26 May 2023

Long-Term Structural Integrity Assessment of the Red Hill Underground Storage Tanks

Joint Base Pearl Harbor-Hickam, Hawaii

26 May 2023

SGH Project No. 221162, Phase 02

SGH

PREPARED FOR:

Naval Facilities Engineering Systems Command (NAVFAC) Pacific
Joint Base Pearl Harbor-Hickam, HI 96860

Via Subcontract to:
Jacobs/B&V
1003 Bishop Street, Suite 1340
Honolulu, HI 96813

PREPARED BY:

Simpson Gumpertz & Heger Inc.
2050 W. Sam Houston Parkway S.
Suite 1625
Houston, TX 77042
Tel: 713.265.6400
Fax: 713.264.6401

26 May 2023

CAPT Darrel E. Frame, P.E.
Naval Facilities Engineering Systems Command (NAVFAC) Pacific
Joint Base Pearl Harbor-Hickam, HI 96860

Project 221162 – Long-Term Structural Integrity Assessment of the Red Hill Underground Storage Tanks, Joint Base Pearl Harbor-Hickam, Hawaii

Dear CAPT Frame:

Please find enclosed our report for the subject project.

We appreciate being of service to NAVFAC, and please do not hesitate to contact us should you have any questions or comments.

Best regards,

Paul B. Summers, P.E., S.E., F.ASCE
Senior Principal
TX License No. 87572
SGH Texas Certificate of Authorization No. F-5107
\\sgh.com\offices\HOU\projects\2022\221162.00-RHDS\WP\008PBSummers-L-221162.00.dkh.docx

Encls.
cc: Dan W. Waddill, Ph.D., P.E. (NAVFAC Atlantic)
CDR Robert E. McCharen, RA (NAVFAC Pacific)
Ashley M. Echevarria, PMP (Jacobs/B&V)
N. Onder Akinci, Ph.D., P.E. (SGH)
Guzhao Li, Ph.D., P.E., S.E. (SGH)
Gayle S. Johnson, P.E. (SGH)
Emily R. McCarthy, Ph.D., P.E. (SGH)

EXECUTIVE SUMMARY

The Navy commissioned Simpson Gumpertz & Heger Inc. (SGH) to assess the long-term structural integrity of the Red Hill underground storage tanks in order to support Closure in Place as the permanent closure method for the Red Hill tanks. The assessment included the following primary tasks:

- Sophisticated computer modeling of earthquake effects on the tanks, both with and without the steel liner of the tank being present. Two earthquake levels were simulated.
    - A "design earthquake" based on the building code requirements for new construction in Honolulu.
    - An "extreme earthquake event" with a 10,000-year return period, which is typically considered only for critical infrastructure such as nuclear power plants.
- Evaluation of the long-term durability of the steel liner and the concrete walls of the tanks.

The following are key results:

- The design earthquake will not cause cracking or other damage to the tanks, with or without the steel liner.
- The extreme earthquake event may cause localized cracking in the concrete without the steel liner but no significant damage. Regardless of the presence of the steel liner, the analysis results indicate the tanks would remain stable and able to withstand the extreme earthquake event.
- The durability evaluation indicated no significant deterioration of the steel liners within the next 50 years. After 100 years, the internal atmosphere will corrode approximately half the thickness of the steel liners. External corrosion of the steel liner will likely be localized and will not affect the overall structural integrity of the liner.
- Significant deterioration of the concrete is not expected to occur for at least 300 years. After that time, localized deterioration of the concrete will likely result from corrosion of the embedded reinforcing steel.

Should a future major earthquake occur, we recommend reviewing the condition of the tanks.

We do not see a need for an extensive inspection and maintenance program for the tanks.

Table of Contents

Letter of Transmittal

EXECUTIVE SUMMARY

CONTENTS **Page**

1. INTRODUCTION 1
   - 1.1 Scope of Work 1
   - 1.2 Project Team 2

2. BACKGROUND AND LITERATURE 4
   - 2.1 Previous Studies and Key Inputs 4
     - 2.1.1 Underground Tank Drawings 4
     - 2.1.2 Borehole Information and Log of Formation in Tank Excavation Areas 12
     - 2.1.3 Other Documents Reviewed 14
     - 2.1.4 Tower Structural Drawings, Literature, and February 2023 Site Visit Observations 15
     - 2.1.5 Tower Access Bridge 19
   - 2.2 Characterization of Rock Formation Properties 22
   - 2.3 Groundwater Properties 23

3. MATERIAL SPECIFICATIONS 25

4. PERFORMANCE CRITERIA 26
   - 4.1 Underground Storage Tanks 27
   - 4.2 Tank Tower 28
   - 4.3 Response Spectra 29
     - 4.3.1 DBE and MCE_R 30
     - 4.3.2 10,000-Year Spectrum 32

5. UNDERGROUND TANK ANALYSIS 34
   - 5.1 Site Response Analyses 34
     - 5.1.1 Assumptions for Site Response Analysis 34
     - 5.1.2 Methodology 35
     - 5.1.3 Calculations 39
     - 5.1.4 Sensitivity Studies 41
     - 5.1.5 Results and Discussion 42
   - 5.2 Soil-Structure Interaction Analysis 44
     - 5.2.1 Model Description 44
     - 5.2.2 Tank Displacements 47
     - 5.2.3 Interface Pressures 48
   - 5.3 3D Nonlinear Structural Response Analysis 50

5.3.1 Finite Element Model 50
5.3.2 Analysis Results for Tank Without Steel Liner 57
5.3.3 Discussion for Tank Without Steel Liner 65
5.3.4 Analysis Results for Tank with a Steel Liner 67
5.3.5 Discussion for Tank with Steel Liner 68
5.3.6 Summary of Analysis Results 69

6. TANK ACCESS TOWER ANALYSIS 70
6.1 Methodology 70
6.2 Analysis Results 76
6.3 Discussion 80

7. LONG TERM DURABILITY 83
7.1 Concrete Components 83
7.1.1 Introduction 83
7.1.2 Effect of Exposure 84
7.1.3 Acid Attack 85
7.1.4 Concrete Leaching 86
7.1.5 Reinforcing Steel Corrosion Due to Carbonation 87
7.1.6 Reinforcing Steel Corrosion Due to Chlorides 87
7.1.7 External Sulfate Attack on Concrete 88
7.1.8 Internal Sulfate Attack 88
7.1.9 Alkali-Silica Reactivity 89
7.1.10 Microbiological attack 90
7.1.11 Salt Crystallization 90
7.1.12 Other Damage 91
7.1.13 Suggestions For Potential Monitoring 91
7.2 Long-Term Corrosion Susceptibility of Red Hill Tank Steel Liners 94

8. SUMMARY, CONCLUSIONS, AND SUGGESTIONS 96
8.1 Summary of Key Tasks 96
8.1.1 Seismic Hazards at the Site 97
8.1.2 Site Response 99
8.1.3 Soil-Structure Interaction Analysis 99
8.1.4 Tank Structural Response Analysis 100
8.1.5 Tank Access Bridge and Support Tower Structural Analysis 102
8.1.6 Tank Durability 103
8.2 Considerations for Future Monitoring 104
8.3 Recommendations 105

9. REFERENCES 106

1. INTRODUCTION

Naval Facilities Engineering Systems Command Hawaii (NAVFAC HI) commissioned Simpson Gumpertz & Heger Inc. (SGH) to assess the long-term structural and seismic risk for the underground storage tanks at the Red Hill Bulk Fuel Storage Facility (Red Hill) under the assumption that the tanks will be left in place after completion of defueling and subsequent cleaning. SGH performed the assessment as a subconsultant to Jacobs/B&V (Jacobs) under Jacobs Agreement No. 149001660, Rev. 1, with the scope of work as defined in the Amendment 26 SAES for IDIQ Contract N62478-20-D-5036 for the Red Hill Closure Structural Analysis at Joint Base Pearl Harbor-Hickam (JBPHH), Hawaii.

1.1 Scope of Work

The scope of work included the following primary tasks:

1. Determine seismic ground motion hazards at bedrock for a range of earthquakes at the site based on the United States Geological Survey (USGS) ground motion data.

2. Perform a site response analysis using a detailed model of the site-specific soil profile to determine soil and rock strains along the height of the soil column and Red Hill tanks, independent of the presence of the tanks.

3. Use the results of the site response analysis as input for a soil-structure interaction (SSI) analysis that considers a detailed model of the soil properties to calculate displacements and the pressures that would be experienced on the tank shell during an earthquake event.

4. Use the loading from the SSI analysis on a detailed FE model of a typical Red Hill storage tank to determine stresses and strains in the concrete tank shell and tank movement due to earthquake loading, both with and without the presence of the steel liner.

5. Perform a seismic evaluation of the access walkway and internal tank tower.

6. Evaluate the likely durability and extent of deterioration of both the steel liner and the concrete in the tank walls for a long exposure period, considering the groundwater chemistry.

Figure 1-1 schematically illustrates the overall analysis approach of Tasks 1 to 4 above. The following sections summarize the analysis results and findings for each item within the scope of work.

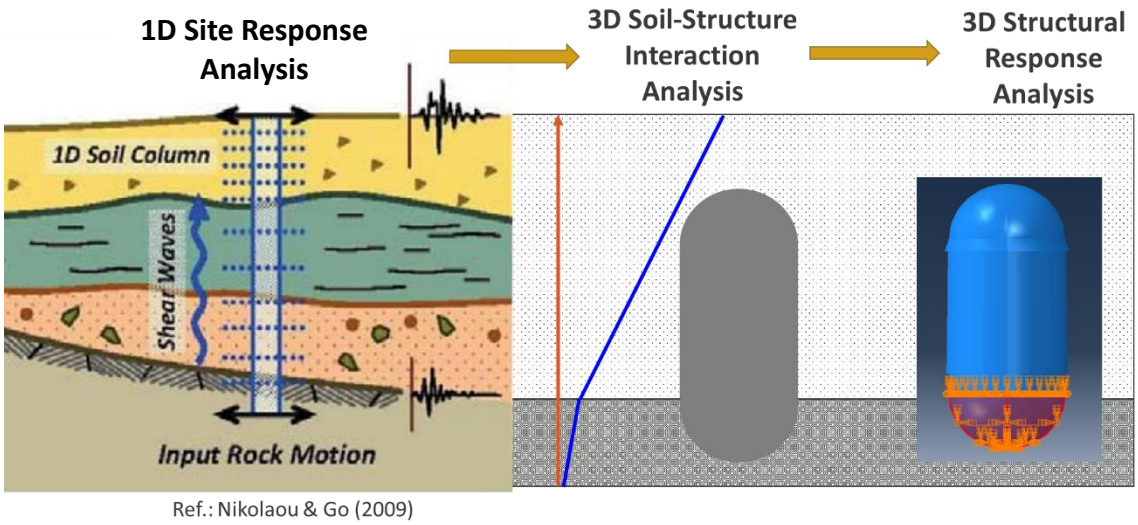

Figure 1-1 – Overall Analysis Approach

1.2 Project Team

Our SGH project team included a number of staff members, as listed below:

- Principal-in-Charge – Paul B. Summers, P.E., S.E.
- Project Manager – Onder Akinci, Ph.D., P.E.
- Geotechnical Engineering – Giuliana Zelada-Tumialan, P.E., G.E.
- Seismic Hazard – Ronald O. Hamburger, P.E., S.E., NAE.
- Underground Storage Tank Analysis.
    - 1D Site Response Analysis – Tianye Yang and Luke Ciarelli.
    - 3D Soil-Structure Interaction – Sean Hsieh and Jeremy Bowers, P.E., S.E.
    - Structural Response – Madhav Parikh, P.E. and Nestor Castaneda, P.E.
- Tank Access Tower Analysis – Emily R. McCarthy, Ph.D., P.E., and Elizabeth A. Washburn.
- Long-Term Durability.

    - Concrete – Matthew R. Sherman, P.E., William P. Konicki, P.E., and Paul C. Scheiner. P.E.
    - Steel – Alan O. Humphreys, Ph.D., P.E.

- Independent Reviewers.

    - Gayle S. Johnson, P.E. – Overall.
    - Daniel W. Eggers, P.E. – Geotechnical Engineering, 1D Site Response Analysis, and 3D Soil-Structure Interaction.
    - Guzhao Li, Ph.D., P.E., S.E. – Structural Response.

2. BACKGROUND AND LITERATURE

2.1 Previous Studies and Key Inputs

2.1.1 Underground Tank Drawings

We reviewed a series of original tank drawings titled Underground Fuel Storage with various dates (from 1941 to 1943) and multiple revisions. For the evaluation of the underground storage tanks, we obtained the pertinent data (such as tank dimensions, steel liner plate details, and reinforced concrete details) from the drawings listed below:

- Drawing No. 293965 – General Plan & Profile of Pipeline Tunnel.
- Drawing No. 294296 – Special Horizontal Steel for Upper Domes #1 to #4.
- Drawing No. 294297 – Dome Steel – Liner Plate Details.
- Drawing No. 294298 – Special Horizontal Steel for Upper Domes #5 to #20.
- Drawing No. 294302 – Reinforcement Steel in Tanks – Lower Dome and Barrel.
- Drawing No. 294303 – Prestressing Grout Detail.
- Drawing No. 294305 – General Design and Construction Details.
- Drawing No. 294307 – Bottom Domes – Typical Section and Plan.
- Drawing No. 294309 – Typical Liner Plates in Lower Dome.
- Drawing No. 294318 – Gen Plan & Gauging Platform.
- Drawing No. 294321 – Upper and Lower Dome Details.

The interior diameter for each tank is 100 ft, based on the drawings. Each tank consists of a bottom dome, a barrel section in the middle, and an upper dome. The overall interior height is approximately 250 ft for Tanks 5 to 20. The barrel section for Tanks 5 to 20 is approximately 150 ft tall, while the upper and lower domes are approximately 50 ft tall. The barrel section for Tanks 1 to 4, built before the other tanks, is 12 ft shorter than that for Tanks 5 to 20, resulting in an overall interior height of about 238 ft for Tanks 1 to 4. The elevations of the tanks (extracted from Drawing No. 294318) are shown in Figure 2-1. The top of the tanks (top of the upper dome) is a minimum of 100 ft below ground, as shown in Figure 2-2 (extracted from Drawing No. 293965).

ELEVATIONS FOR TANKS

	Tanks 1,2,3,4	Tanks 5 & 6	Tanks 7 & 8	Tanks 9 & 10	Tanks 11 & 12	Tanks 13 & 14	Tanks 15 & 16	Tanks 17 & 18	Tanks 19 & 20
Elev. Fin. Floor of Tunnel.	102.36	105.36	109.36	113.36	117.36	121.36	125.36	129.36	133.36
Fin. Floor to Top of Arch of Tunnel	15.09	15.09	15.09	15.09	15.09	15.09	15.09	15.09	15.09
Elev. Bottom of Sub-Grade	117.45	120.45	124.45	128.45	132.45	136.45	140.45	144.45	148.45
Thickness of Bottom	3.00	3.00	3.00	3.00	3.00	3.00	3.00	3.00	3.00
Elev. Inside of Bottom	120.45	123.45	127.45	131.45	135.45	139.45	143.45	147.45	151.45
Vertical Height of Bottom	48.99	48.99	48.99	48.99	48.99	48.99	48.99	48.99	48.99
Elev. Bottom of Barrel Section	169.44	172.44	176.44	180.44	184.44	188.44	192.44	196.44	200.44
Height of Barrel Section	139.42	151.41	151.41	151.41	151.41	151.41	151.41	151.41	151.41
Elev. at Springline	309.86	323.85	327.85	331.85	335.85	339.85	343.85	347.85	351.85
Elev. Inside Top of Dome	359.86	373.85	377.85	381.85	385.85	389.85	393.85	397.85	401.85
Thickness of Dome	4.00	4.00	4.00	4.00	4.00	4.00	4.00	4.00	4.00
Elev. Outside Top of Dome	365.03	380.02	384.02	388.02	392.02	396.02	400.02	404.02	408.02

Note: Grade Level to Station 30+00
+2% Grade Beyond Sta 30+00

Figure 2-1 – Elevations for the Red Hill Tanks
(Extracted from Drawing No. 294318)

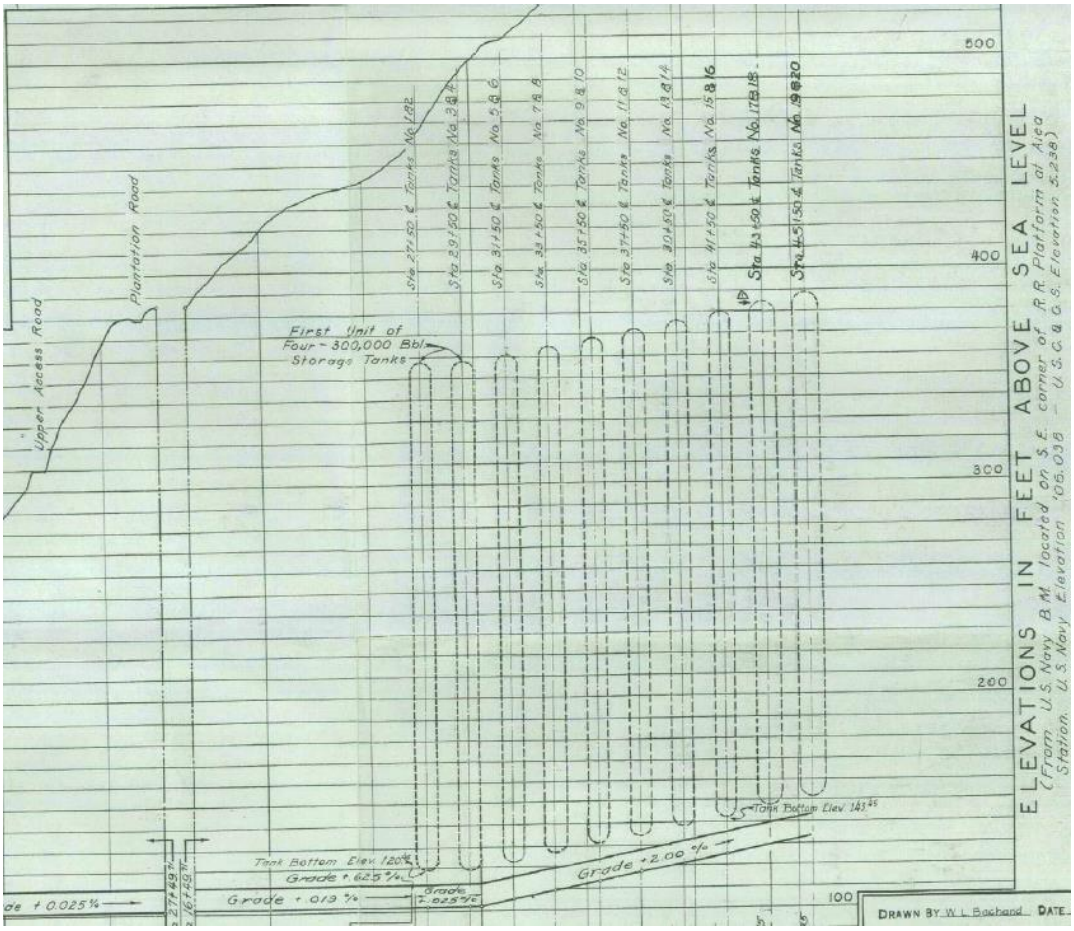

Figure 2-2 – Elevation View of the Tanks
(Extracted from Drawing No. 293965)

The construction of each tank consists of a minimum of 2.5 ft thick reinforced concrete (2.5 ft minimum at the top of a barrel section and 4 ft minimum at the bottom of a barrel section) with 1/4 in. thick interior steel liner plate (1/2 in. thick steel plate at the floor of the bottom dome). Each tank was constructed by excavating the lava rock formation of Red Hill. The excavated wall was washed, and a 6-in. layer of gunite was applied, followed by a spray-applied coating of red earth to prevent bonding with the concrete lining (ASCE 1993). Therefore, the reinforced concrete shell of each tank was surrounded and laterally supported either by basalt (sound rock) or clinker (a softer, less stiff layer), as shown in Figure 2-3. Soft material was compacted with gunite plugs (dry-gun concrete) before reinforced concrete was placed. Figure 2-4 shows the gunite plug detail.

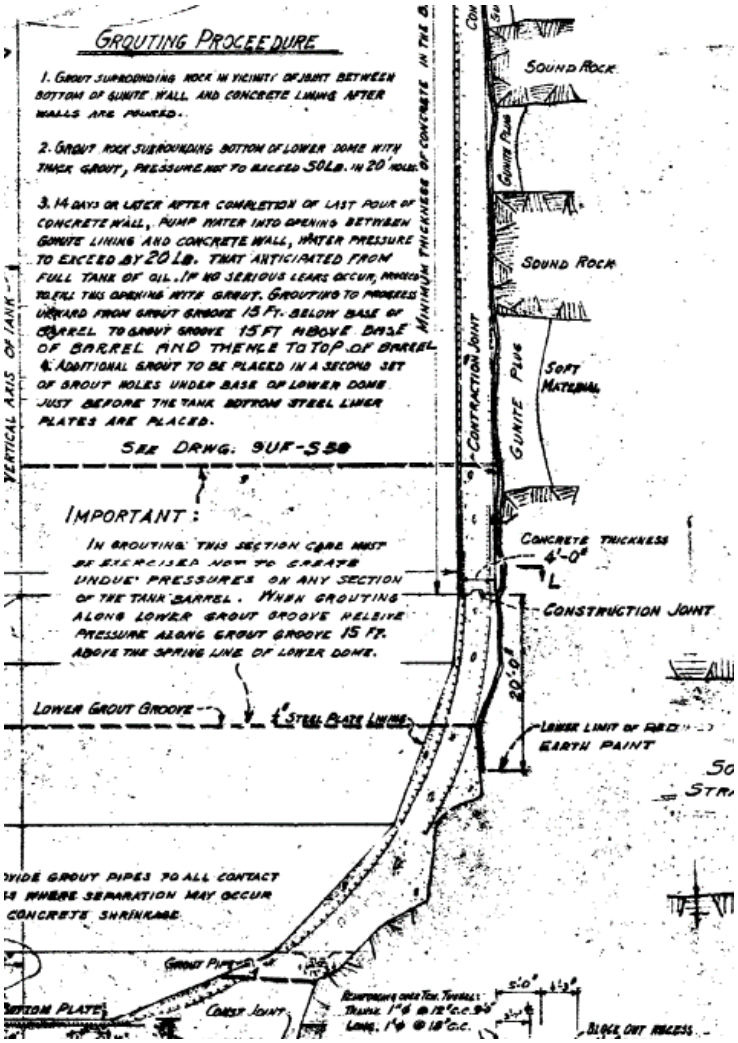

Figure 2-3 – Partial Section of Tank
(Extracted from Drawing No. 294305)

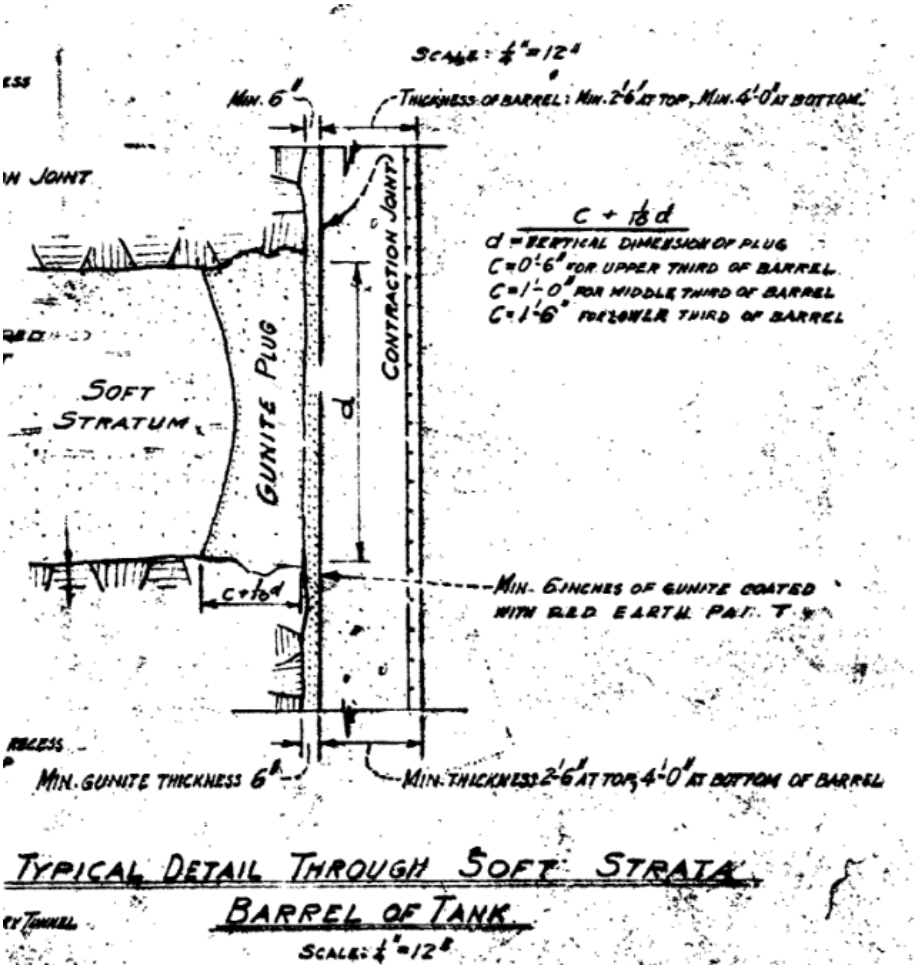

Figure 2-4 – Typical Detail Through Soft Strata for Barrel Section of Tank (Extracted from Drawing No. 294305)

The reinforcement details for the barrel section concrete (extracted from Drawing No. 294302) are shown in Figure 2-5. The steel liner plates on the barrel section are arranged as 5 ft tall horizontal courses. The liner plates are connected by 3 in. x 2-1/2 in. x 5/16 in. horizontal steel angles welded to the backside of the steel liner plates at the top and bottom of the plates, and the angles are embedded or anchored into the reinforced concrete using 3/4 in. diameter steel rods. Figure 2-6 shows a typical section of barrel liner plate anchorage details (extracted from Drawing No. 294321).

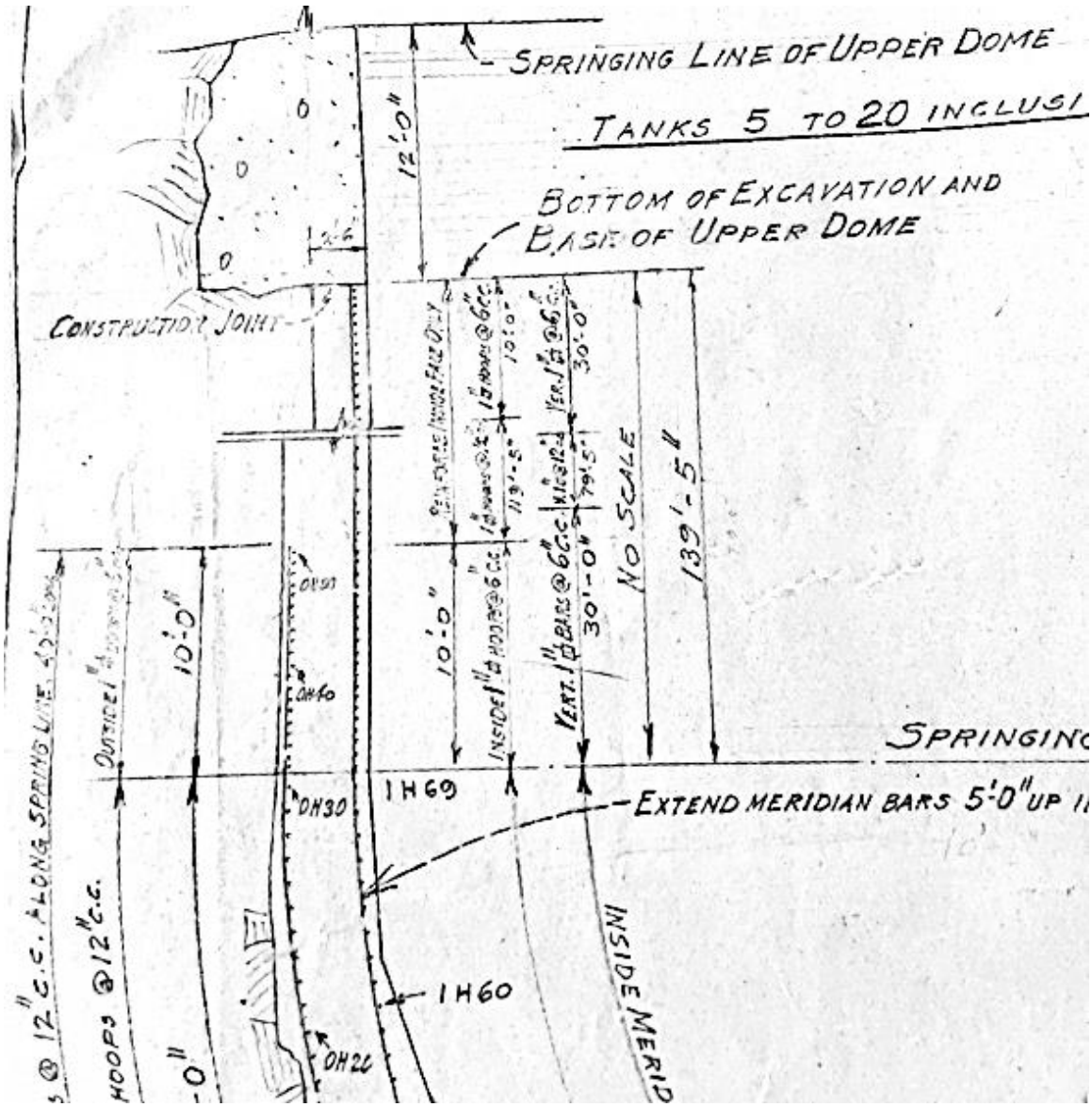

Figure 2-5 – Typical Tank Barrel Section Reinforcement Details
(Extracted from Drawing No. 294302)

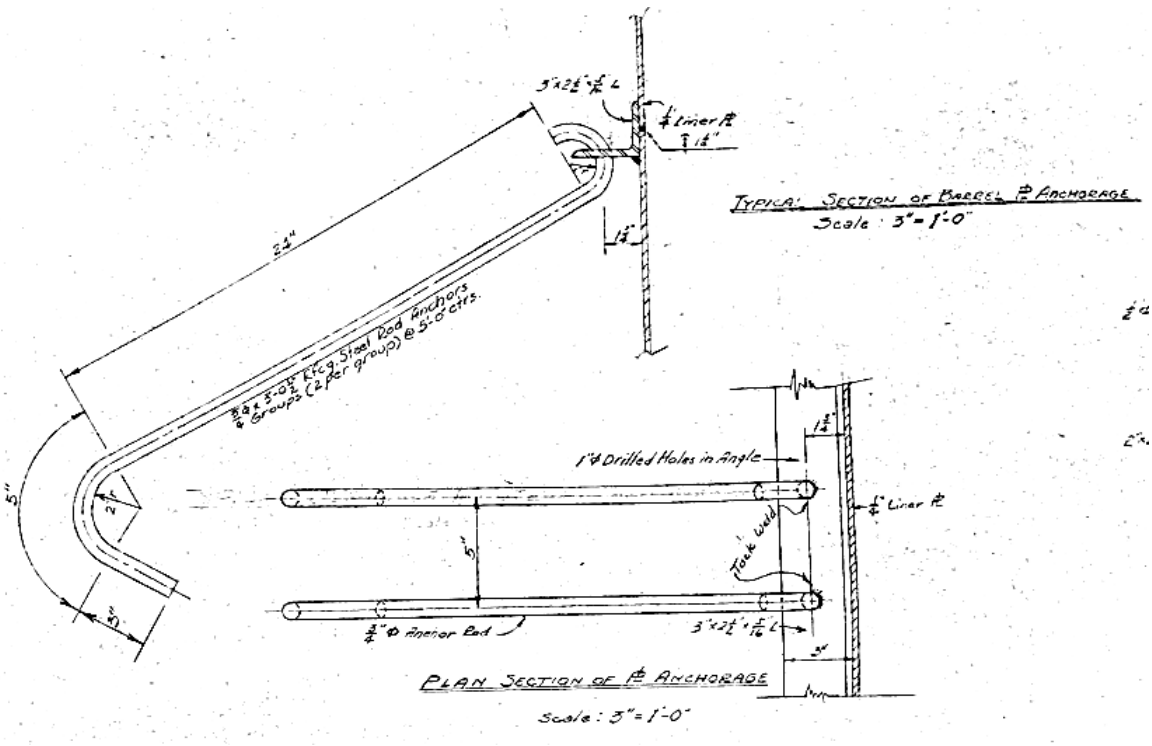

Figure 2-6 – Typical Liner Plate Anchorage Details of Tank Barrel Section (Extracted from Drawing No. 294321)

After the construction of the tank wall, prestressing grout was injected through the grout pipes between the tank wall and the surrounding strata (basalt or gunite plug at softer soil layers). This prestressing grout puts concrete in the tank wall under compression. The minimum thickness of this grout or gunite lining specified in the drawings is 6 in. for the upper portion of the barrel. Figure 2-7 shows the vertical section through the tank with locations of the grout grooves along the tank height. A typical horizontal section through the tank barrel at a grout groove is shown in Figure 2-8. Eight grout pipes and four strain gauges are used along the perimeter of each grout groove. Figure 2-9 shows a typical grout groove detail in the cross-section.

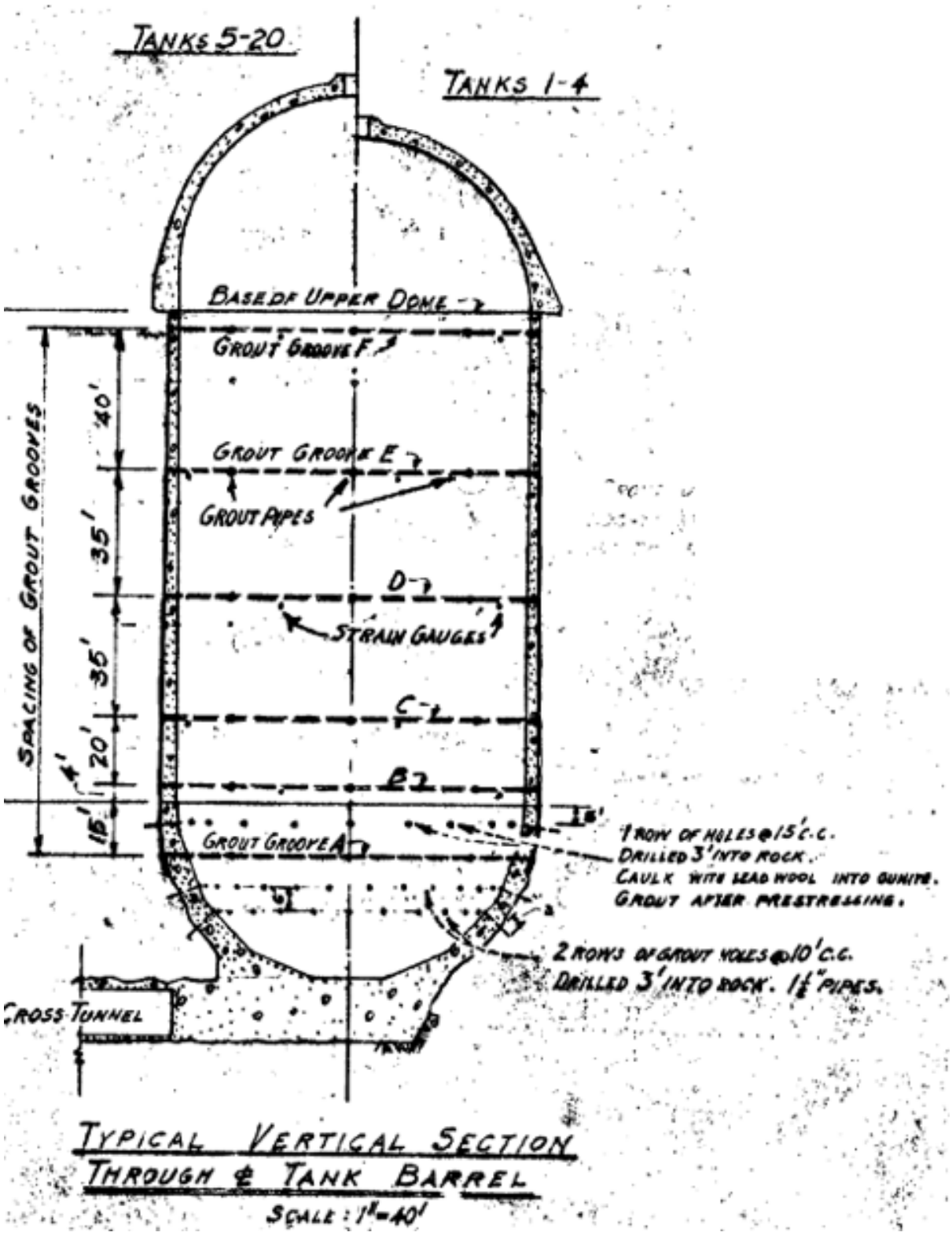

Figure 2-7 – Typical Vertical Section Through Centerline of Tank with Grout Grooves (Extracted from Drawing No. 294303)

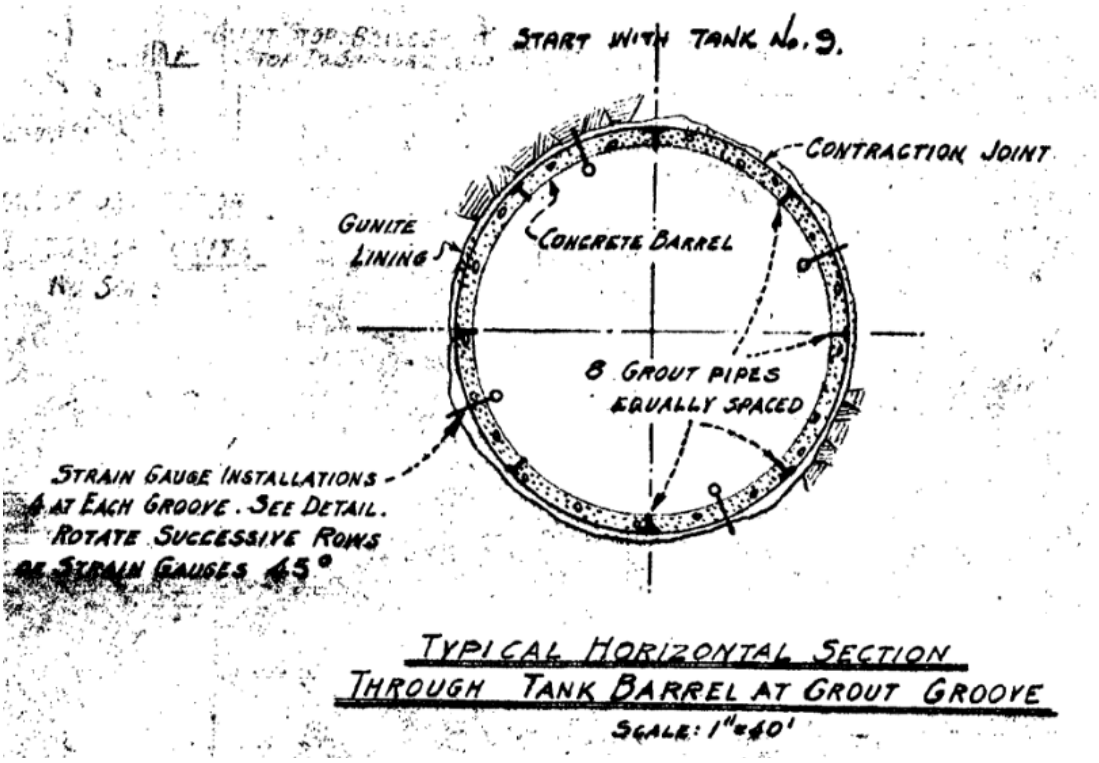

Figure 2-8 – Typical Horizontal Section Through Tank Barrel at Grout Groove (Extracted from Drawing No. 294303)

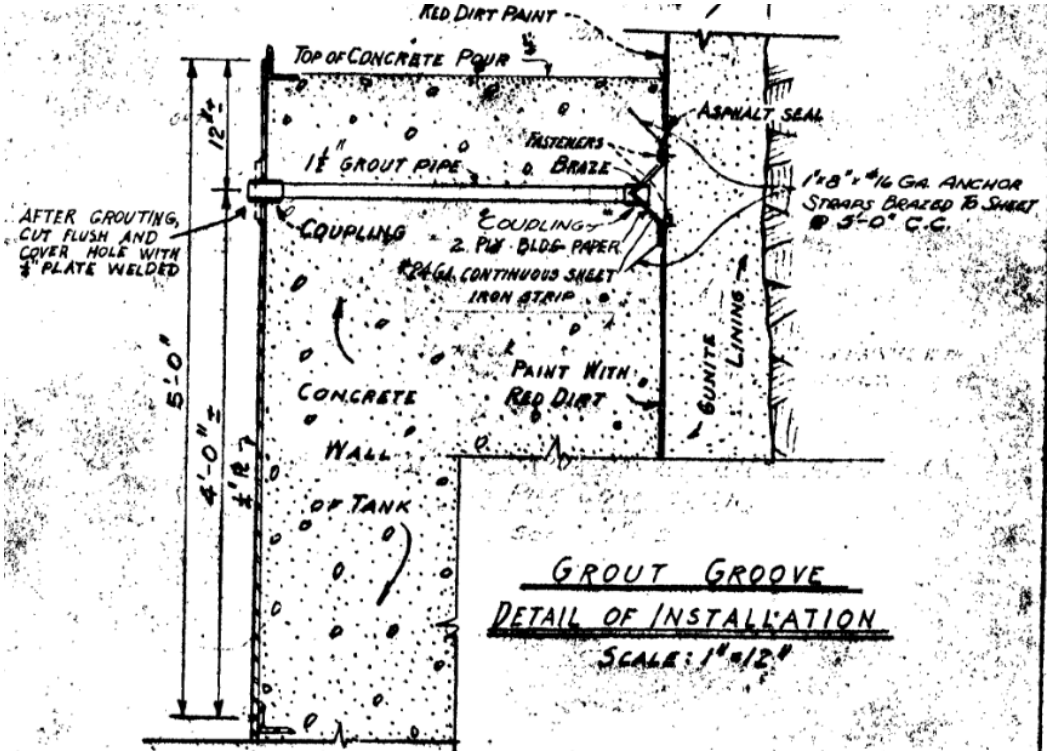

Figure 2-9 – Tank Grout Groove Detail of Installation (Extracted from Drawing No. 294303)

2.1.2 Borehole Information and Log of Formation in Tank Excavation Areas

We reviewed the following drawings containing the borehole information and log of formation observed during tank excavation:

- Drawing No. 293906 – Pearl Harbor Fuel Storage Log of Diamond Drill Holes 1940.
- Drawings No. 293962 to No. 293979 – Log of Formations in Tank Excavation from Tank 1 to Tank 18.
- Drawing No. 293981 – Log of Formations in Tank Excavation for Tank 20.

Borehole No. 2B, included in Drawing No. 293906, is adjacent to Tanks 9 and 10. However, Borehole No. 2B only extends to El. 244.5 ft, while the base elevation of the bottom domes of Tanks 9 and 10 is El. 131.45 ft. Between El. 244.5 and El. 350 ft, the borehole shows interlayered "hard, gray basalt" and “hard caving clinker.” Portions of the basalt rock were described as “of a clinker character, caves badly and leaks” or “with frequent cavities. Very leaky.”

During the construction of the tanks, the rock formations observed at the perimeter of the tank excavations were logged by Contractors Pacific Naval Air Bases (CPNAB). For example, Figure **2-10** shows the log of formation recorded during Tank 6 excavation (extracted from Drawing No. 293967). Figure 2-11 shows a 3D rendering of the twenty tanks with their respective log formations, highlighting the trend of rock, clinker, grout, etc., along the height of the tanks and along the length of the tank gallery tunnel (AECOM 2019).

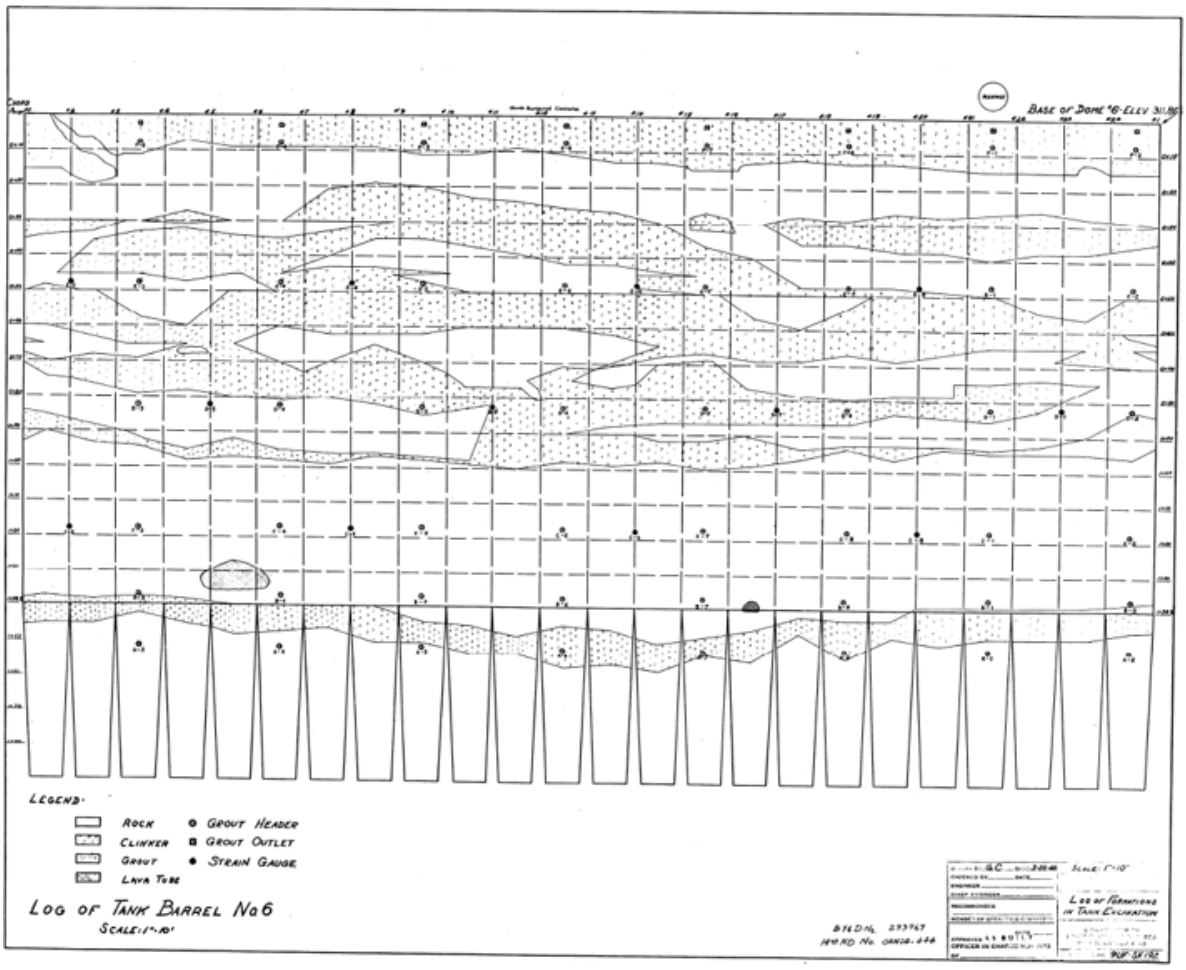

Figure 2-10 – Tank 6 Log of Formation During Excavation for Construction of Tanks

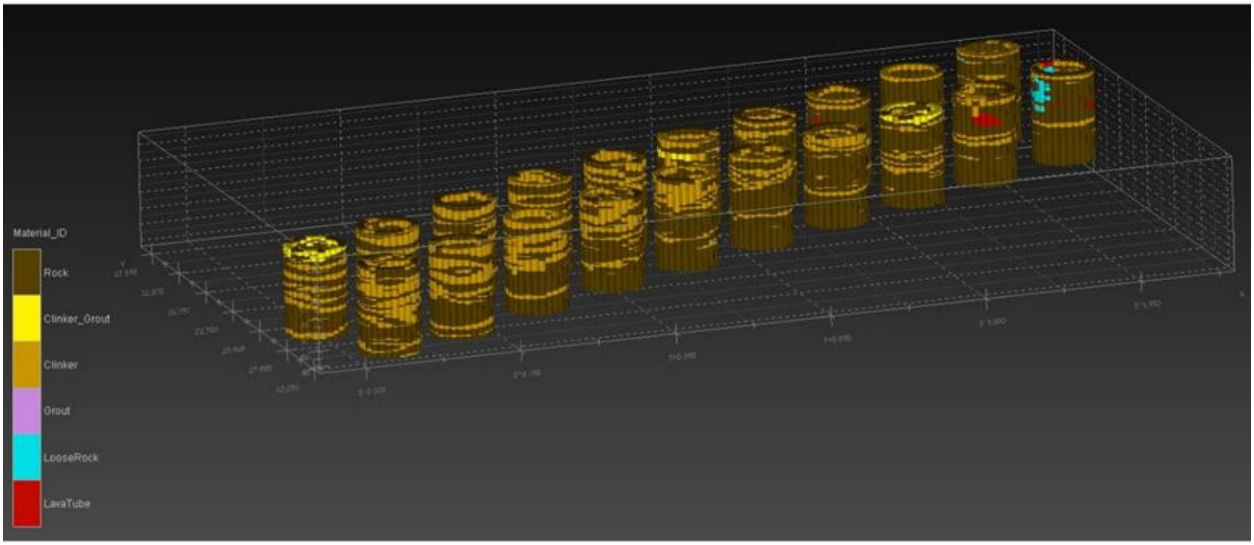

Ref.: AECOM 2019

Figure 2-11 – 3D Rendering of Formations Around the Tanks Excerpted from Conceptual Site Model

2.1.3 Other Documents Reviewed

We reviewed the following document to determine the material properties of the steel liner plate and current conditions:

- Red Hill Bulk Fuel Storage Facility Destructive Testing Report, AOC/SOW 5.3.3, SSR-NAVFAC EXWC-CI-1941, 7 July 2019.

This report presents data on ten steel liner coupon samples from Tank 14. Eight of these samples were taken from the tank barrel, one from the lower part of the upper dome and the other from the upper part of the lower dome of Tank 14. This report indicates that the steel tank liner was made from steel that generally conformed to ASTM A36 specifications based on testing the ten coupons (with dimensions of 12 in. x 12 in. for each coupon) in 2018. This report also indicates that the remaining liner plate thickness at the thinnest location for Coupon 3 (top course of steel liner in the barrel) was about 53% of the original liner plate thickness of 1/4 in. Figure 2-12 shows a cross-section of Coupon 3 at the location of maximum wall loss.

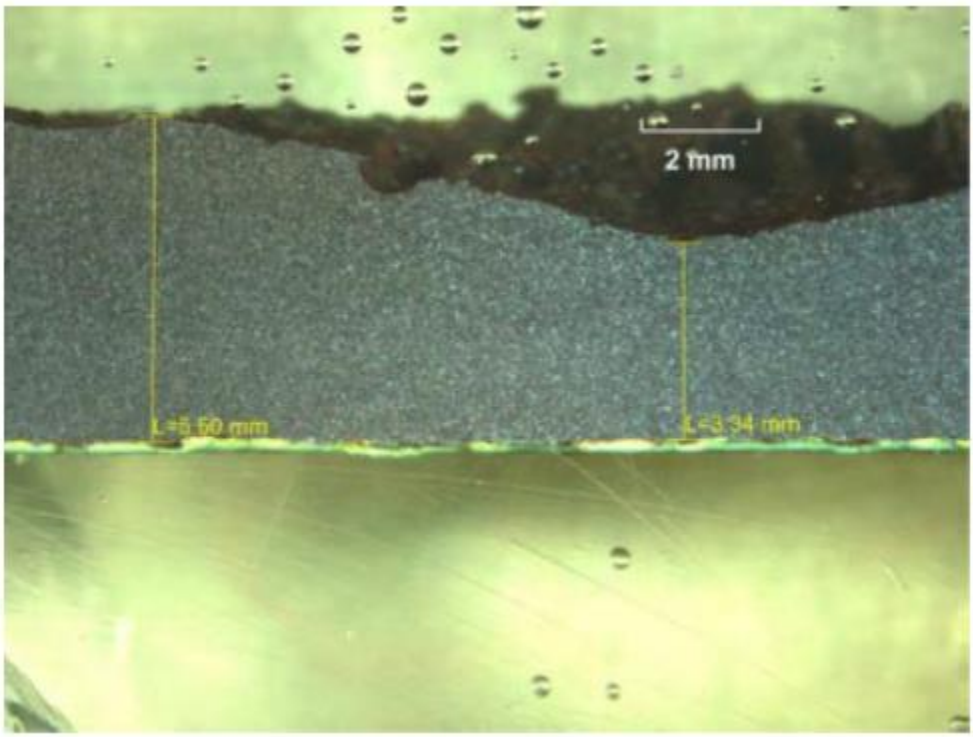

Figure 2-12 – Cross Section of Coupon 3 at Area of Maximum Wall Loss (Tank 14)

2.1.4 Tower Structural Drawings, Literature, and February 2023 Site Visit Observations

We reviewed the following document to determine the layout and design of the internal tank tower:

- Drawing No. 294318 – General Plat of Tank – Sheet No. 1 Reinforcing Steel, Access Gallery Vent Pipes & Grout Grooves.
- Drawing No. 294365 – Details of Tower Footings.
- Drawing No. 294368 – Oil Storage Tanks: Details of Service Scaffold & Tugger Platform.

The internal tank tower is 7 ft x 7 ft in plan and varies in overall height with the tanks, i.e., for Tanks 1 to 4, the tower is approximately 238 ft tall, while for Tanks 5 to 20, the tower is approximately 250 ft tall. The tower comprises crossed-braced bays that are approximately 10 ft tall (each face of the tower) that continue the full tower height. SGH performed a site visit of Tank 19 on 1 February 2023 and measured the tower legs as 6 in. x 4 in. x 3/8 in. angles, with the long leg parallel to the cantilevering access platforms. We note that Drawing No. 294365 cites each tower leg as 6 in. x 6 in. x 3/8 in. angles. This drawing additionally specifies that the column legs are bolted to batter foundations that are inset in mass concrete below the lower tank dome (Figure 2-13).

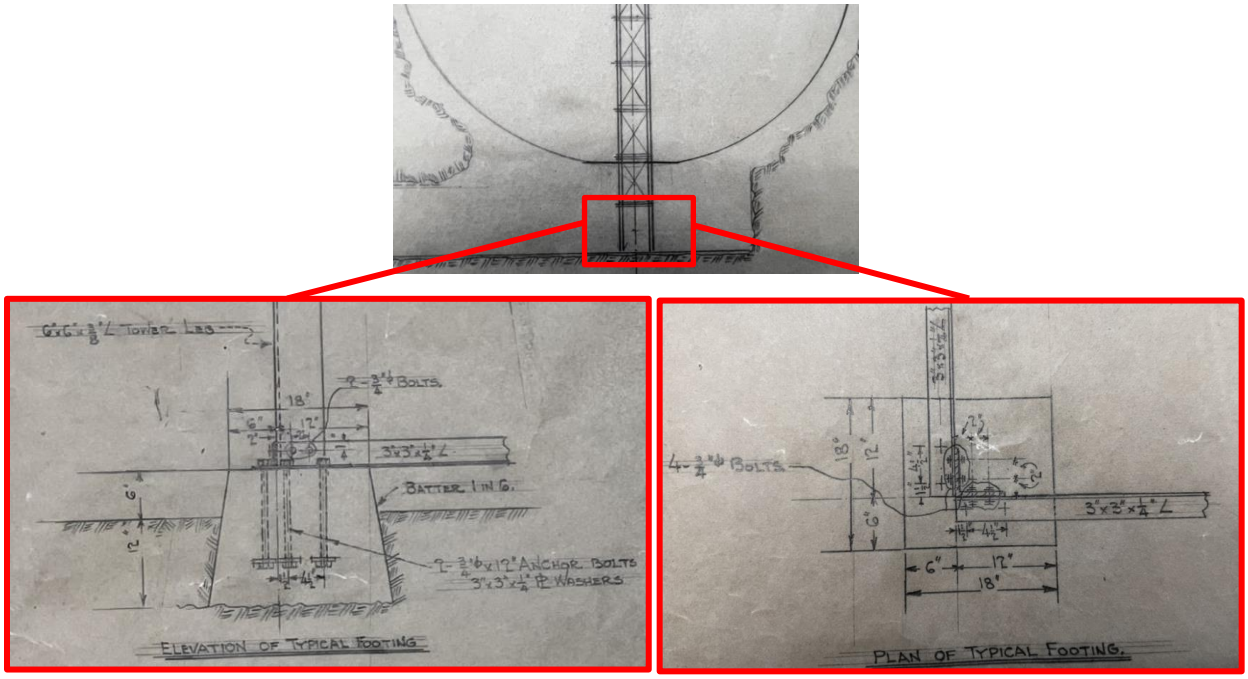

Figure 2-13 – Structural Drawing 294365 – Details of Tower Footings

Four 3/4 in. x 12 in. anchor bolts (two along each column angle leg) with 3 in. x 3 in. x 1/4 in. plate washers attach the columns to their batter foundations at each anchor bolt. Figure 2-14 shows a photo of the invert of Tank 2 during construction, showing the tank tower inset into the mass concrete portion of the tank prior to pouring the mass concrete. Additionally, we received photos of the Tank 5 tower taken during the clean inspection repair (CIR) program (Figure 2-15), which show the base connection of the tower to the tank.

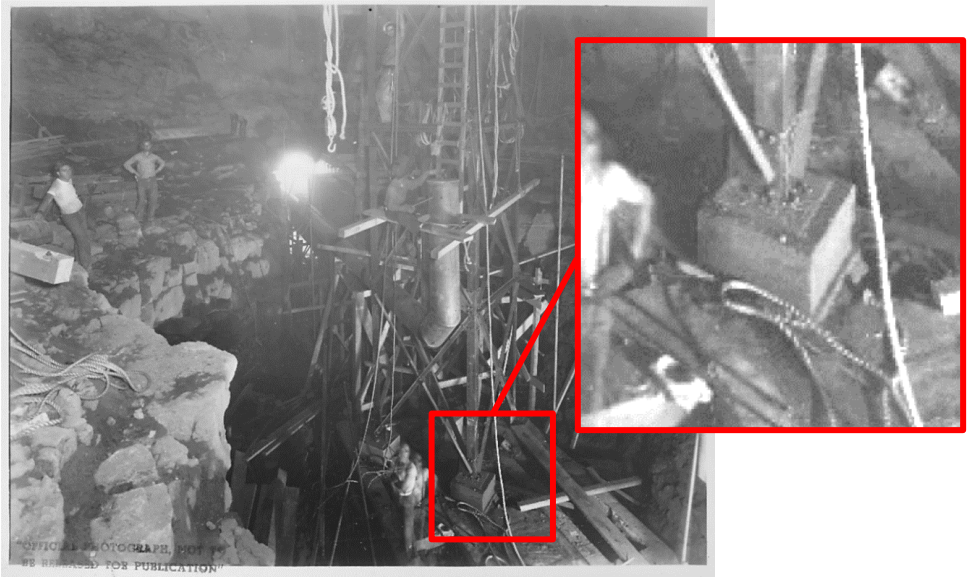

Figure 2-14 – Photo of Invert Construction of Tank 2 Prior to Placement of Mass Concrete Plug, with Tank Tower Foundation Connection Below Tank Invert

Figure 2-15 – Base of Tank 5 Tower

Drawing 294318 shows that the tower legs at the top of the tower penetrate the concrete upper dome, although no details are given in this drawing about how the column is secured in the concrete (Figure 2-16).

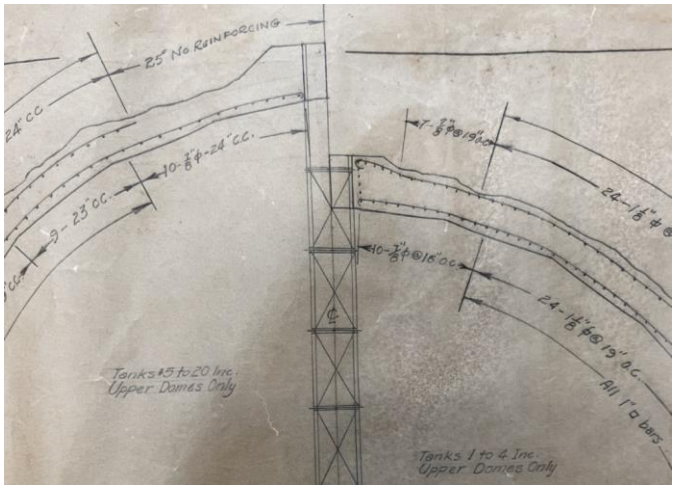

Figure 2-16 – Structural Drawing 294318 – General Plan of Tank, Showing Tank Tower Penetrating Upper Tank Dome

From SGH field measurements in Tank 19 during the February 2023 site visit, each horizontal beam in the tower is a double angle 3 in. x 3 in. x 1/4 in., and each diagonal X-brace is a 2-1/2 in. x 2 in. x 3/8 in. angle with a vertically-oriented long leg. The braces and beams are bolted to gusset plates that are bolted to each column leg. The braces are connected at their midsection by a bolted gusset plate connection.

Per Drawing 294365, the tank tower is stabilized by 3/4 in. guy wires at four locations along the height of the tower. However, we only observed three sets of 1/2 in. diameter guy wires along the height of Tank 19 during our site visit on 1 February 2023.

In February 2023, we additionally observed eight access platforms with caged ladders that connect each platform level. At the upper access tunnel, a bridge connects the tunnel entrance to the tank tower at the main access platform that encircles the tank tower. Drawing 294368 presents member sections and a layout for the main access platform connecting the upper access tunnel via the bridge. The remaining seven access platforms do not fully encircle the tank tower; instead, they project from one face of the tank tower. Additionally, there is piping and conduit running the full height of the tower (Figure 2-17). During our document review, we did not find drawings related to these elements.

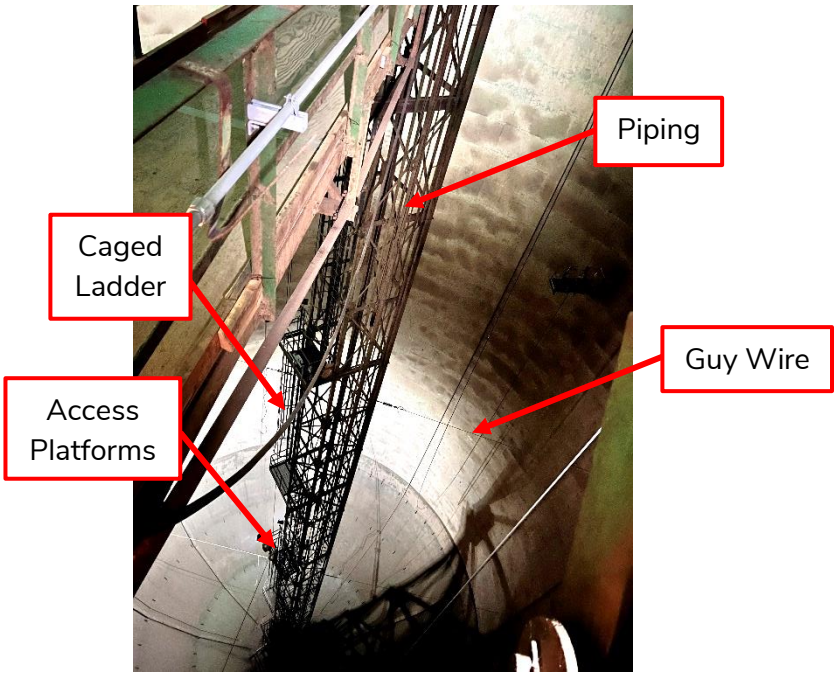

Figure 2-17 – Tank 19 Tower with Piping/Conduit, Platforms, Bridge, and Ladders

2.1.5 Tower Access Bridge

During the site visits in January 2022 and February 2023, we observed the tower access bridge spans from the internal tank wall to the tank tower and consists of steel and timber construction (Figure 2-18). The bridge comprises steel girders and support beams, steel braces, timber panels and beams along the walking surface, cable stays, and steel railing.

Figure 2-18 – Tank Tower Access Bridge (Left) and Entry Platform (Right)

Drawing 294368 shows the access bridge consists of timber structural members and steel connection hardware (Figure 2-19). Per the original drawing, truss members at the center and rods stabilize the bottom of the bridge; however, we did not observe the truss members during the site visit in February 2023.

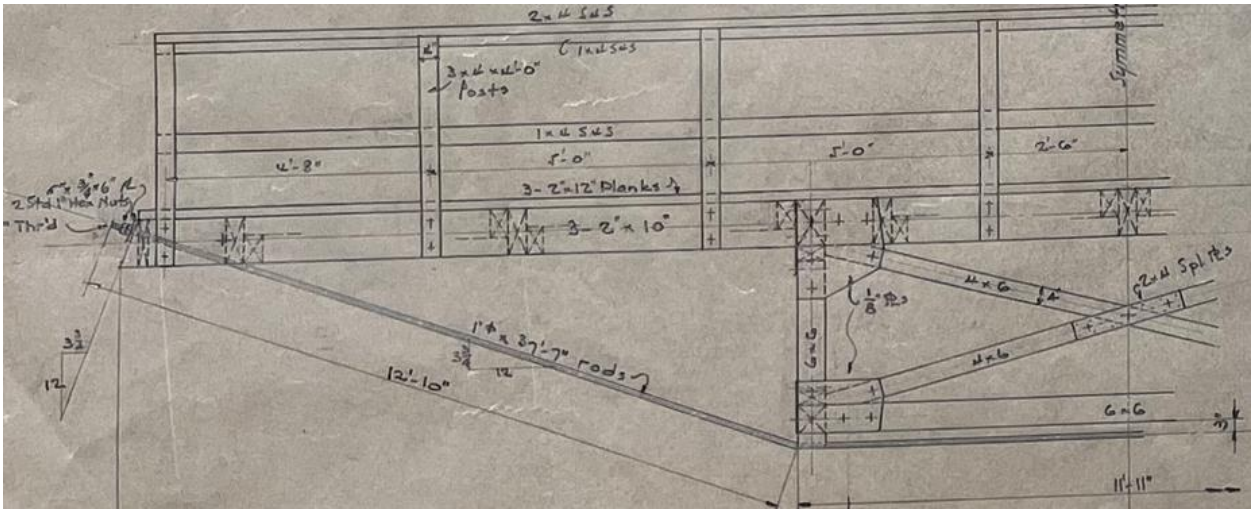

Figure 2-19 – Half Elevation of Tank Tower Access Bridge
(Extracted from Structural Drawing 294368)

According to Drawing 294368, the bridge is bolted to the tank tower platform and supported by a wide flange beam (Figure 2-20 and Figure 2-21). Details of the access bridge connections are unknown.

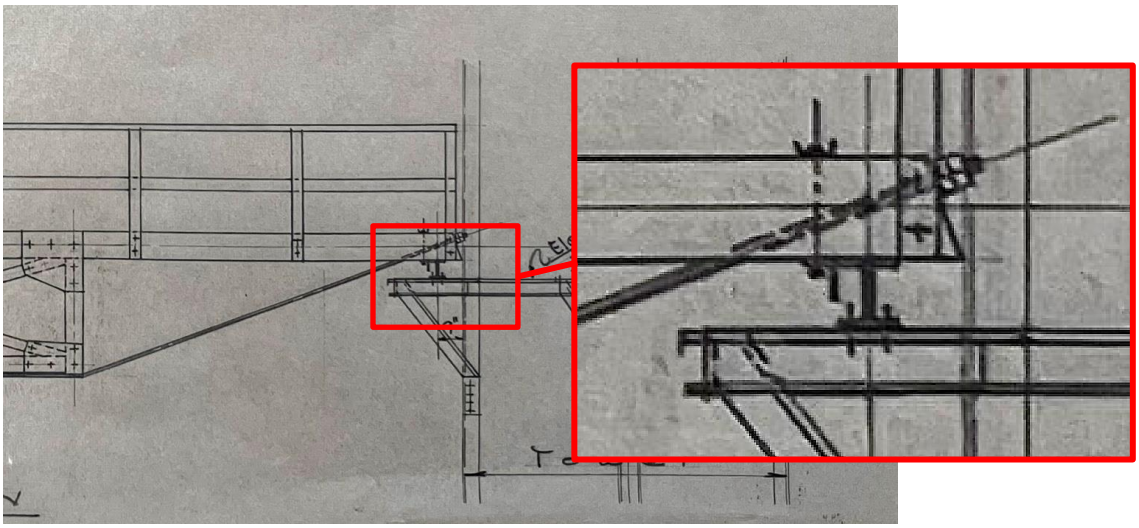

Figure 2-20 – Tank Tower Access Bridge Details
(Extracted from Structural Drawing 294368)

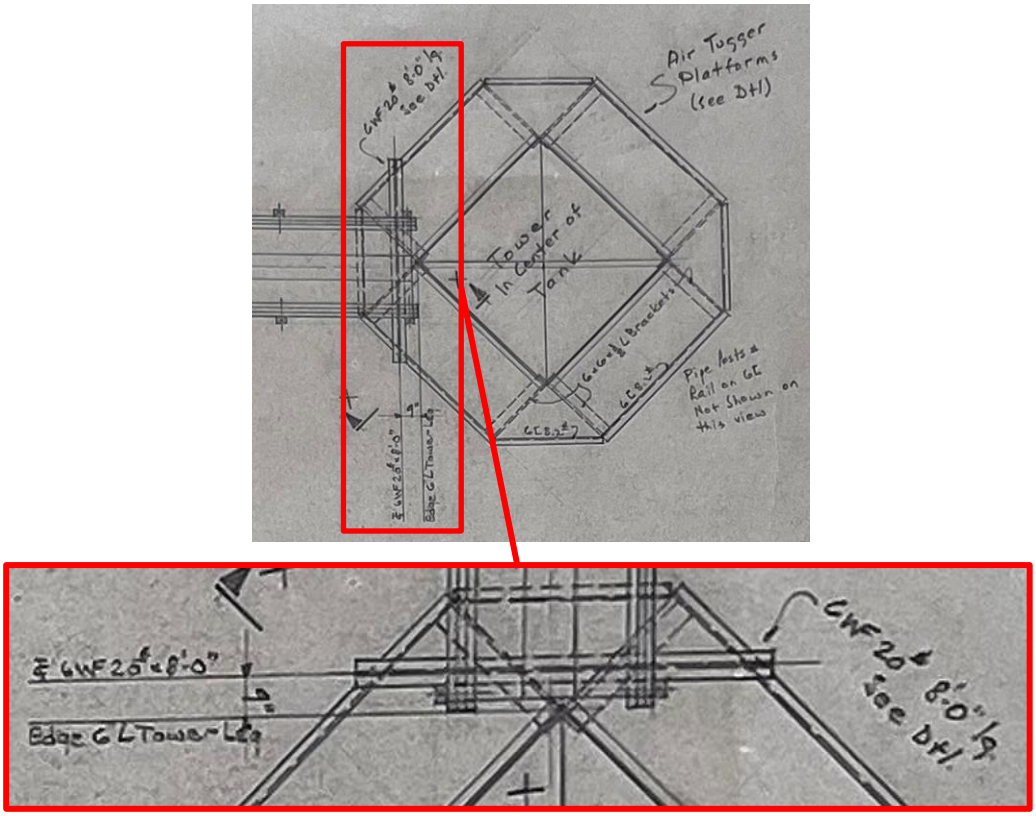

Figure 2-21 – Tank Tower Access Bridge Details
(Extracted from Structural Drawing 294368)

2.2 Characterization of Rock Formation Properties

Given that the available borehole information did not provide a sufficient description of the clinker and basalt formations around the tank to develop design soil/rock properties, we reviewed published documents related to Hawaiian geology to assist in developing the material properties. Specifically, we reviewed the following publications:

- "Soil and Rock Properties in a Young Volcanic Deposit on the Island of Hawaii," H.G. Brandes et al., Journal of Geotechnical and Geoenvironmental Engineering, June 2011.
- "Shear-Wave Velocity Characterization of the USGS Hawaiian Strong-Motion Network on the Island of Hawaii and Development of a NEHRP Site-Class Map," I.G. Wong et al., Bulletin of the Seismological Society of America, Vol. 101, No. 5, pp. 2252-2269, October 2011.

Brandes et al. describe clinker as thick units of "disorganized, jagged, and spiny basalt blocks and rubble" and indicate that the clinker is found alternating with thinner intervals of more homogeneous solid rock. Based on this description and considering the field observations during tank construction which indicate that the clinker caved easily, we conservatively assumed the clinker acts as a granular soil with a friction angle of 33°, a unit weight of 130 pcf, and a Poisson's ratio of 0.3.

In addition, we assumed unit weights of 120 pcf and 140 pcf for the upper soil layer and the basalt rock, respectively.

To develop a site-specific response, we assigned shear wave velocities to the three main materials being modeled (upper soils, clinker, and basalt rock) following Figure 12 by Wong et al. (2011), as shown in Figure 2-22 of this report.

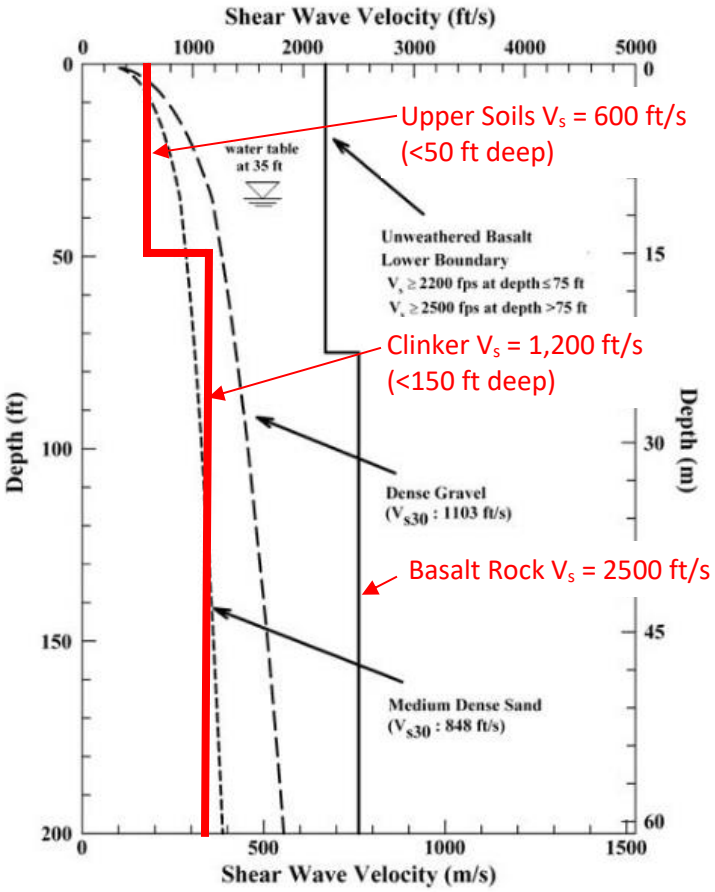

Figure 12. Template of V_S-depth relationships used to categorize geotechnical materials of the 22 sites.

Figure 2-22 – Recommended Shear Wave Velocities

2.3 Groundwater Properties

We compiled the summary of groundwater characteristics reported for groundwater monitoring wells RHMW01, RHMW02, and RHMW03, as shown in Table 2-1. These wells are located along the crest of the hill directly in line with the tanks with a bottom elevation at approximate elevation zero, well below the bottom of the tanks. As such, we expect that they will best represent water passing down past and interacting with the tanks. We also compiled the groundwater characteristics for well nearby well RHWM04, located upstream of the groundwater flow, for comparison.

Table 2-1 – Summary of Groundwater Testing (NAVFAC 2023)

Parameter	Wells RHMW01 – RHMW03 (average)	Well RHMW04
Chloride (ppm)	42.6	76.1
Sulfate (ppm)	16.9	10.4
Total Dissolved Solids (ppm)	355	291.4
pH	6.78	7.3
Dissolved Oxygen (mg/l)	0.97	8
Oxidation Reduction Potential (mV)	3.85	145

3. MATERIAL SPECIFICATIONS

Detailed material properties were not shown in the available drawings. Based on the time of construction (the underground storage tanks in the 1940s) and testing data described in Section 2.1.3, we assumed the following typical material types and properties in our assessment:

- Concrete Compressive Strength and Steel Grades:

    1. Concrete – Nominal compressive strength at twenty-eight days, fc'= 3,000 psi.
    2. Reinforcing steel – ASTM A15 Gr. 40 (minimum yield stress = 40 ksi).
    3. Steel liner – ASTM A36 (minimum yield stress = 36 ksi).

- Modulus of Elasticity:

    1. Reinforcing bars and steel, modulus of elasticity E_s = 29,000 ksi.
    2. For concrete with f_c'= 3,000 psi, per ACI 318, the modulus of elasticity is given by:

$$E_c = 57{,}000\sqrt{f_c'}$$

- Material Density:

    1. Reinforcing bars and steel: 490 lbs/ft^3.
    2. Reinforced concrete: 150 lbs/ft^3.

4. PERFORMANCE CRITERIA

We evaluated both the underground storage tanks and the internal access tower for the following two levels of earthquakes:

- Code defined Design Basis Earthquake (DBE).
- Conservative earthquake with 10,000-year mean recurrence interval (MRI).

The DBE is also referred to as the Design Earthquake (DE) in American Society of Civil Engineers (ASCE) Standard, ASCE 7-22, "Minimum Design Loads and Associated Criteria for Buildings and Other Structures." It is defined as two-thirds of the Maximum Considered Earthquake (MCE) associated with a 2,475-year MRI. Note that ASCE 7 defines a risk-targeted MCE, notated as MCE_R. Within this report, MCE and MCE_R are used interchangeably.

For the DBE, we considered both Risk Category II (with importance factor, $I_e = 1.0$) and Risk Category III (with $I_e = 1.25$). Risk categories are classifications within the building code that depend on the risk associated with the unacceptable performance of the structure. ASCE 7-22 Risk Categories are defined in Table 4-1. Note that Risk Category I (the lowest risk category) applies to buildings and other structures that represent a low risk to human life. Since the Red Hill tanks will be permanently closed in place and will not be occupied structures, Risk Category I can also apply.

Table 4-1 – Risk Category of Buildings and Other Structures for Floor, Wind, Tornado, Snow, Earthquake, and Ice Loads (ASCE 7-22)

Use or Occupancy of Buildings and Structures	Risk Category
Buildings and other structures that represent low risk to human life in the event of failure	I
All buildings and other structures except those listed in Risk Categories I, III, and IV	II
Buildings and other structures, the failure of which could pose a substantial risk to human life	III
Buildings and other structures not included in Risk Category IV, with potential to cause a substantial economic impact and/or mass disruption of day-to-day civilian life in the event of failure	
Buildings and other structures not included in Risk Category IV (including, but not limited to, facilities that manufacture, process, handle, store, use, or dispose of such substances as hazardous fuels, hazardous chemicals, hazardous waste, or explosives) containing toxic or explosive substances where the quantity of the material exceeds a threshold quantity established by the Authority Having Jurisdiction and is sufficient to pose a threat to the public if released*	
Buildings and other structures designated as Essential Facilities	IV
Buildings and other structures, the failure of which could pose a substantial hazard to the community	
Buildings and other structures (including, but not limited to, facilities that manufacture, process, handle, store, use, or dispose of such substances as hazardous fuels, hazardous chemicals, or hazardous waste) containing sufficient quantities of highly toxic substances where the quantity of the material exceeds a threshold quantity established by the Authority Having Jurisdiction and is sufficient to pose a threat to the public if released*	
Buildings and other structures required to maintain the functionality of other Risk Category IV structures	

*Buildings and other structures containing toxic, highly toxic, or explosive substances shall be eligible for classification to a lower risk category if it can be demonstrated to the satisfaction of the Authority Having Jurisdiction by a hazard assessment as described in Section 1.5.3 that a release of the substances is commensurate with the risk associated with that risk category.

4.1 Underground Storage Tanks

We performed a nonlinear FE stress analysis, as permitted in Section 6.9 of American Concrete Institute (ACI) Standard, ACI 318-19, "Building Code Requirements for Structural Concrete," to evaluate the tank's performance subjected to seismic loads. We used the seismic loading from our SSI analysis as input to our 3D nonlinear FE stress analysis model.

We used the FE analysis software package, ABAQUS, to perform the stress analysis. ABAQUS is a general-purpose, nonlinear FE analysis method software developed by Dassault Systems. ABAQUS is widely used to perform complex civil, structural, and mechanical systems analyses in critical applications, including the aerospace, nuclear, and petrochemical industries.

Performance criteria for the evaluation of the underground storage tanks are as follows:

- To preclude visible concrete cracking when the tank is subjected to DBE ground motion.
- To maintain structural integrity with localized concrete cracking permitted when the tank is subjected to a 10,000-year MRI earthquake.

According to American Water Works Association (AWWA) Standard, AWWA C304-14, "Design of Prestressed Concrete Cylinder Pipe," and other references, the onset of visible cracking of concrete occurs when the total tensile strain reaches about eleven times the tensile strain at the elastic limit in tension (which is an equivalent plastic strain in the tension of about ten times the tensile strain at the elastic limit), as shown Figure 4-1 (excerpted from Figure 2 of AWWA C304-14).

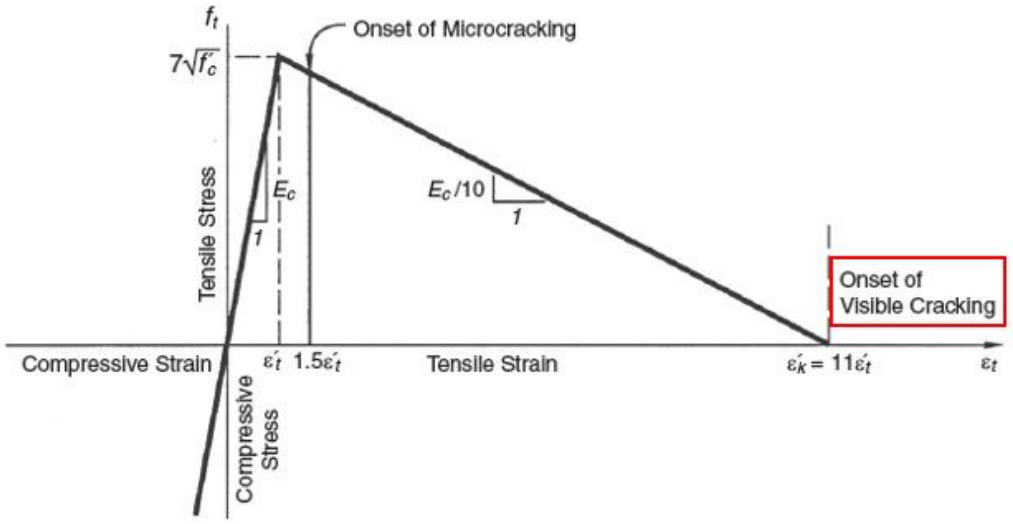

Figure 4-1 – Stress-strain Curve of Concrete in Tension Showing Onset of Visible Cracking (AWWA 2014)

For normal concrete with compressive strength of f'_c = 3,000 psi at twenty-eight days, the corresponding elastic modulus (E_c) and tensile strength ($f'_t = 7\sqrt{f'_c}$) are 3,122 ksi and 383 psi, respectively. This results in an elastic tensile strain limit (f'_t/E_c) of 0.00012. The onset of visible cracking of concrete would occur when the total tensile strain reaches about 0.00135 (eleven times elastic strain limit), equivalent to a plastic strain in the tension of about 0.0012 (ten times elastic strain limit). In our analysis, we conservatively used a concrete tensile strength of $f'_t = 6\sqrt{f'_c}$, resulting in a plastic strain in the tension of about 0.0010 at the onset of concrete visible cracking.

4.2 Tank Tower

For the tower, we targeted an acceptance criterion for the ASCE 7-22 DBE (for both Risk Category II and III) of an Immediate Occupancy (IO) limit state, i.e., no damage and ongoing use with no required repairs after the DBE. For the 10,000-year MRI event, we considered Collapse Prevention (CP) as the appropriate acceptance criterion. ASCE 7-22 defines Immediate Occupancy as the post-earthquake damage state in which a structure remains safe to be occupied and essentially retains its pre-earthquake strength and stiffness. ASCE 7-22 defines Collapse Prevention as the post-earthquake damage state in which a structure has damaged components and continues to support gravity loads but retains no margin against collapse. We

used a response modification coefficient (R) = 1.5 for both DBE assessments to achieve this criterion. The response modification coefficient represents the ratio of the forces that would develop under the specified ground motion if the structure had an entirely linear-elastic response to the prescribed design forces. While a larger R could have been used for the 10,000-year MRI event, we conservatively maintained an R = 1.5, given the importance of the tank tower for future access.

Our American Institute of Steel Construction (AISC) Specification, AISC 360-16, "Specification for Structural Steel Buildings" member strength checks for the tower are based on ASCE 7-22 load combinations with orthogonal horizontal inertial demands and vertical seismic effects in combination with gravity loads. We used a resistance factor of 1.0 for the CP limit state when determining the margin against collapse.

4.3 Response Spectra

We developed 5% damped elastic ground motion spectra for the Red Hill site for the MCE_R, DBE, and 10,000-year MRI motions. To determine the MCE_R and DBE spectra, we used the online ASCE 7 Seismic Hazards tool available at https://asce7hazardtool.online/. This tool, maintained by the American Society of Civil Engineers, references the national seismic hazard database maintained by the United States Geologic Survey and returns values of 5% damped spectral ordinates (coordinates of the multi-period response spectrum) at twenty periods ranging from 0 to 10 sec based on the input of site longitude, latitude, and site class, as defined in the *ASCE 7-22*. We determined the spectral ordinates for the 10,000 mean recurrence interval motion using a seismic hazard tool maintained by the United States Geologic Survey online at https://earthquake.usgs.gov/nshmp/.

For all spectra, we assumed site conditions associated with Site Class B (soft rock) since our site response analysis will propagate this ground motion from the bedrock to the surface.

4.3.1 DBE and MCE_R

Table 4-2 summarizes the input data we used to determine the DBE and MCE_R spectra.

Table 4-2 – Input Data for DBE and MCE_R Spectra

Parameter	Value
Latitude	21.3724
Longitude	-157.8959
Site Class	B
Risk Category	II

Figure 4-2 presents the DBE spectrum, and Figure 4-3 the MCE_R spectrum. Table 4-3 presents the spectral ordinates for both spectra at twenty periods. All spectral ordinates are for maximum direction, that is, RotD-100 motions, in accordance with ASCE 7-22.

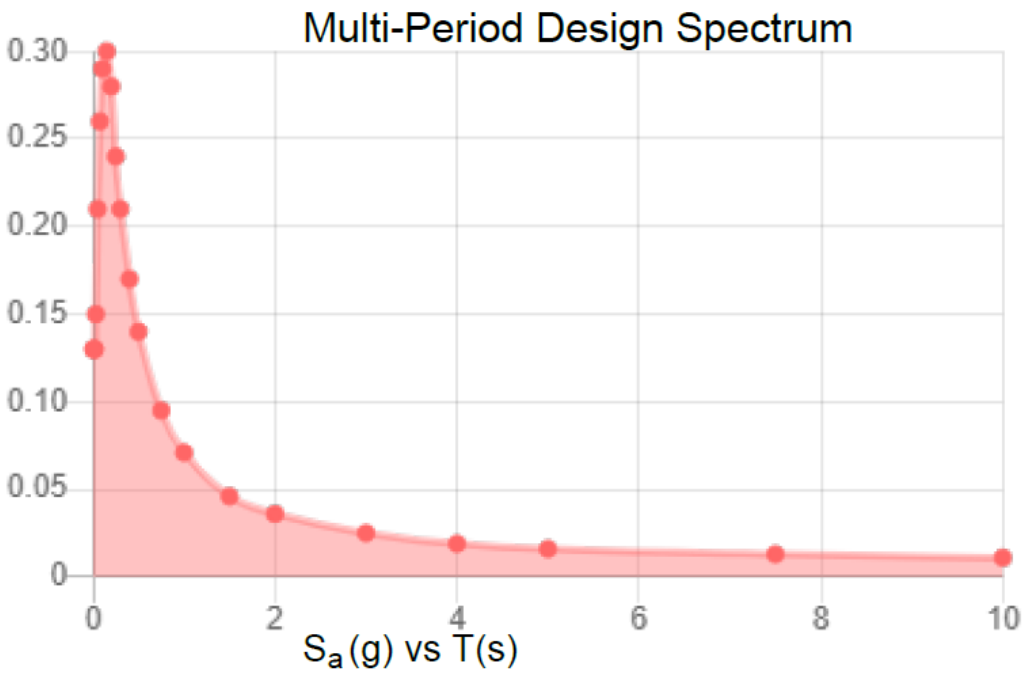

Figure 4-2 – DBE 5% Damped Elastic Response Spectrum

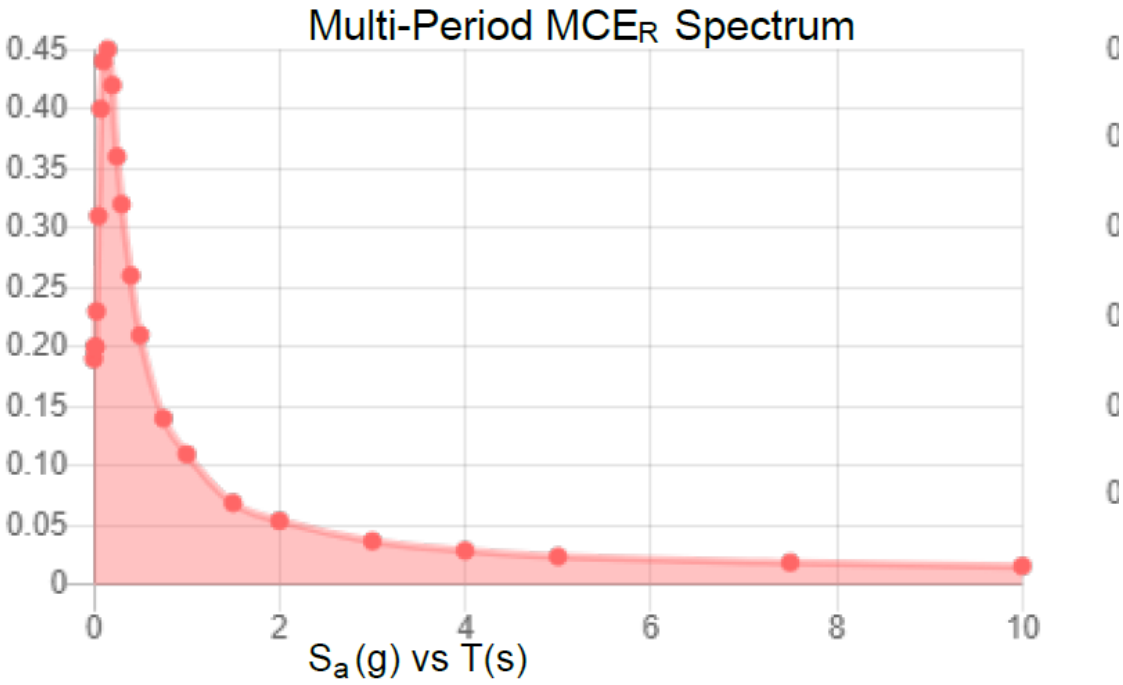

Figure 4-3 – MCE_R 5% Damped Elastic Response Spectrum

Table 4-3 – Spectral Ordinates for DBE and MCE_R Spectra – g

Period – sec	S_a(DBE) – g	S_a(MCE_R) – g
0	0.13	0.195
0.01	0.13	0.195
0.02	0.13	0.195
0.03	0.15	0.225
0.05	0.21	0.315
0.075	0.26	0.39
0.1	0.29	0.435
0.15	0.3	0.45
0.2	0.28	0.42
0.25	0.24	0.36
0.3	0.21	0.315
0.4	0.17	0.255
0.5	0.14	0.21
0.75	0.095	0.1425
1	0.071	0.1065
1.5	0.046	0.069
2	0.036	0.054
3	0.025	0.0375
4	0.019	0.0285
5	0.016	0.024

4.3.2 10,000-Year Spectrum

We computed the 5% damped spectral ordinates for the 10,000-year mean recurrence spectrum using the national seismic hazard tool maintained by the United States Geologic Survey. We used the 2021 National Seismic Hazard Model for Hawaii. The tool returned outputs for vibration periods of 0.01, 0.02, 0.03, 0.05, 0.075, 0.1,0.15, 0.2, 0.25, 0.3, 0.4, 0.5, 0.75, 1, 1.5, 2, 3, 4, 5, 7, and 10 sec. Figure 4-4 presents the hazard curves we obtained. The dark solid horizontal line on the plot represents the 10,000-year mean recurrence interval. The data points on each line indicate discrete periods for each hazard, at which it is possible to read spectral values. All spectral values are for the median, that is, RotD-50, motions.

In general, data points from which it is possible to read spectral values directly are unavailable at the mean recurrence interval of 10,000 years. Therefore, to obtain the 10,000-year values, we interpolated between the values at available data points with return periods immediately above and below the 10,000-year recurrence. We interpolated in $\ln(S_a)$ vs. $\ln(RP)$ space. We performed this interpolation at periods of 0, 0.02, 0.03, 0.05, and 0.075 sec, as we understand ground response would be most sensitive to short-period (high frequency) motion. Table 4-4 presents the spectral ordinates we obtained.

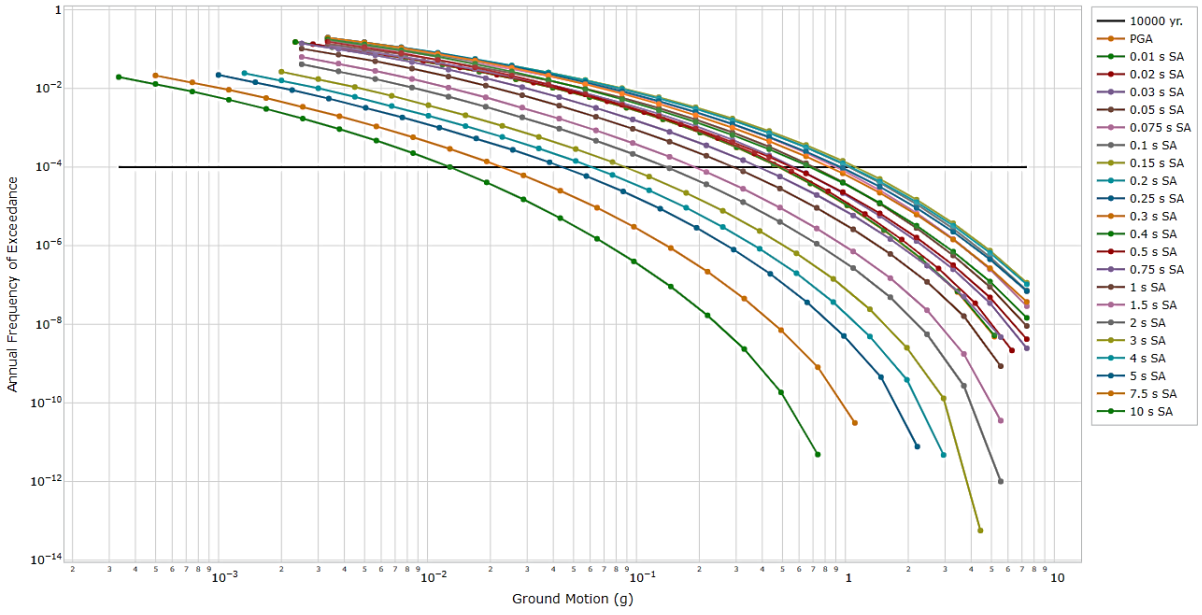

Figure 4-4 – Hazard Curves for Red Hill Site, Class B Conditions

Table 4-4 – 10,00 Year Mean Recurrence Interval, 5%-Damped, Spectral Ordinates

Period T – Seconds	$S_a(T)$ – g
0	0.424
0.01	0.429
0.02	0.460
0.03	0.532
0.05	0.758
0.075	0.858
0.1	0.954
0.15	0.954
0.2	0.865
0.25	0.752
0.3	0.667
0.4	0.667
0.46	0.532
0.5	0.442
0.51	0.437
0.75	0.320
1	0.324
1.5	0.165
2	0.126
3	0.082

5. UNDERGROUND TANK ANALYSIS

Under the seismic ground motion, the site soils and rock will shake, and that motion will be transmitted to the tank. Three analyses were performed to evaluate the structural integrity of the tank. Site response analyses were performed to evaluate the seismically induced ground motion displacements. Three-dimensional soil-structure interaction analyses were performed using the input displacements at the boundary to evaluate the local effects of the interaction of the tank with the surrounding soil and rock. Then, the pressures and displacements from the soil-structure interaction analyses were used to define the loads for a nonlinear structural response analysis to evaluate structural behavior.

5.1 Site Response Analyses

Site response analyses calculate the seismic ground motion as the seismic waves propagate through the soil. We performed one-dimensional site response analyses to calculate the maximum soil strains and displacement with the site soil identified in Section 2.2 and the earthquake motions presented in Section 4.3. The results of site response analysis are subsequently used in soil-structure interaction analysis (Section 5.2) as boundary displacement inputs.

5.1.1 Assumptions for Site Response Analysis

We made the following justified assumptions for the use of equivalent linear site response:

- The one-dimensional analysis assumes a horizontally layered site and neglects horizontal propagation and scattering of seismic waves and horizontal soil property variations.
- The analysis uses an iterative approach to achieve effective strain-compatible properties. We set the ratio of equivalent uniform strain to peak instantaneous strain of 0.65 in accordance with Kramer, Geotechnical Earthquake Engineering 1996. This iterative approach resolves to a user-defined tolerance of 0.5%, which we judge as appropriate given the other uncertainties in soil properties and other parameters.

There are several assumptions regarding the distribution and layering of rock and clinker due to the variable nature at the site. The methodology section below identifies the approach we used to address this uncertainty. We further made assumptions regarding the soil degradation and

upper soil layer properties, which were shown not to be major factors in the resulting soil strains. These items are further discussed below.

5.1.2 Methodology

Using the program Strata, we performed dynamic site response analysis on the representative soil columns for the previously designated input response spectra. We used Strata with random vibration theory (RVT) to generate a ground motion matching a target response spectrum. We additionally validated the use of RVT for this case by comparing multiple scaled time-history analyses to the RVT analysis at the 10,000-year event level. The subsequent sections identify inputs for this analysis.

Soil Types

Based on the as-built excavation logs, the clinker and rock are horizontally interspersed and interconnected throughout the site and over the structure's height, as shown in Figure 2-10, Figure 2-11, Figure 5-1, and Figure 5-2. The response is based on motion through layers that are part clinker and part rock and acting independently so that any layer of clinker can act independently. Therefore, instead of characterizing individual layers of these materials over the height of a representative soil column, we estimated the percentage of clinker and rock, and from that, we calculated the equivalent densities and stiffnesses. The upper soil layer above the tanks, which is much softer, is characterized separately. Due to uncertainties in the distribution of rock and clinker, we estimated that the profile consists of approximately 50% of each rock and clinker (50/50 case) as a lower stiffness estimate of the profile near the tanks. We also considered a profile of 75% rock and 25% clinker (75/25 case) as an upper stiffness estimate. These estimates are based on the excavation logs shown in Figure 5-1 and Figure 5-2 are selected to be representative of a soft and stiff profile, respectively. Rock is represented by solid white and clinker by dotted areas in these figures.

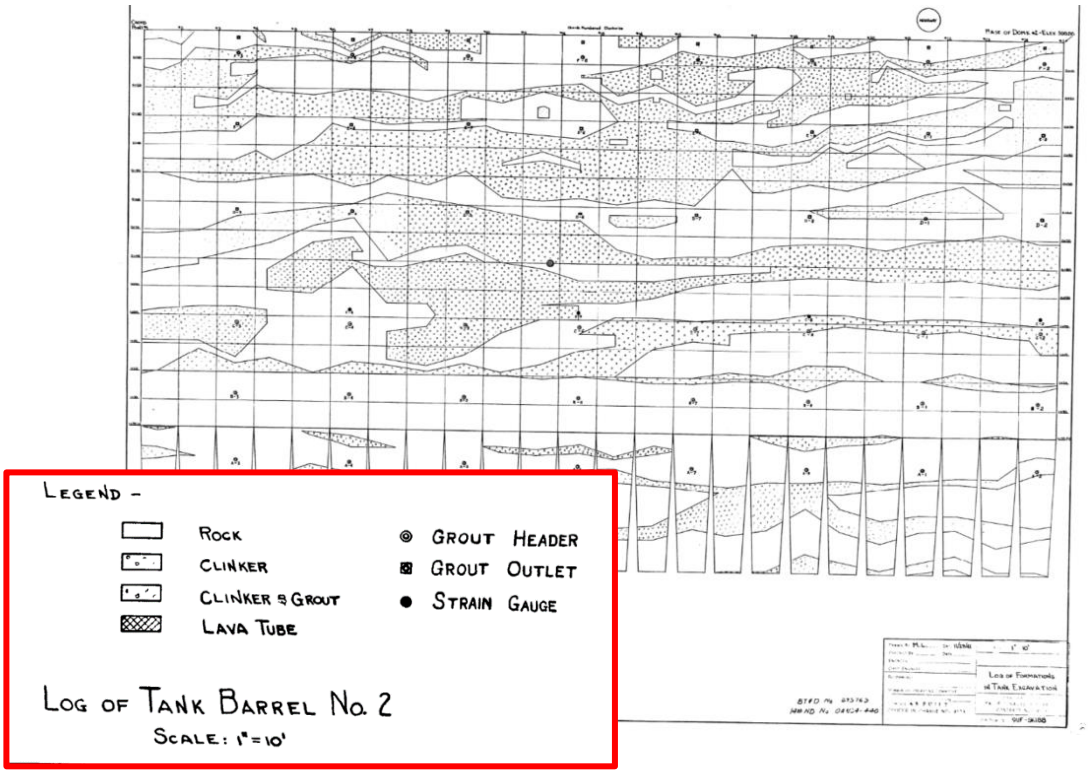

Figure 5-1 – As-Built Drawing, Underground Fuel Storage, Log of Formations in Tank Excavation – Tank 2

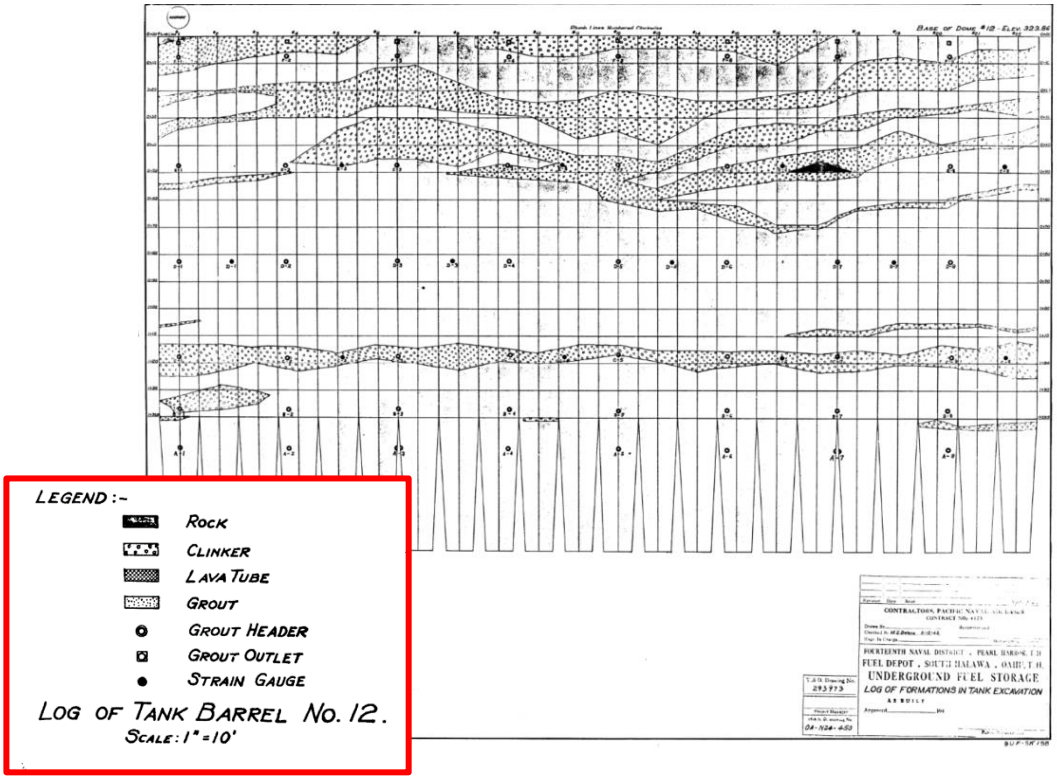

Figure 5-2 – As-Built Drawing, Underground Fuel Storage, Log of Formations in Tank Excavation – Tank 12

Based on the inputs from Section 2.2 (unit weights of 130 pcf and 140 pcf and shear wave velocities of 1,200 ft/s and 2,500 ft/s, respectively, for clinker and rock), we calculated equivalent properties using average shear stiffness and mass. This results in a shear wave velocity of 1,984 ft/s and a unit weight of 135 pcf for the 50/50 case and a shear wave velocity of 2,261 ft/s, and a unit weight of 138 pcf for the 75/25 case. We designated the upper soil layer a shear wave velocity of 600 ft/s and a unit weight of 120 pcf. Finally, the bedrock half-space is given a 140 pcf density (equivalent to the basalt rock layers) and a damping ratio of 1%. Since there was no data about the bedrock beneath these soil columns, we assumed a stiffer rock layer with a shear wave velocity of 5,000 ft/s, which is conservative when calculating the maximum strain above the bedrock.

In addition to elastic properties, we assigned a degradation curve to the upper soil and smeared clinker and basalt layers. A degradation curve is a set of functions that modifies the stiffness and damping of soil based on its maximum cyclic strain to provide equivalent dynamic properties for the linear numerical analysis. No site-specific degradation curves were available for the clinker, nor were we able to locate any degradation curves for material closely related to the clinker present at the site. Therefore, for this site, we selected the generic Eastern North America modulus reduction and damping curves from Electric Power Research Institute (EPRI) document TR-102293 “Guidelines for Determining Design Basis Ground Motions.” These curves were developed for a range of soils, from gravelly sand to low-plasticity clays at varying depths, and we selected these curves as reasonable for the clinker/rock mixture in this case. Evaluation of the entire site using an alternative higher degradation level (a degradation curve corresponding to a shallower depth) is presented as a sensitivity study. It demonstrates only small increases in relative displacement with increased degradation. Because rock behaves elastically at small strains, we assumed that rock remains elastic in this analysis.

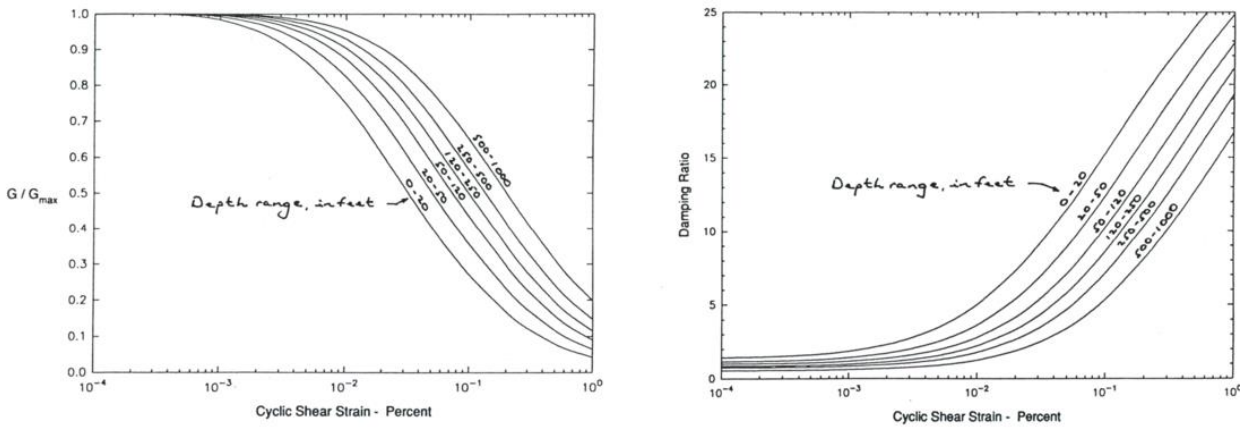

Figure 5-3 – Degradation Curves from Electric Power Research Institute, Guidelines for Determining Design Basis Ground Motions (EPRI TR-102293, 1993)

Soil Profile

Based on Figure 5-1, we assigned a representative soil column, Soil Column 1 (SC1), according to the following layering pattern (beginning at the surface):

- 50 ft of upper soil.
- 100 ft of smeared* rock/clinker (above the height of the tank).
- 240 ft of smeared* rock/clinker (along the height of the tank).
- 80 ft of rock (below the tank).

*In this context, smeared refers to the effective response as an averaging of stiffness and mass. This effectively takes into account the response of the region around the tank without modeling of the undulating rock and clinker local features.

We discretized this soil profile into 10-ft layers in the Strata model and assigned each layer the shear wave velocity corresponding to the soil type. Table 5-1 gives layer-by-layer detail for the 50/50 and 75/25 cases. Shaded cells indicate that they are layers consistent with the tank elevation.

Table 5-1 – Discretized Soil Profile

Depth	Layer Type	Vs., 50/50	Vs., 75/25	Depth	Layer Type	Vs., 50/50	Vs., 75/25
(ft)		(ft/s)	(ft/s)	(ft)		(ft/s)	(ft/s)
0	Soil	600.0	600.0	240	Smeared	1983.5	2261.2
10	Soil	600.0	600.0	250	Smeared	1983.5	2261.2
20	Soil	600.0	600.0	260	Smeared	1983.5	2261.2
30	Soil	600.0	600.0	270	Smeared	1983.5	2261.2
40	Soil	600.0	600.0	280	Smeared	1983.5	2261.2
50	Smeared	1983.5	2261.2	290	Smeared	1983.5	2261.2
60	Smeared	1983.5	2261.2	300	Smeared	1983.5	2261.2
70	Smeared	1983.5	2261.2	310	Smeared	1983.5	2261.2
80	Smeared	1983.5	2261.2	320	Smeared	1983.5	2261.2
90	Smeared	1983.5	2261.2	330	Smeared	1983.5	2261.2
100	Smeared	1983.5	2261.2	340	Smeared	1983.5	2261.2
110	Smeared	1983.5	2261.2	350	Smeared	1983.5	2261.2
120	Smeared	1983.5	2261.2	360	Smeared	1983.5	2261.2
130	Smeared	1983.5	2261.2	370	Smeared	1983.5	2261.2
140	Smeared	1983.5	2261.2	380	Smeared	1983.5	2261.2
150	Smeared	1983.5	2261.2	390	Rock	2500.0	2500.0
160	Smeared	1983.5	2261.2	400	Rock	2500.0	2500.0
170	Smeared	1983.5	2261.2	410	Rock	2500.0	2500.0
180	Smeared	1983.5	2261.2	420	Rock	2500.0	2500.0
190	Smeared	1983.5	2261.2	430	Rock	2500.0	2500.0
200	Smeared	1983.5	2261.2	440	Rock	2500.0	2500.0
210	Smeared	1983.5	2261.2	450	Rock	2500.0	2500.0
220	Smeared	1983.5	2261.2	460	Rock	2500.0	2500.0
230	Smeared	1983.5	2261.2	470	Bedrock	5000.0	5000.0

Motion

We analyzed the motions described in Section 4.3, considering a 5% damped outcrop motion. We selected the base of the soil column (80 ft below the bottom of the tank elevation, at a depth below the ground surface of 470 ft) as appropriate for the input of the ground motion.

5.1.3 Calculations

Post Processing

We calculated the displacement profiles of the site based on the maximum shear strain of each layer. Displacements relative to the base of the tank are provided in Table 5-2.

Table 5-2 – Relative Displacements to Tank Base

Depth	Relative Displacement, 50/50 Case			Relative Displacement, 75/25 Case		
	DE	MCE	10,000-yr	DE	MCE	10,000-yr
(ft)	(in.)	(in.)	(in.)	(in.)	(in.)	(in.)
140	0.28	0.35	1.05	0.21	0.27	0.79
150	0.27	0.34	1.01	0.20	0.26	0.76
160	0.26	0.32	0.97	0.20	0.25	0.73
170	0.24	0.31	0.92	0.19	0.24	0.70
180	0.23	0.29	0.88	0.18	0.22	0.66
190	0.22	0.28	0.83	0.17	0.21	0.63
200	0.21	0.26	0.78	0.16	0.20	0.59
210	0.19	0.24	0.73	0.15	0.19	0.56
220	0.18	0.23	0.68	0.14	0.17	0.52
230	0.17	0.21	0.63	0.13	0.16	0.48
240	0.15	0.19	0.58	0.12	0.15	0.44
250	0.14	0.17	0.52	0.11	0.13	0.40
260	0.12	0.15	0.47	0.09	0.12	0.35
270	0.11	0.14	0.41	0.08	0.10	0.31
280	0.09	0.12	0.36	0.07	0.09	0.27
290	0.08	0.10	0.30	0.06	0.08	0.23
300	0.06	0.08	0.24	0.05	0.06	0.18
310	0.05	0.06	0.18	0.04	0.05	0.14
320	0.03	0.04	0.12	0.02	0.03	0.09
330	0.02	0.02	0.06	0.01	0.02	0.05
340	0.00	0.00	0.00	0.00	0.00	0.00

Validation of Response Spectra

We compared the surface acceleration response spectra from the 50/50 case under DBE motion to the ASCE 7-22 Site Class D DBE response spectrum, with Site Class D chosen as a comparison because it most closely matches the actual site conditions at the surface. Both spectra show peak spectral acceleration of approximately 0.55g, which indicates that the site response analysis is not overdriving the soil column for the given site conditions.

Validation of Random Vibration Theory (RVT)

We performed two separate validation checks to check that RVT has produced reasonable results for this analysis. First, we compared the target input response spectra with the calculated response spectra from the Strata program. Second, we compared the output

response spectrum for the 10,000-year event with a scaled set of ten time-history motions. Both checks demonstrated good performance of RVT for this profile.

5.1.4 Sensitivity Studies

We performed two sensitivity studies to assess the sensitivity of the results to different assumptions made for our main analysis. All sensitivity cases were performed on the 50/50 soil case. We found that the site response is slightly sensitive to variations in degradation and upper soil layer stiffness. We expect our selected values for these factors to be conservative for generating maximum strains at tank elevations. Comparisons for each study are presented for the bounding input motions (DBE and 10,000-year MRI.)

Reduced Upper Soil Layer Stiffness

We reduced the shear wave velocity of the upper soil layer from 600 ft/s to 450 ft/s. The analysis results from this case (Figure 5-4) had slightly decreased relative displacement at tank elevations compared to the stiffer soil. Therefore, the assumed 600 ft/s soil shear wave velocity is accepted as reasonable and more conservative.

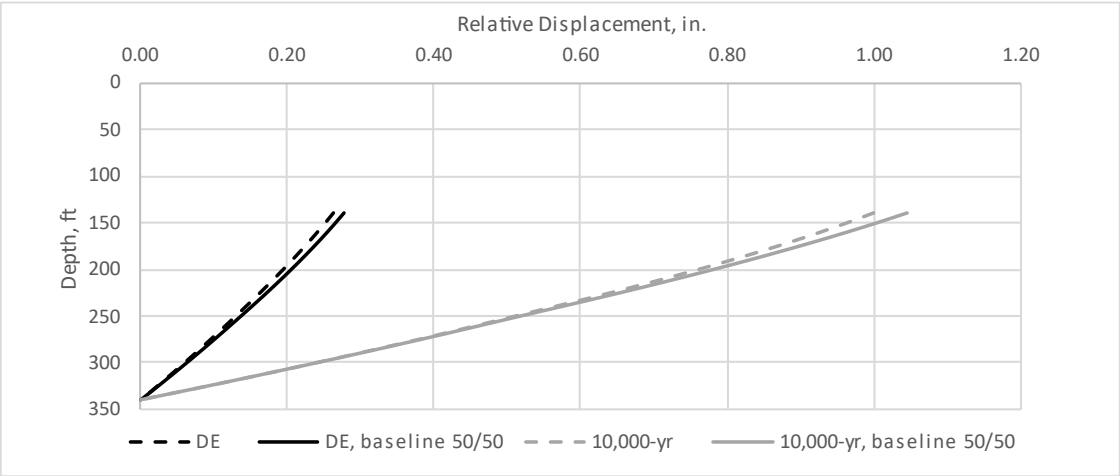

Figure 5-4 – Comparison of Relative Displacements for Reduced Upper Soil Layer Stiffness

Increased Degradation

Because we assumed a degradation curve for soils that have different characteristics than the smeared rock/clinker, we calculated results with increased degradation of the smeared rock/clinker layers (Figure 5-5). To perform this, we used degradation curves for soils at depths of 50 – 120 ft instead of those corresponding to actual layer depth. This resulted in a maximum increase in degradation of approximately 10% at maximum effective strain for the 10,000-year event. We observed slight to moderate increases in relative displacement for design earthquakes, of 2.6% for DBE and 3.2% for MCE to 11.7% for the 10,000-year case. This demonstrates that this analysis is somewhat sensitive to the degradation curves, especially at higher strains. However, at this level of analysis, we believe this difference is reasonable given the uncertainty of the site conditions.

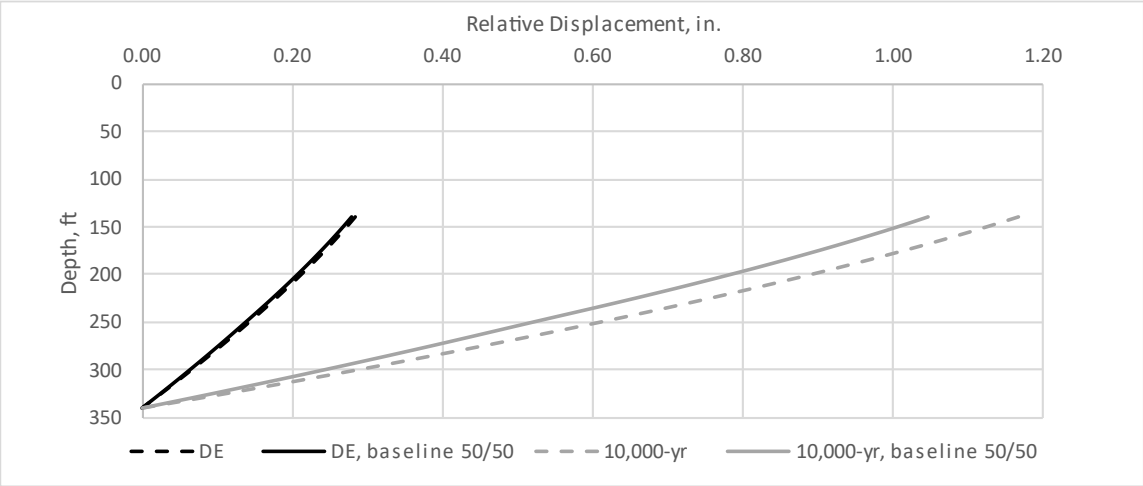

Figure 5-5 – Comparison of Relative Displacements for Increased Degradation

5.1.5 Results and Discussion

Strain/Displacement Outputs

As shown below in Figure 5-6, the strain profiles for both stiffness cases are qualitatively similar within the tank region. Over the depth of the tanks, strain tends to increase with depth in the smeared clinker/rock layer and then sharply decrease in the rock layer, which matches the expected behavior at such a stiffness boundary. The 50/50 case is less stiff and thus allows

higher strains and displacements over the height of the tank. However, both sets of results are used for soil-structure interaction, as stiffer soil may result in higher soil pressures.

Displacements relative to the bottom of the tank wall are shown in Figure 5-7 for the DBE and 10,000-year motions (with MCE results not included for clarity).

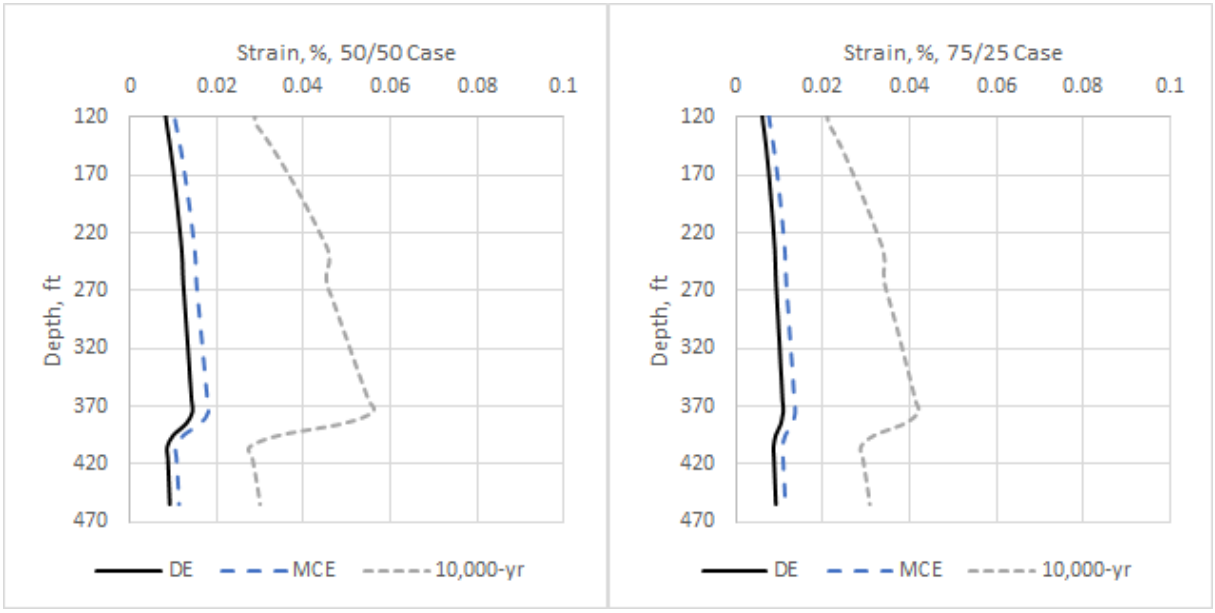

Figure 5-6 – Strain Profiles, 50/50 and 75/25 Cases

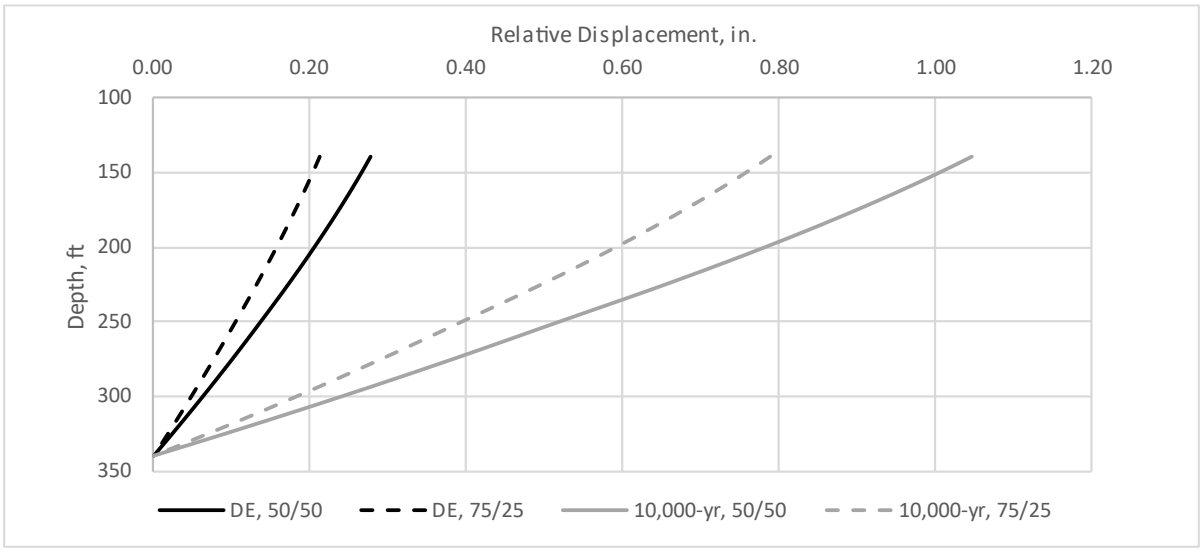

Figure 5-7 – Displacements Relative to Base of Tank

5.2 Soil-Structure Interaction Analysis

Following the 1D site response analysis, we developed a FE model to analyze the soil-structure interaction between the tank and the surrounding clinker/rock. The objective of the analysis was to obtain the soil pressure distribution on the exterior of the tank barrel under an equivalent seismic load in the form of imposed displacements from the 1D site response analysis. We could then apply the resulting soil pressure distribution on the tank in a separate FE analysis which incorporates more accurate nonlinear behavior of the tank structure through the inclusion of embedded reinforcing bar elements and concrete damage plasticity.

We estimated the stiffness of the tank through the use of a simplified 3D FE model that captures the general tank shape and the distribution of the surrounding soils. We checked the displacements due to two of the 1D site response analysis cases 1) smeared layer with 50% rock/50% clinker properties and 2) smeared layer with 75% rock/25% clinker. The development of the 3D model and the results of the analysis are summarized in the following sections.

5.2.1 Model Description

We modeled a 600-ft by 600-ft soil body centered on the tank along the full depth of the soil column analyzed in the 1D site response. We used the same soil stratigraphy in our model as soil column SC1 in the 1D site response analysis, which consists of upper soil for the first 50 ft, followed by 290 ft of smeared rock/clinker, and 80 ft of rock at the bottom. The upper soil layer and bottom rock layer were modeled using linear elastic properties, while the intermediate layer was modeled using a nonlinear Mohr-Coulomb model, except for within 50 ft of the model boundaries where a linear elastic material model was used. The soil stiffness of the upper soil layer is consistent with the same shear modulus in the 1D site response analysis. For the bottom rock layer, we increased the stiffness to a value representative of the concrete material which embeds the bottom dome of the tank. This assumption is conservative as stiffer material results in higher forces transferred to the tank. The stiffness of the intermediate layer is dependent on the seismic displacement applied. For Case 1 (50% rock/50% clinker), the shear modulus matches the 50% rock/50% clinker modulus from the 1D site response analysis. For

Case 2 (75% rock/25% clinker), the shear modulus is conservatively modeled as equivalent to the rock modulus from the 1D site response analysis. Figure 5-8 shows a cross-section through the center of the model, with a planar slice to show the soil stratigraphy.

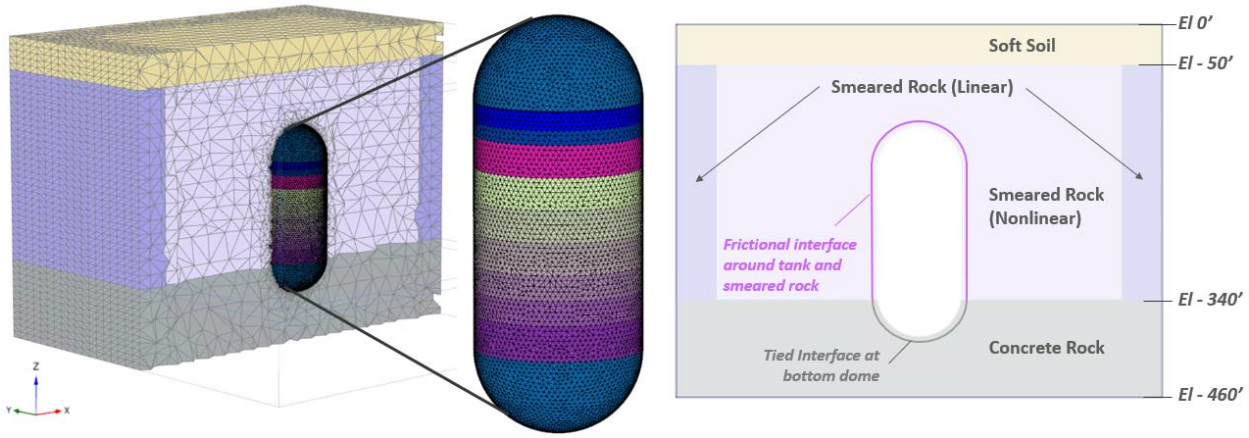

Figure 5-8 – Finite Element Model Mesh and Soil Stratigraphy

We prescribed a displacement profile at the side boundaries obtained from the 1D site response output to simulate a seismic event (Figure 5-9). It is worth noting that the displacement profile was inverted such that the base of the model was fixed, and relative displacements were applied along the height of the soil column. The side boundaries orthogonal to the earthquake direction were normally fixed, while the top of the intermediate smeared rock/clinker layer and the base of the model were vertically fixed. It is prudent to restrain the vertical motion at the top of the smeared rocker/clinker layer to force the seismic soil load through the full length of the soil body. Displacement from both the design earthquake and the 10,000-year earthquake was considered, but only results from the 10,000-year earthquake are presented, as the design earthquake soil pressures are very low in comparison.

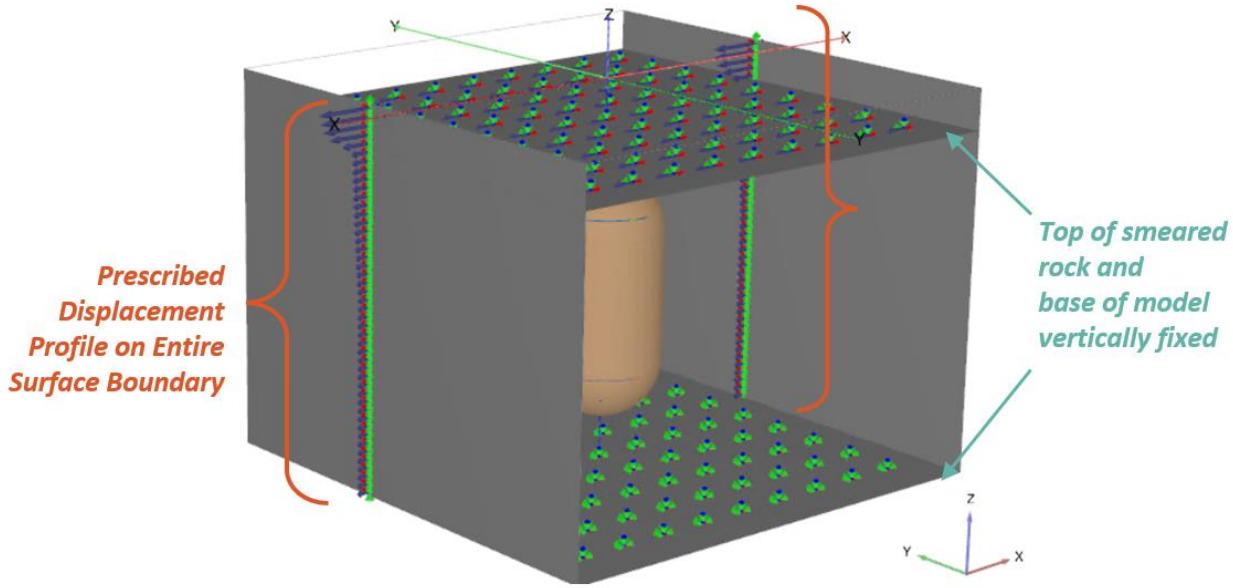

Figure 5-9 – Boundary Conditions on Soil-Structure Interaction Analysis

The tank was modeled using plate elements with linear elastic properties corresponding to a higher concrete strength to provide a slightly stiffer tank, which results in higher pressures on the tank wall. Consideration of stronger and stiffer concrete for this analysis is therefore conservative for demand generation and accounts for the fact that concrete is typically delivered at higher than the design minimum to avoid rejection and continues to gain strength over time. We simplified the tank geometry to ignore local protrusions at the top and bottom of the tank barrel by considering the wall to be vertical between the upper and lower domes. The tank barrel was discretized into different sections with increasing thicknesses along the depth of the barrel to account for the tapered wall section. We accounted for the presence of gunite in the shell element thickness, as a stiffer cross section will attract more load and result in more conservative soil pressures. We also included interface elements around the tank which incorporate frictional behavior with the surrounding smeared rock/clinker based on reduced soil strength. The lower tank dome is embedded in the bottom rock layer with a tied interface.

Based on the analyses conducted in the 1D site response, we analyzed the following two cases, with the latter producing higher soil pressures on the tank.

1. Seismic displacements from 1D site response with 50% rock/50% clinker and the same smeared material properties for the intermediate 240 ft layer.

2. Seismic displacements from 1D site response with 75% rock/25% clinker and 100% rock material properties for the intermediate 240 ft layer for conservatism.

A summary of the soil material inputs is shown in Table 5-3.

Table 5-3 – Soil Properties for Controlling Analysis Case

Property	Upper Soil Layer	Smeared Rock/Clinker	Rock
Depth	0 ft – 50 ft	50 ft – 390 ft	390 ft – 470 ft
Soil Model	Linear Elastic	Mohr-Coulomb, except within 50 ft of model boundary	Linear Elastic
Density (pcf)	120	135	140
Shear Wave Velocity, V_s (ft/s)	600	2500	-
Elastic Modulus[a], E (ksi)	24	453[b]	4415[e]
Poisson Ratio, ν	0.3	0.2	0.2
Cohesion (psi)	-	1 [c]	-
Friction Angle (°)	-	33	-

a. Calculated directly from shear wave velocity used in 1D site response analysis.
b. Rock stiffness instead of a smeared rock/clinker stiffness for conservatism.
c. Small cohesion value needed for numerical stability.
d. Assumed standard friction angle for granular material.
e. Concrete stiffness for embedded rock material around the lower dome of the tank.

5.2.2 Tank Displacements

Table 5-4 summarizes relative displacements for our analysis cases and shows that for the 10,000-year seismic event considering displacements for 75%/25% smeared rock/clinker, the tank moves 0.79 in. laterally relative to its base, which is identical to the movement from the 1D response. When the 50%/50% material is considered, our 3D analysis shows an additional 0.1 in. of lateral displacement occurs compared to the movement from the 1D response. This result is expected as the 50%/50% smeared rock/clinker has less stiffness and provides less passive soil resistance on the backside of the tank. The displaced shape of the tank from the 3D soil-structure interaction analysis provides an essential benchmark for the subsequent nonlinear pushover analyses discussed in Section 5.3.

Table 5-4 – Summary of Relative Tank Displacements

Seismic Motion	Relative Displacement at Top of Tank Barrel Relative to Bottom Dome (in.)			
	50%/50% Rock/Clinker		75%/25% Rock/Clinker	
	1D (Strata)	3D (PLAXIS)	1D (Strata)	3D (PLAXIS)
DBE	0.28	0.31	0.21	0.24
1.25DBE	0.35	--	0.27	--
10,000-year	1.05	1.15	0.79	0.79

Figure 5-10 below shows a magnified deformed shape of a section cut of the soil mesh across the center parallel to the seismic loading direction, along with lateral displacement contours of the tank. The displaced shape and contour plots indicate a combination of rigid body rotation and global bending deformation along the tank height.

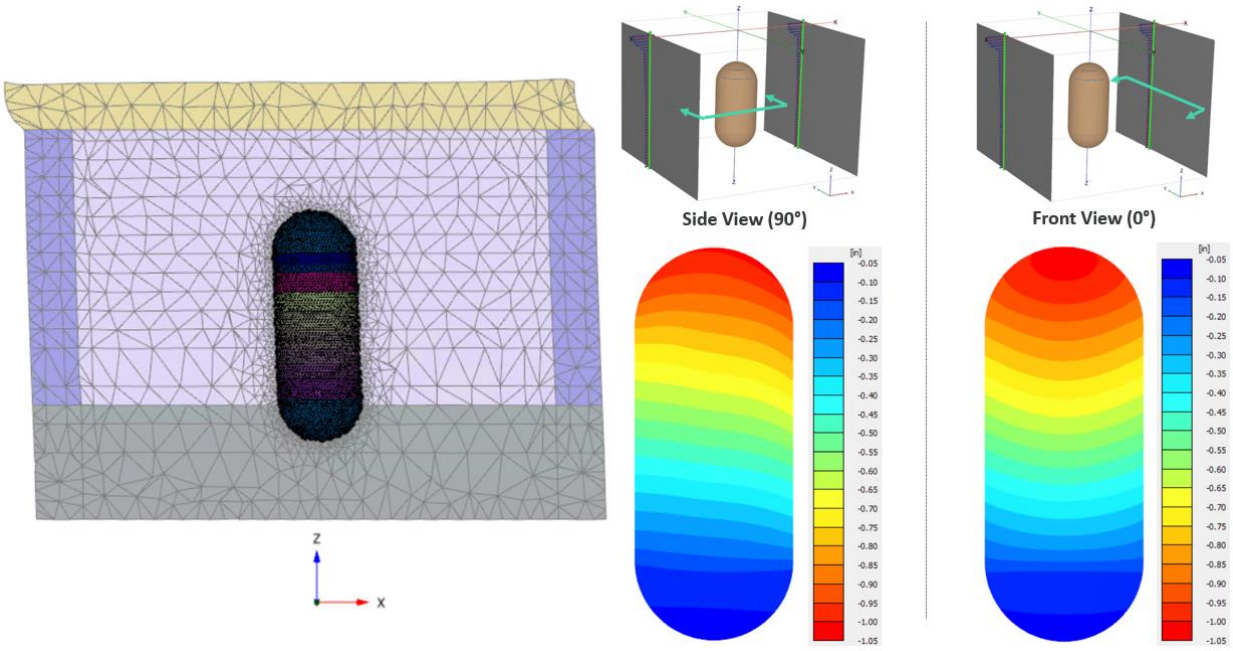

Figure 5-10 – Deformed Shape of Center Section (scaled 100x) and Lateral Displacement Contour Plots of the Tank

5.2.3 Interface Pressures

Figure 5-11 shows the soil pressures acting on the front and back of the tank for the 10,000-year seismic event, using displacements from the 75%/25% smeared rock/clinker case and 100% rock properties. Although the tank displacements are smaller compared to the

50%/50% smeared rock/clinker case, the stiffer soil surrounding the tank transfers more force onto the tank resulting in higher and more conservative soil stresses.

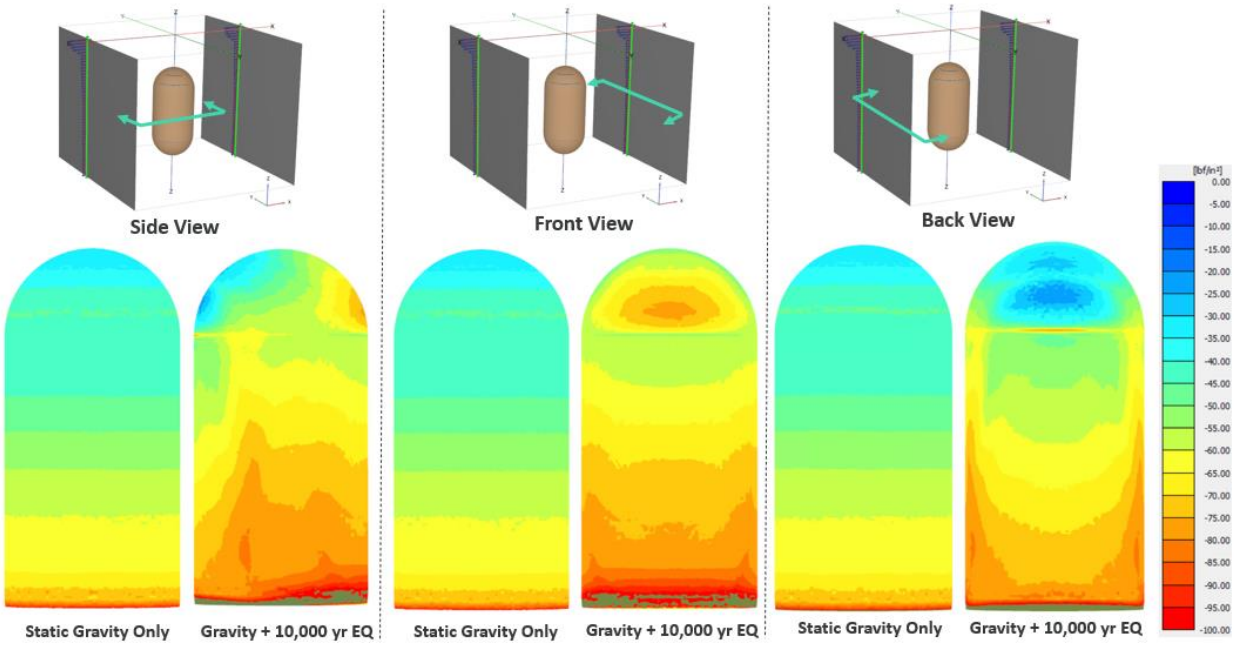

Figure 5-11 – Soil Pressure Around Tank

We understand that due to the self-supporting nature of the rock/clinker during construction, no static soil pressures were expected to develop in the tank's existing condition. Therefore, we subtracted out the static soil pressures in the gravity initialization phase of the analysis to obtain soil stresses due to earthquakes only. We extracted the soil stresses by performing five radial section cuts along the perimeter to get representative pressures around the entire circumference. Figure 5-12 shows an elevation plot of the soil pressures around the front and back of the tank, where 0° corresponds to the direction in line with the imposed seismic displacements and 90° corresponds to the direction perpendicular to the seismic direction. We observe that at 0°, the soil pressures are higher on the front of the tank, and the pressures decrease with depth since the imposed seismic displacement is higher at the top of the barrel. The soil pressures increase sharply near the bottom of the tank barrel due to the effect of embedding the lower dome in the significantly stiffer concrete/rock material. Near the perpendicular direction at 67.5° and 90°, soil pressures are higher due to the local ovalization of the cylindrical tank causing the sides to bulge out and push against the soil.

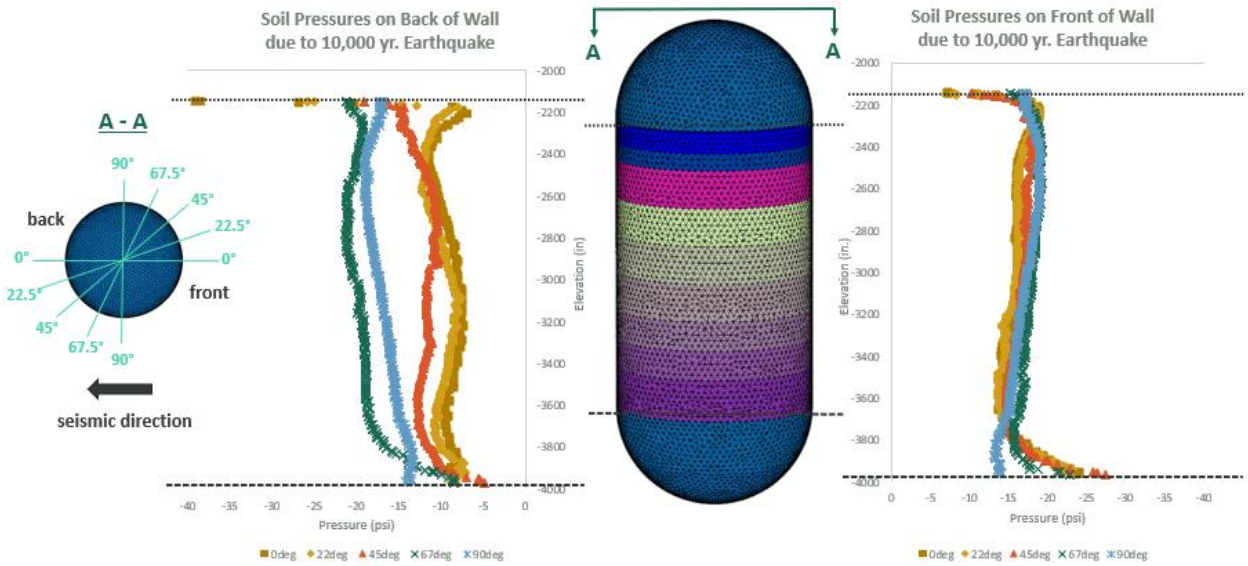

Figure 5-12 – Soil Pressure Profile at Front and Back of Tank

5.3 3D Nonlinear Structural Response Analysis

Following our SSI analyses, we developed a FE model of a typical tank in ABAQUS and conducted a nonlinear stress analysis using the seismic soil pressures estimated from our SSI analysis. The objective of this analysis is to assess the structural response of the tank due to a design basis earthquake considering Risk Categories II and III and a 10,000-year event.

5.3.1 Finite Element Model

In this FE model, we simulated a typical underground tank. Figure 5-13 shows our FE model. We modeled the concrete wall with varying thicknesses (4 ft at the base of the barrel section and 2.5 ft at the top of the barrel section) and the vertical and hoop reinforcement (both 1 in. diameter bars at 12 in. center-to-center spacing) near the interior face of the barrel section. We also modeled additional vertical and hoop reinforcement near the exterior face at the barrel-bottom dome interface. We developed the models, including the 1/4 in. thick steel liner plate, to represent the as-designed condition.

We also developed the models excluding the 1/4 in. thick steel liner plate to represent a severely corroded liner plate, an unlikely condition but a conservative assumption. Figure 5-14 shows typical reinforcement in the barrel section.

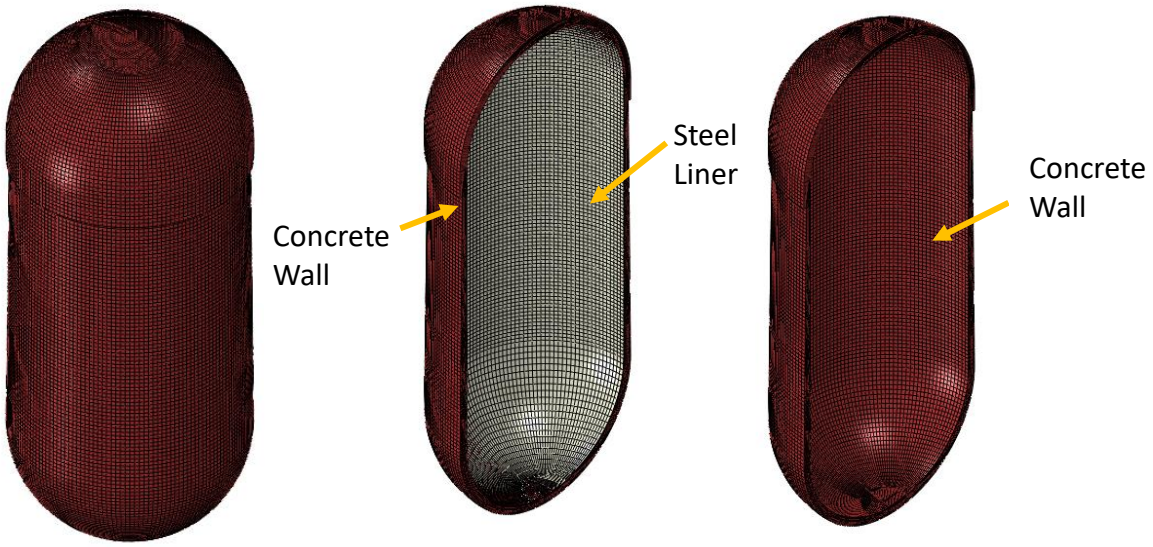

Figure 5-13 – Global FE Model of a Typical Underground Tank

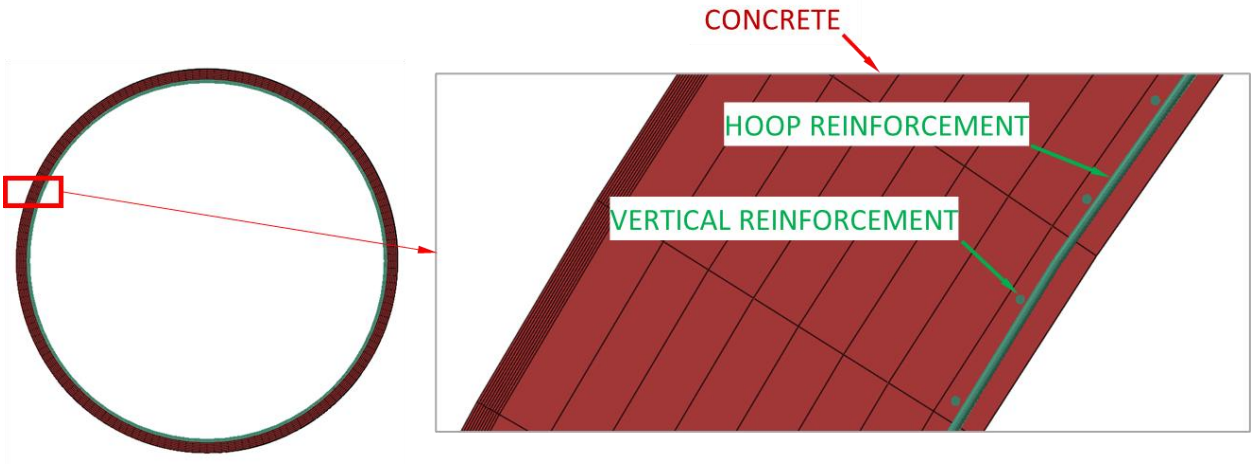

Figure 5-14 – Typical Reinforcement in Barrel Section of Tank (Partial Plan)

We modeled the concrete walls using solid elements. We modeled the liner plate using shell elements. We modeled the steel reinforcement using beam elements. We embedded the liner plate and reinforcement in concrete. Since the drawings did not indicate a concrete

compressive strength, we used a characteristic concrete compressive strength of 3,000 psi. We used a yield strength of 36 ksi for the liner plate and 40 ksi for reinforcement. These material properties fall within the suggested minimum ranges of the material properties to use based on the time of construction of the facility per ASCE 41-17 “Seismic Evaluation and Retrofit of Existing Buildings.” We used nonlinear material properties for both steel (bilinear relationship, Figure 5-15 and Figure 5-16) and concrete (damaged plasticity model) in our FE model. The damaged plasticity model was initially developed by Lubliner et al. (Lubliner, 1989) with modifications proposed by Lee and Fenves (Lee, 1998) to account for the different behavior in tension and compression. This model is a continuum, plasticity-based damage model. We simplified the stress-strain curve in tension to a triangular shape. Concrete stress-strain curves used in our material model are shown in Figure 5-17 and Figure 5-18.

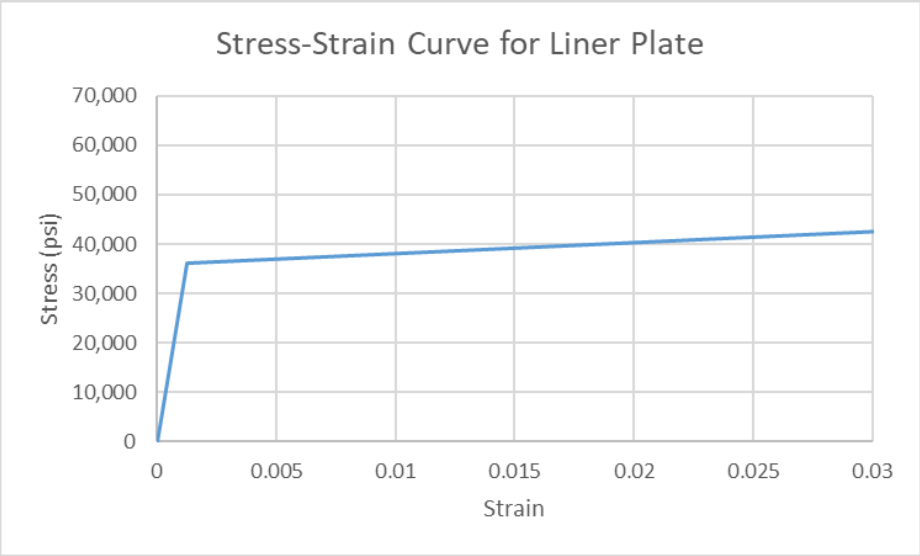

Figure 5-15 – Liner Plate Stress-Strain Curve

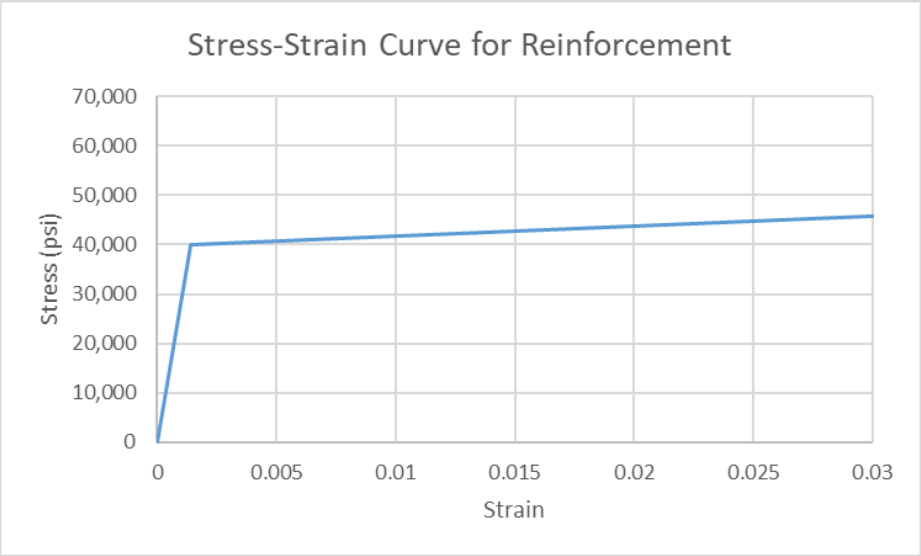

Figure 5-16 – Reinforcement Stress-Strain Curve

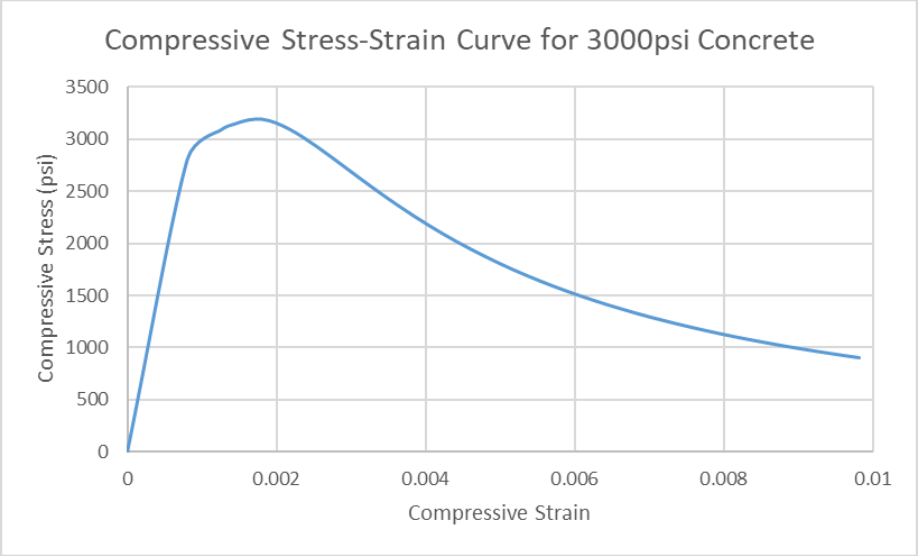

Figure 5-17 – Concrete Stress-Strain Curve in Compression

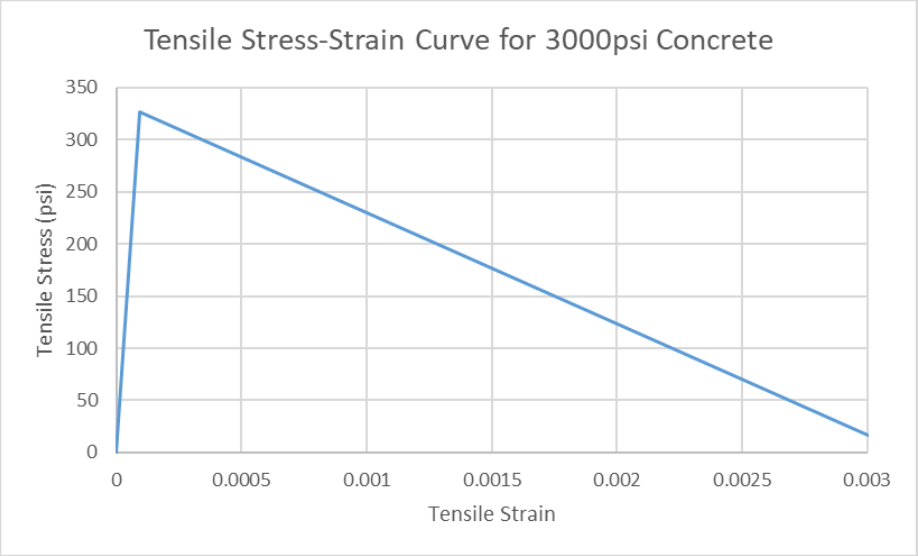

Figure 5-18 – Concrete Stress-Strain Curve in Tension

Boundary Conditions

We used pinned boundary conditions for the nodes at the exterior of the bottom dome to represent the bottom dome encased in mass concrete and at the bottom 20 ft of the barrel section to represent the resistance provided by the sound rock layer, as shown in Figure 5-19. Note that these boundary conditions are representative of the strata around tanks based on our review of the log of formations of all the underground tanks.

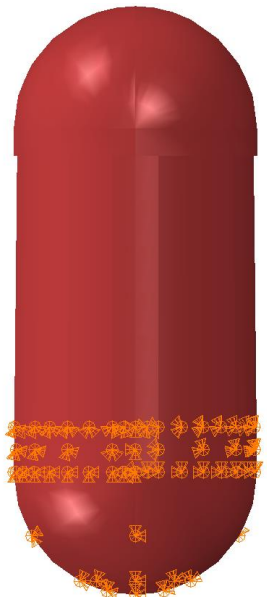

Figure 5-19 – Boundary Conditions in the Model, Tank Elevation

Application of Loads

We used the soil pressures predicted from our SSI analysis. As described in Section 5.2, the SSI analysis predicts the normal pressures and tangential and vertical shear pressures at the periphery of the tank caused by the strata around the tank due to a design basis earthquake considering Risk Categories II and III and a 10,000-year event. We used the soil pressures for the case of 75% rock/25% clinker strata around the tank, which is a representative case for most of the tanks at Red Hill. For a few of the tanks, 50% rock/50% clinker strata consideration is deemed more appropriate. Since the 75% rock/25% clinker strata model represents a conservative case yielding in higher soil pressures compared to 50% rock/50% clinker strata models, we used soil pressures calculated based on 75% rock/25% clinker strata in our response analysis.

We first applied gravity loads, which include the self-weight of the tank and the weight of a 1 ft thick gunite (assumed gunite thickness to consider the weight of the gunite applied at clinker layers) distributed uniformly along tank height. We then applied the normal soil pressures and tangential shear pressures with the magnitude and direction estimated from our SSI analysis. Figure 5-20 shows the distribution of soil pressures along the height of the tank at 0°, 22°, 45°, 67°, and 90° from SSI analysis. Negative normal pressures indicate an inward direction (towards the tank shell). The tangential shear stresses are positive in a counterclockwise direction about a vertical axis. Figure 5-21 shows the qualitative representation of the application of normal and tangential shear pressures. Note the tangential shear pressures are zero at 0° in Figure 5-20. We also applied representative vertical shear pressures in our model.

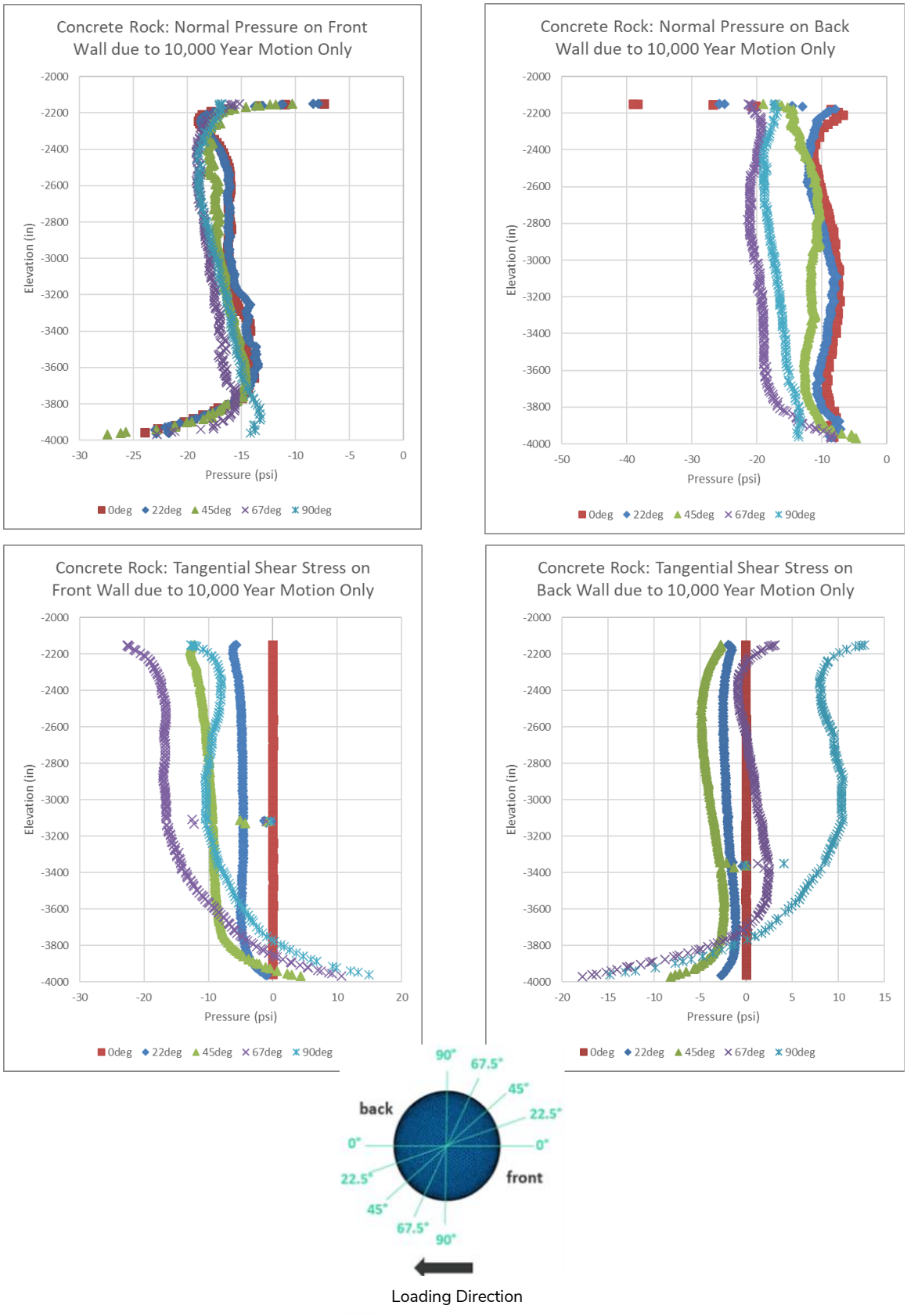

Figure 5-20 – Normal and Tangential Soil Pressure Distribution from SSI Analysis

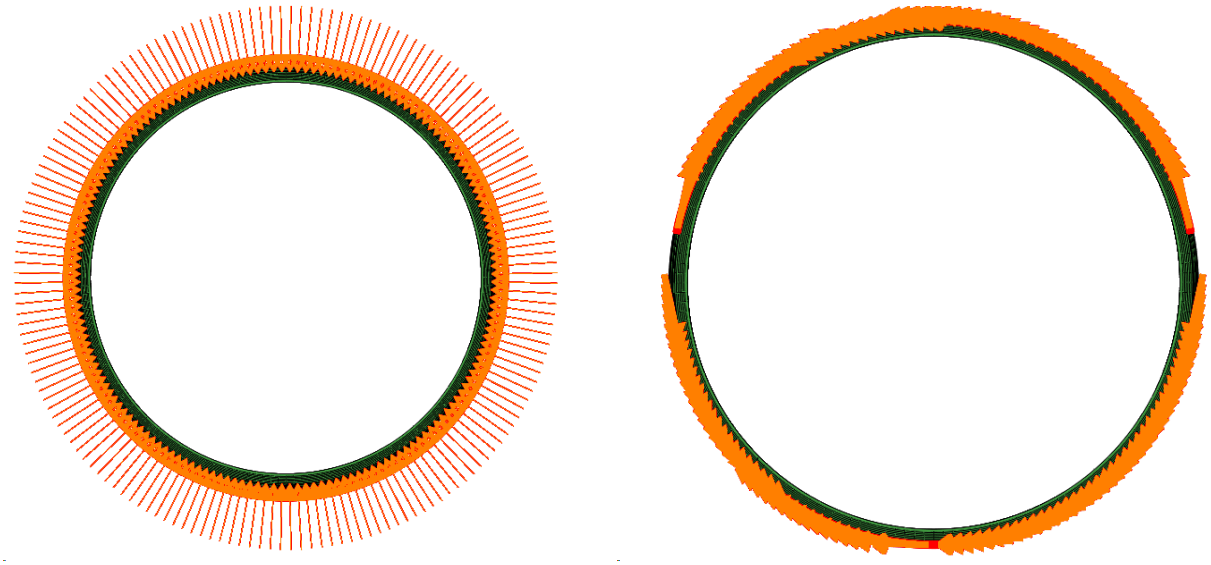

Figure 5-21 – Seismic Soil Pressure Application – Normal Pressure (Left) and Tangential Pressure (Right)

5.3.2 Analysis Results for Tank Without Steel Liner

The analysis results presented in this section are based on the analysis model without considering the steel liner, as this case resulted in a higher response compared to the case with the liner.

Figure 5-22 shows the load vs. displacement response of the tank subjected to seismic soil pressures for 75% rock/25% clinker strata. The displacement demands a design basis earthquake considering Risk Categories II and III, and a 10,000-year event from SSI analysis are shown in the graph. The response is linear for the DBE with both Risk Category II and III demands. The response is in the nonlinear range for the 10,000-year event demand.

Figure 5-23 shows the deflected shape of the tank for DBE Risk Category II demand, where the displacement demand is 0.24 in. at the top of the tank. The tank deflects from right to left in the direction of the seismic loading. Figure 5-24 shows the equivalent plastic tensile strains in concrete for a DBE Risk Category II demand. The maximum strains are located near the base of the barrel and are on the order of 0.0001.

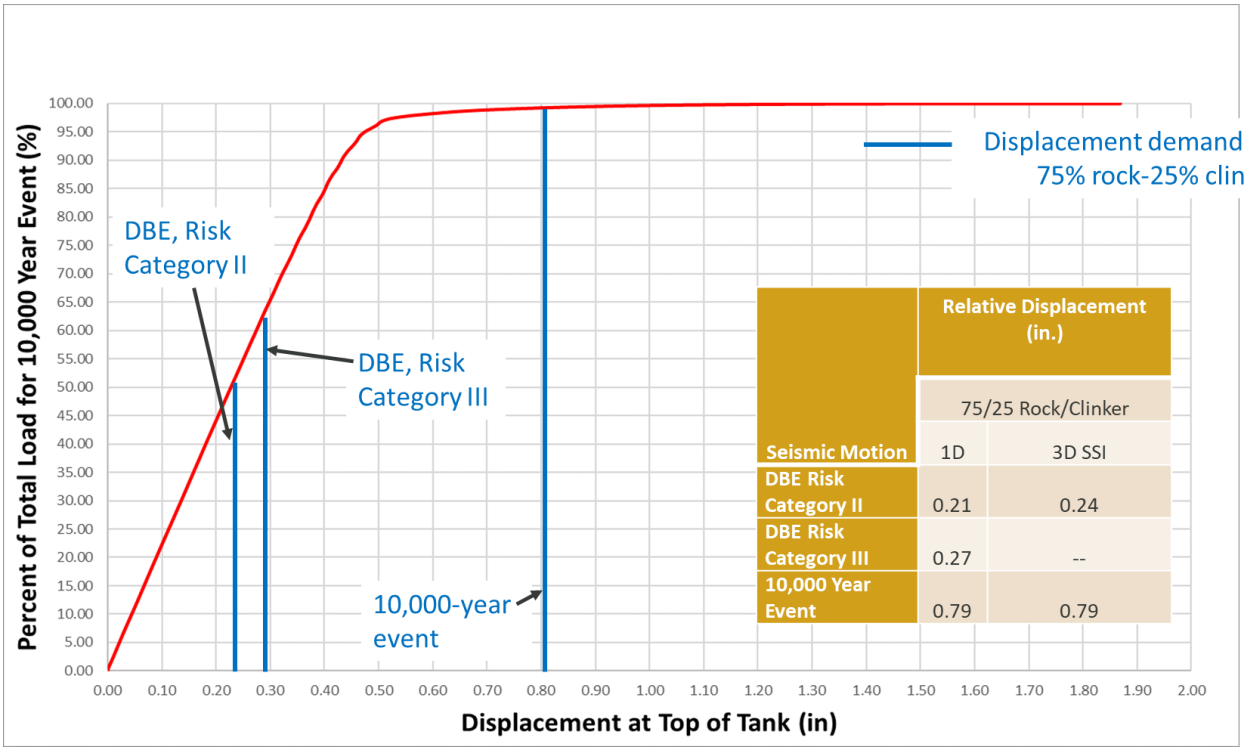

Figure 5-22 – Load vs. Displacement Curve for Tanks Subjected to Seismic Soil Pressures (No Liner Case)

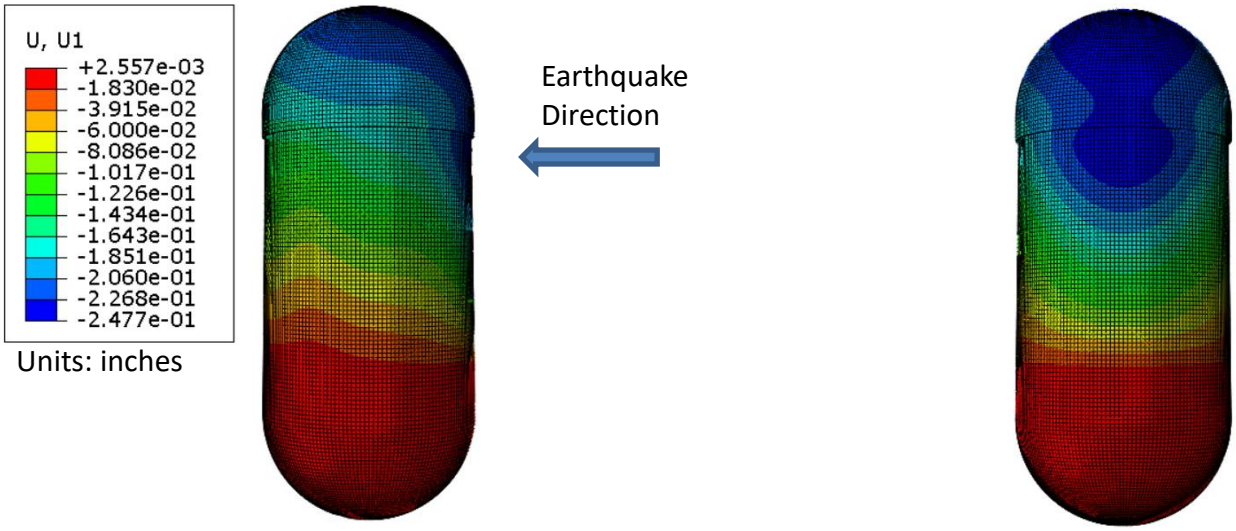

Figure 5-23 – Deflection Contours Shown on Deformed Shape for DBE Risk Category II Seismic Demand (No Liner Case)

Figure 5-24 – Equivalent Plastic Tensile Strains in Concrete for DBE Risk Category II Seismic Demand (No Liner Case)

Figure 5-25 shows the deflected shape of the tank for a DBE Risk Category III demand, where the displacement demand is 0.3 in. at the top of the tank. The tank deflects from right to left in the direction of the seismic loading. Figure 5-26 shows the equivalent plastic tensile strains in concrete for a DBE Risk Category III demand. The maximum strains are located near the base of the barrel and are on the order of 0.0003.

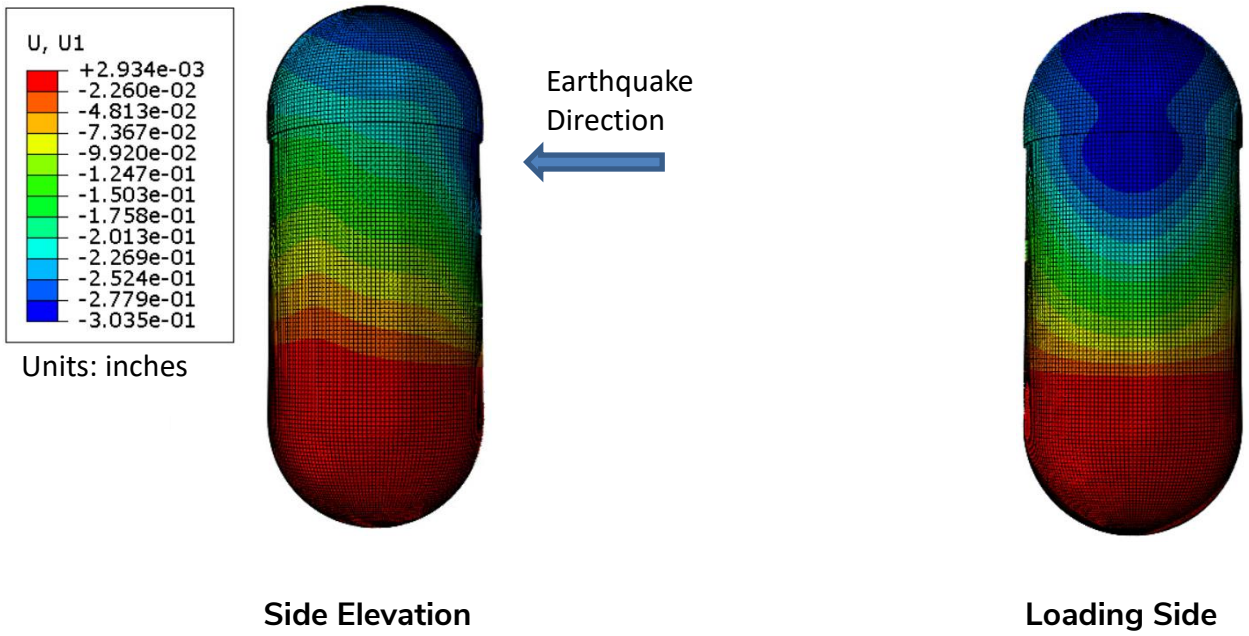

Figure 5-25 – Deflection Contours Shown on Deformed Shape for DBE Risk Category III Seismic Demand (No Liner Case)

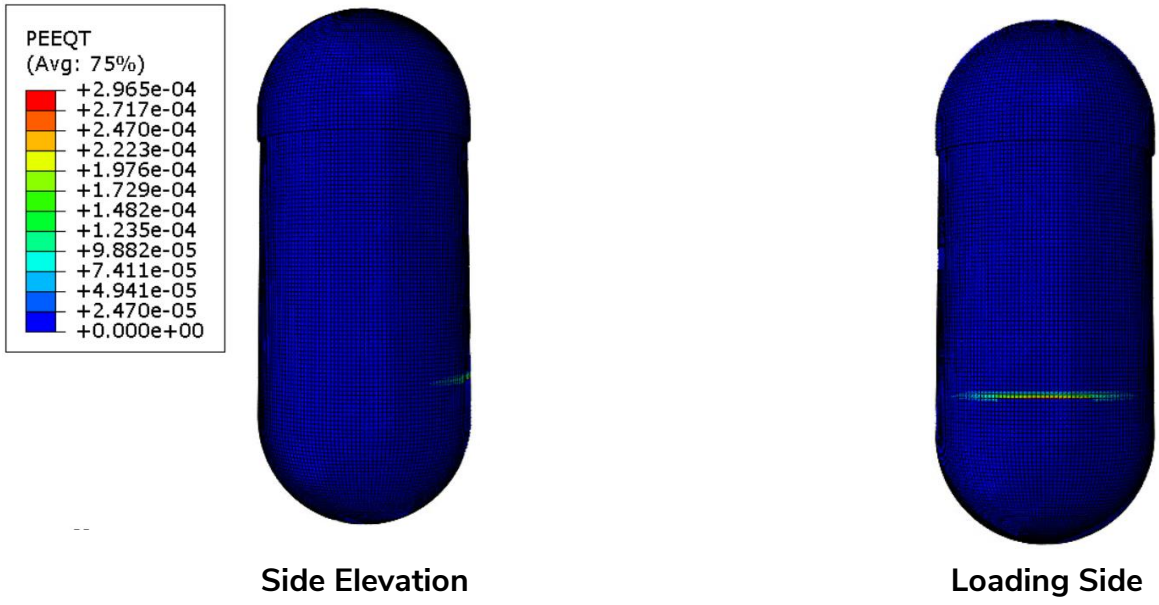

Figure 5-26 – Equivalent Plastic Tensile Strains in Concrete for DBE Risk Category III Seismic Demand (No Liner Case)

Figure 5-27 shows the deflected shape of the tank for 10,000-year event demand, where the displacement demand is 0.8 in. at the top of the tank. The tank deflects from right to left in the

direction of the seismic loading. Figure 5-28 shows the equivalent plastic tensile strains in concrete for a 10,000-year event demand. The maximum strains are observed near the base of the barrel and are on the order of 0.005.

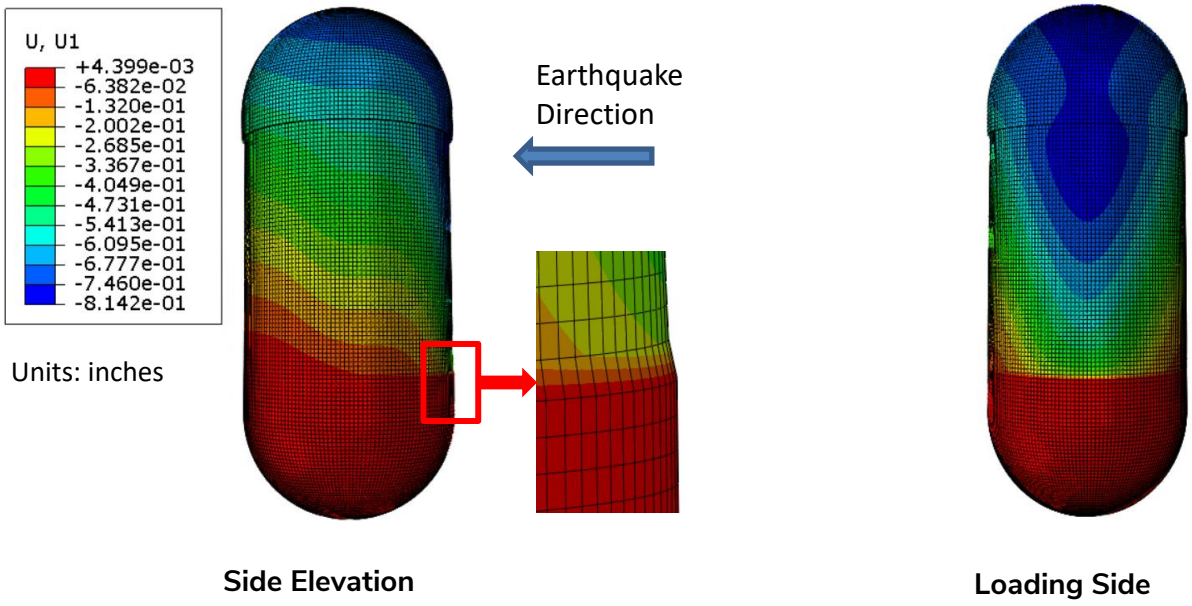

Figure 5-27 – Deflection Contours Shown on Deformed Shape for a 10,000-Year Earthquake (No Liner Case)

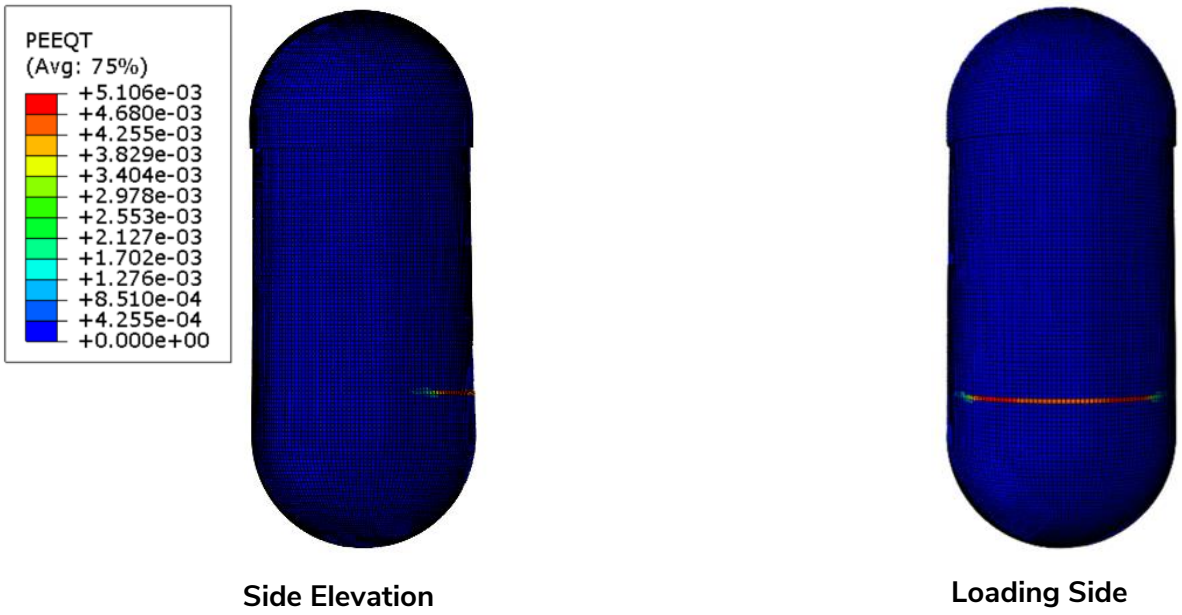

Figure 5-28 – Equivalent Plastic Tensile Strains in Concrete for 10,000-Year Earthquake (No Liner Case)

Figure 5-29 shows the von Mises stress in the reinforcement for a 10,000-year event demand. The stress in the reinforcement has reached the yield stress of 40 ksi, and the reinforcement yielding is concentrated near the base of the barrel section.

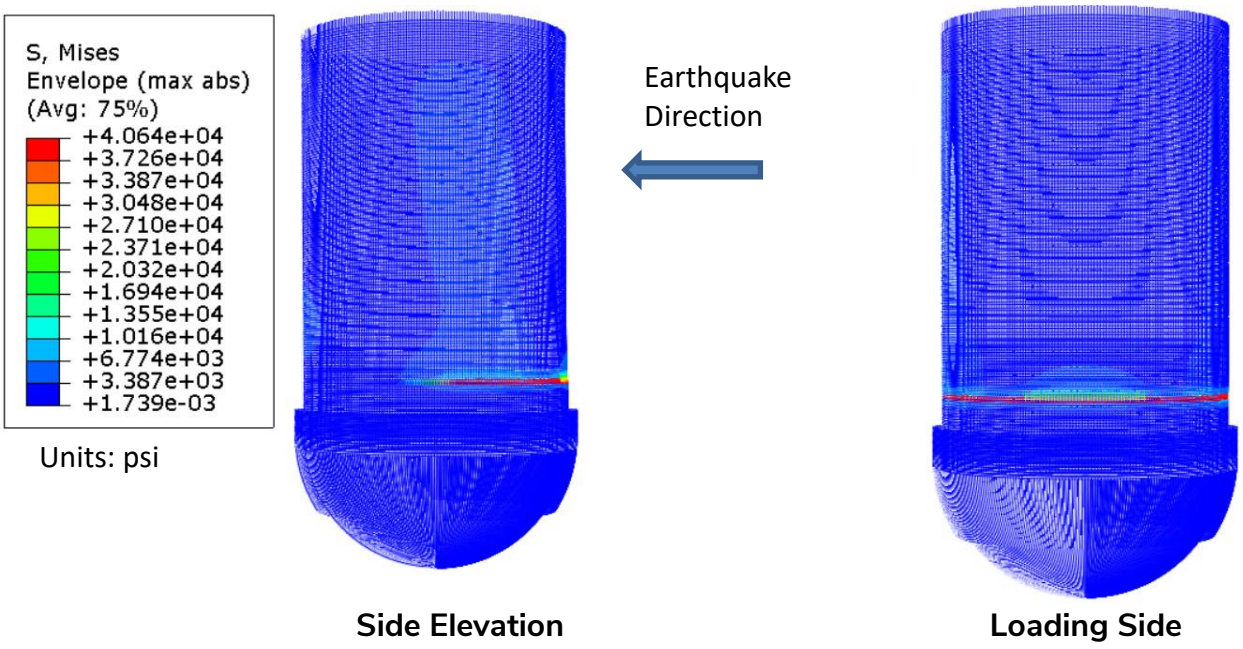

Figure 5-29 – Von Mises Stresses in Reinforcement for 10,000-Year Earthquake (No Liner Case)

Figure 5-30 shows the comparison of the displacement demands a design basis earthquake considering Risk Categories II and III and a 10,000-year event for both 75% rock/25% clinker and 50% rock/50% clinker strata without a steel liner. Note the displacement demands estimated in our SSI analysis for 50% rock/50% clinker strata are higher than those for 75% rock/25% clinker strata. The response is linear for the DBE with Risk Category II or III demands 50% rock/50% clinker strata. The response is in the nonlinear range for the 10,000-year event demand for 50% rock/50% clinker strata.

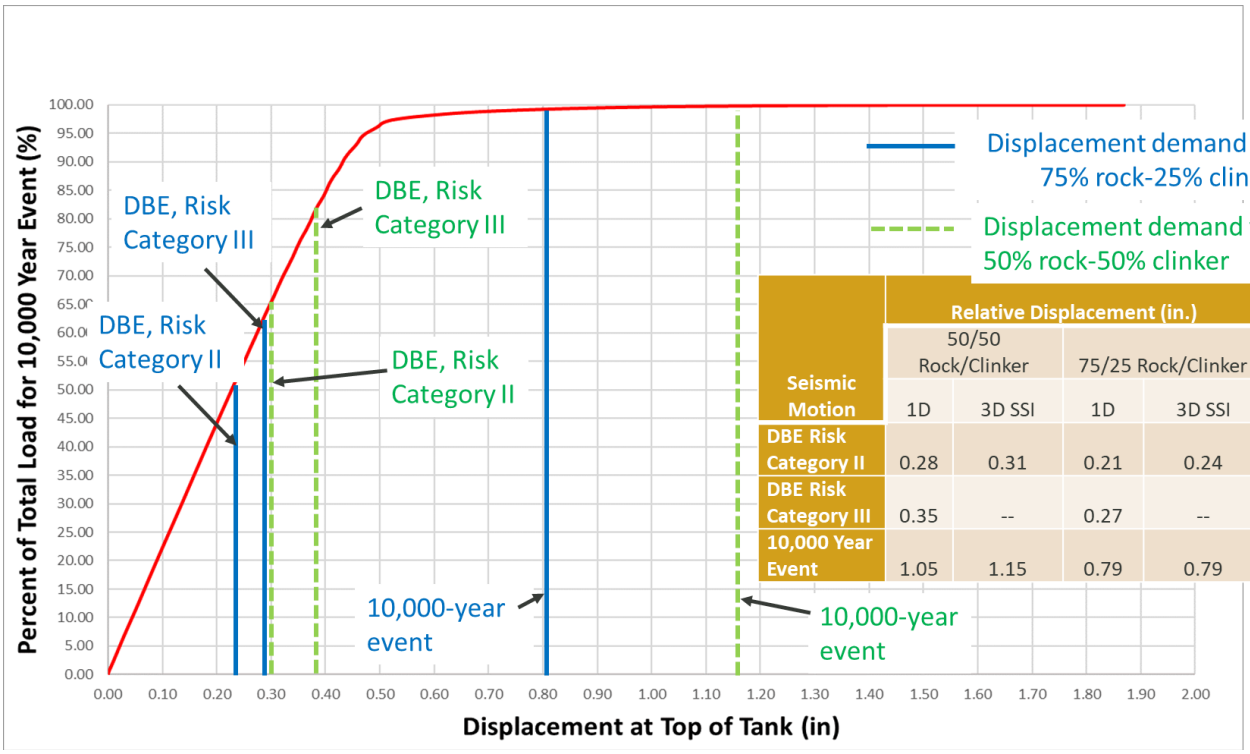

Figure 5-30 – Load vs. Displacement Curve for Tank Subjected to Seismic Soil Pressures with Comparison of 75% Rock/25% Clinker and 50% Rock/50% Clinker (No Liner)

Figure 5-31 shows the deflected shape of the tank for a 10,000-year event demand for 50% rock/50% clinker strata, where the displacement demand is 1.14 in. at the top of the tank. The tank deflects from right to left in the direction of the seismic loading. Figure 5-32 shows the equivalent plastic tensile strains in concrete for this case. The maximum strains are located near the base of the barrel and are on the order of 0.007.

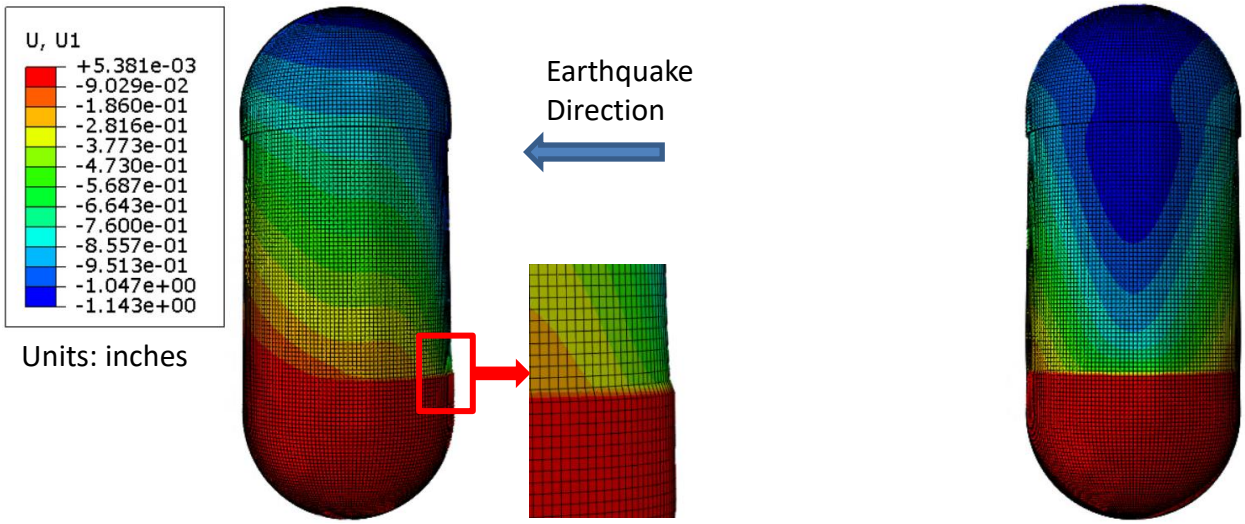

Figure 5-31 – Deflection Contours Shown on Deformed Shape for Seismic Demand for a 10,000-Year Earthquake (50% Rock/50% Clinker Strata, No Liner Case)

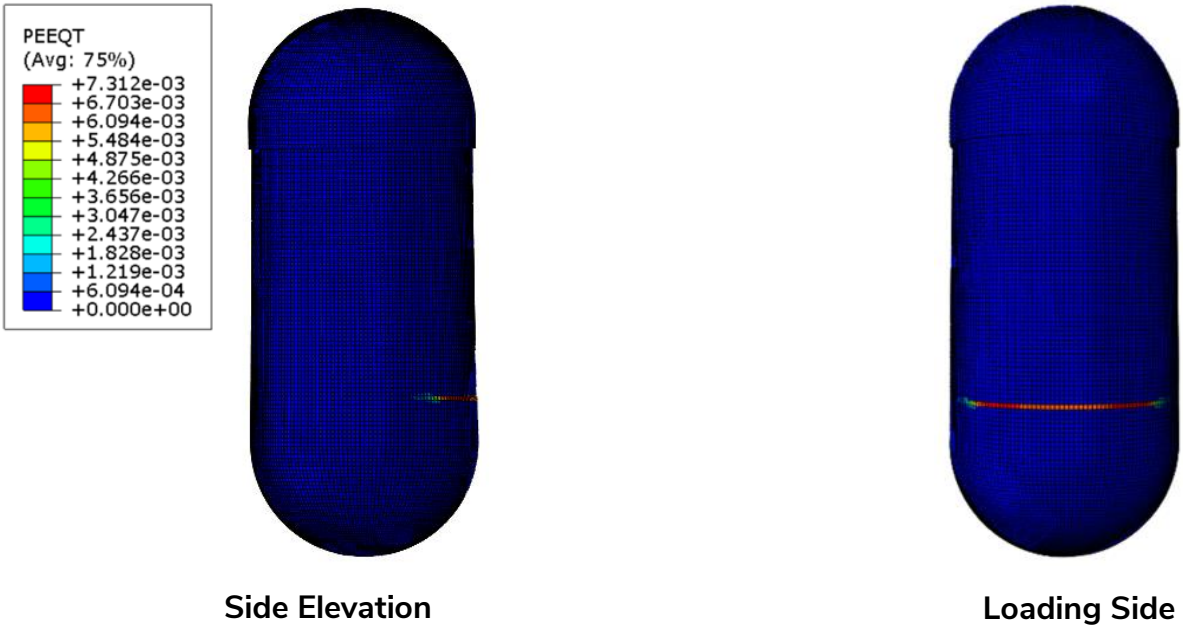

Figure 5-32 – Equivalent Plastic Tensile Strains in Concrete for Seismic Demand for a 10,000-Year Event (50% Rock/50% Clinker Strata, No Liner Case)

Figure 5-33 shows the von Mises stress in the reinforcement for a 10,000-year event demand for 50% rock/50% clinker strata. The stress in the reinforcement has reached the yield stress of 40 ksi, and the reinforcement yielding is concentrated near the base of the barrel section.

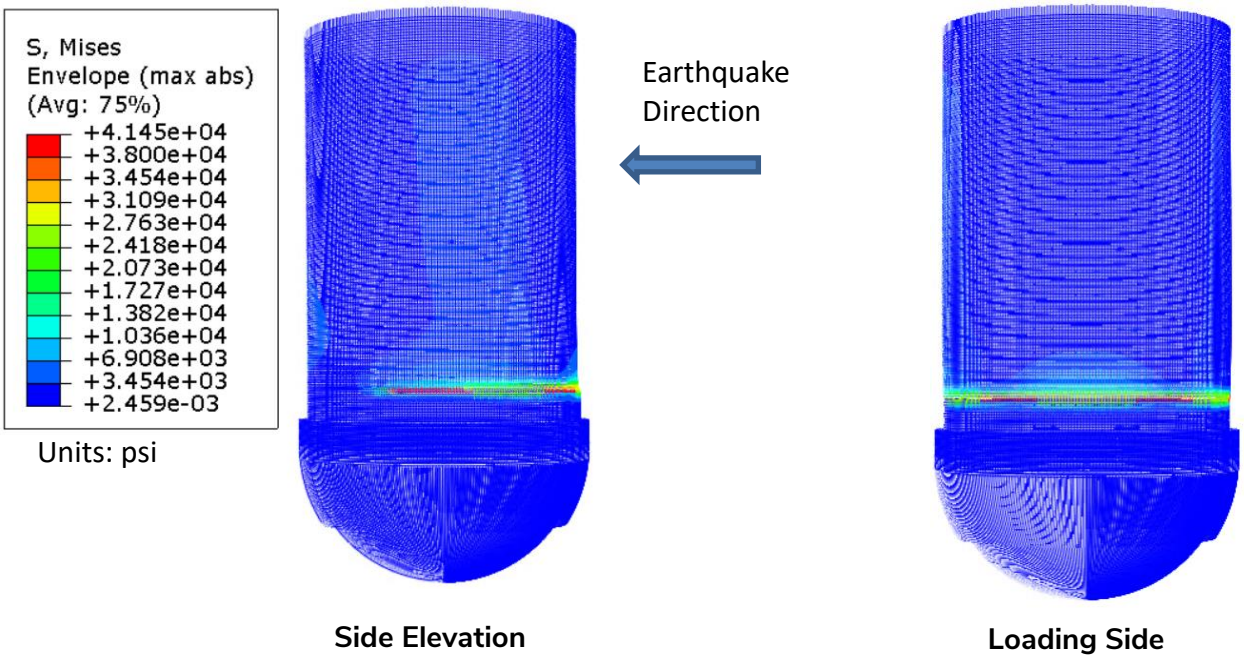

Figure 5-33 – Von Mises Stress in Reinforcement for Seismic Demand for a 10,000-Year Earthquake (50% Rock/50% Clinker Strata, No Liner Case)

5.3.3 Discussion for Tank Without Steel Liner

Displacement Corresponding to 75% Rock/25% Clinker Strata

The analysis predicted that the concrete cracking for the DBE Risk Categories II and III demands is minor, as indicated by the small equivalent plastic tensile strains ranging from 0.0001 to 0.0003. Since both these strain levels are smaller than 0.001, the strain corresponding to the onset of visible concrete cracking as defined in the performance criteria in Section 4.1, the tank meets the performance criteria and is able to resist the soil pressures due to seismic demands for DBE Risk Categories II and III without any damage.

The analysis results indicate that the concrete cracks for the 10,000-year event demand maximum equivalent plastic tensile strains of 0.005, but the concrete cracking is concentrated in the localized area near the base of the barrel on the loading side. As the concrete develops

this localized cracking, a kink in the displacement can be observed near the cracked area in Figure 5-27. The analysis also predicts the reinforcement yields providing a ductile response of the tank. The plastic strains in the reinforcement are relatively small (less than 2%). Since the concrete cracking is only concentrated in the localized region near the base of the barrel section on the loading side, the tank performance is adequate to meet the performance criteria.

As a result, the tank is stable and able to sustain the soil pressures due to an earthquake as large as a 10,000-year event.

Displacement Corresponding to 50% Rock/50% Clinker Strata

The displacement corresponding to a 50% rock/50% clinker strata is greater than that corresponding to a 75% rock/50% clinker strata.

For the DBE Risk Categories II and III demands, the analysis indicated no damage. Therefore, the tank meets the performance criteria and is able to resist the soil pressures due to seismic demands for DBE Risk Categories II and III.

The analysis results also indicate that the concrete can crack for the 10,000-year event demands due to the maximum equivalent plastic tensile strains of 0.007, but the concrete cracking is concentrated in the localized area near the base of the barrel on the loading side. As this localized cracking develops on the loading side of the barrel portion of the tank, a kink in the displacement can be observed near the cracked area in Figure 5-31. The analysis also predicts the reinforcement yields and provides a ductile response. The plastic strains in the reinforcement are relatively small (less than 2%). Since the concrete cracking is only concentrated in the localized region near the base of the barrel section on the loading side and is not through the thickness, the tank performance is deemed adequate to meet the performance criteria.

Therefore, the tank is stable and able to sustain the soil pressures due to a seismic event as large as a 10,000-year event.

5.3.4 Analysis Results for Tank with a Steel Liner

Figure 5-34 shows the deflected shape of the tank for a 10,000-year event demand. The maximum displacement is 0.52 in. at the top of the tank using the seismic soil pressure from our SSI analysis. The lateral displacement of 0.52 in. at the top of the tank is less than the displacement corresponding to 75% rock/25% clinker strata (0.8 in.) and the displacement corresponding to a 50% rock/50% clinker strata (1.15 in.), indicating that the overall lateral stiffness is larger with a steel liner compared to the tank model without a steel liner. The tank deflects from right to left in the direction of the seismic loading. Figure 5-35 shows the equivalent plastic tensile strains in concrete for a 10,000-year event demand. The maximum strains are located near the base of the barrel and are on the order of 0.0025.

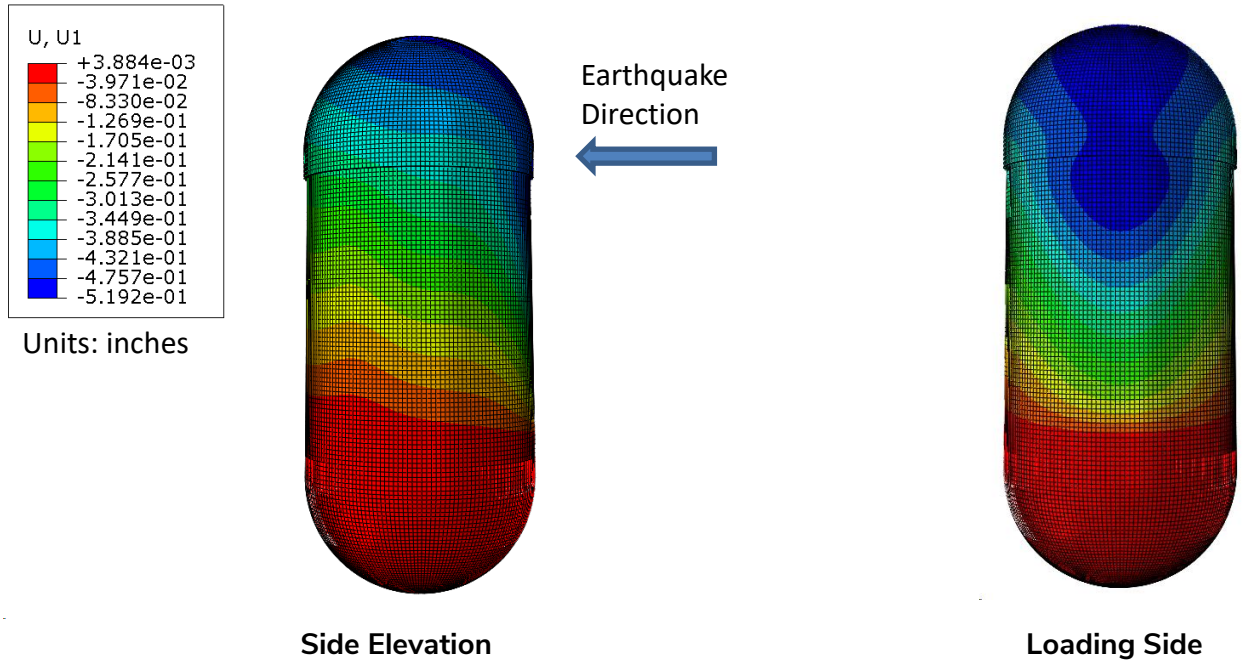

Figure 5-34 – Deflection Contours Shown on Deformed Shape for Seismic Demand for a 10,000-Year Earthquake (With Liner Case)

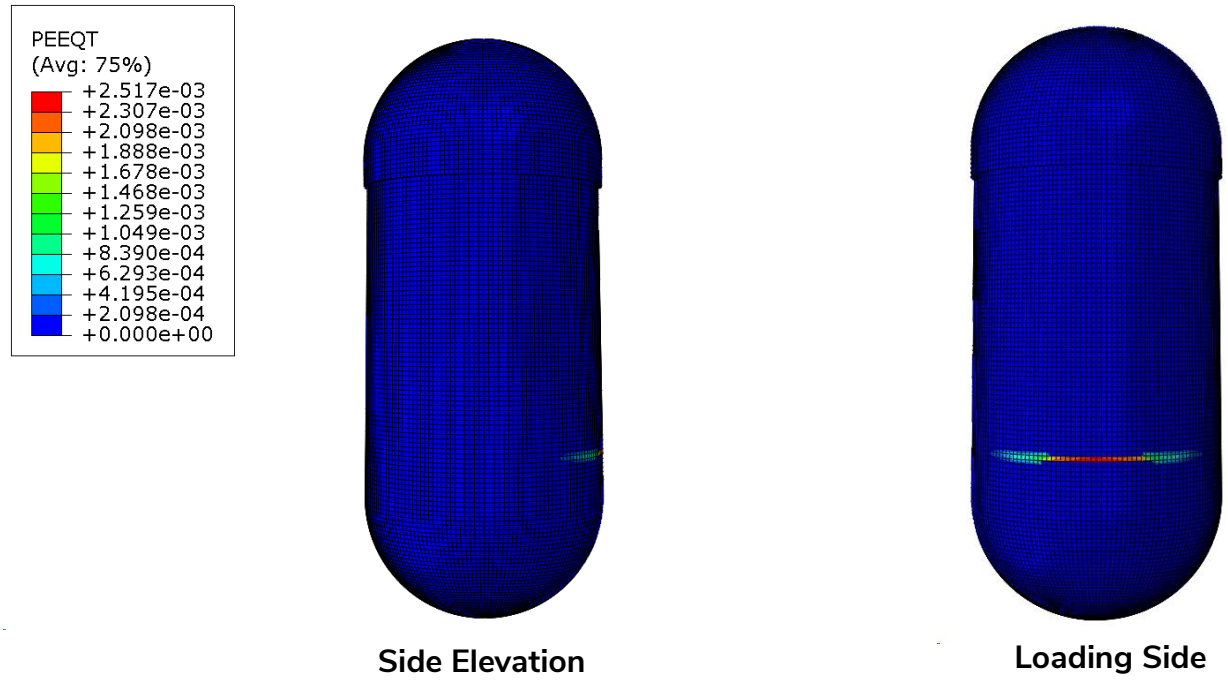

Figure 5-35 – Equivalent Plastic Tensile Strains in Concrete for Seismic Demand for 10,000-Year Earthquake (With Liner Case)

5.3.5 Discussion for Tank with Steel Liner

For the DBE Risk Categories II and III demands, the analysis indicated no damage. The tank meets the performance criteria and is able to resist the soil pressures due to seismic demands for DBE Risk Categories II and III.

The analysis predicted that the concrete cracking for the 10,000-year event demand is minor, as indicated by the equivalent plastic tensile strain of 0.0025, slightly larger than the strain of 0.001 corresponding to the onset of visible concrete cracking. Note that this cracking is limited to a localized area near the base of the barrel on the loading side. Both the reinforcement and steel liner remain elastic in the analysis. The tank meets the performance criteria and is able to resist the soil pressures due to a seismic event as large as a 10,000-year event. The presence of the steel liner improves the tank's seismic performance compared to the performance of the tank without a liner.

5.3.6 Summary of Analysis Results

The analysis results indicate that the performance of both tank analysis models, with and without steel liner, meet the performance criteria defined in Section 4.1 for a design basis earthquake considering Risk Categories II and III and a 10,000-year event. The tank is stable and able to sustain the seismic soil pressures due to a seismic event as large as a 10,000-year event.

6. TANK ACCESS TOWER ANALYSIS

The internal tank towers were constructed to facilitate tank construction and periodic maintenance throughout the life of the tanks. After the primary tank cavity was excavated and the gunite layer placed on the rough cavity wall, the tower was constructed from the lower to the upper dome. These towers enabled concrete placement and steel liner installation. The towers historically have been used by contractors to conduct the clean, inspect, repair (CIR) program during the life of the tanks. During this CIR process, the first step after taking a tank out-of-service and creating a vapor-free space for workers is to inspect and repair the tank towers so that they are structurally sound for cleaning, inspecting, and repairing the tank. After completion of the defueling process, these towers will remain in the empty tanks. Among other methods the Navy may employ, these towers can facilitate periodic tank condition assessments, especially after a seismic event. Therefore to provide the Navy with multiple options as they plan for tank closure, it is important to understand the long-term seismic performance of these towers. Given our visual assessment of Tank 19 in February 2023, where observations differ from our document review, we used our Tank 19 observations as a generalization across all tanks.

6.1 Methodology

We analyzed the tank tower using SAP2000 software v24. The tank tower analysis model considered self-weight, superimposed dead loads, and earthquake loads. Earthquake loads are defined as the ASCE 7-22 design earthquake for both Risk Category II (I_e = 1.0) and III (I_e = 1.25), as well as the 10,000-year mean recurrence of earthquakes (see Section 4 for more details). Our tank tower model geometry, sections, connections, and superimposed dead loads are as described in Section 2.1.4 (see Figure 6-1 for geometry and primary structural members).

We defined the boundary conditions of the tank tower based on available drawings and supplemented by field observations. Photos during construction (Figure 2-14) show the tower legs penetrating several feet into the tank bottom, effectively fixing the tower base to the tank's lower dome. Conservatively, we modeled the bottom of the tank tower as a pinned connection

with a connection capacity the same as the member capacity. Tank tower drawings show the top tower legs penetrating the upper dome concrete (Figure 2-16). However, we do not have details about the mechanical attachment within the concrete section. Therefore, we conservatively assigned roller support, which allows vertical movement such that a hanging gravity reaction is not imposed at the top of the tank dome. The roller connection is restrained in both lateral directions.

Steel elements are assigned ASTM A36 material properties consistent with the AISC Steel Manual for structural steel angles.

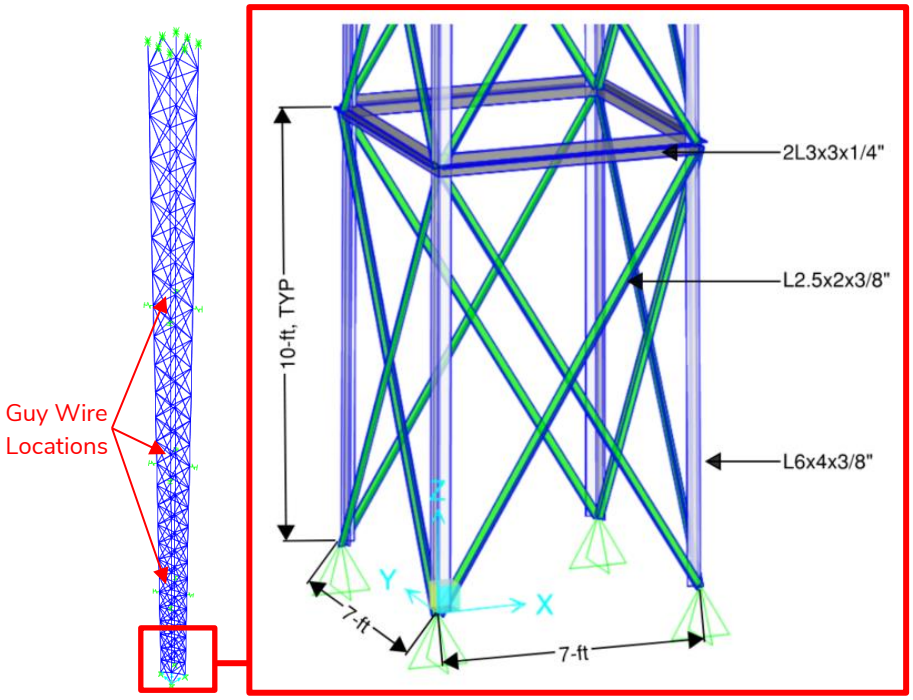

Figure 6-1 – Finite Element Model of Internal Tank Tower, Structural Elements, and Dimensions

The structure is a vertical box truss; therefore, beams and cross-bracing should primarily transfer axial loads at the panel points, i.e., at the joints. All bracing and beam structural members are modeled as frame elements with the moment and torsion releases at the ends. Columns are modeled as continuous frame elements. The cross-braces are connected at their midsection by a bolted gusset plate which reduces their effective length in the major and minor axis to 70% of the total length (KL=0.7) (Picard and Beaulieu 1987 and 1988). Considering this

effective length, the structural members have approximate axial capacities as summarized below:

- Cross-bracing: compression capacity = 6 kips, tension capacity = 50 kips.
- Columns: compression capacity = 75 kips, tension capacity = 213 kips.
- Double-angle beams: compression capacity = 60 kips, tension capacity = 93 kips.

To accurately capture the gravity load path of the vertical box truss, we established a staged construction load case in SAP2000 such that the cross-bracing contributes to resisting the gravity demands of their self-weight and that of the superimposed dead loads. The self-weight of the columns and beams is taken by the columns directly.

As mentioned in Section 2.1.4, in Tank 19, we measured the diameter of the guy wires in the field to be 1/2-in., although the original drawings specify 3/4-in. guy wires. We extracted section properties for the guy wires (cables) from ASTM A603, as shown in Figure 6-2 and Figure 6-3 and summarized below.

- Gross area = 0.119 in^2.
- Minimum breaking strength = 21 kips.
- Minimum modulus of elasticity = 20,000 ksi.

TABLE 1 Properties of Single-Class Metallic-Coated Steel Structural Wire Rope (Inch-Pound Units)

Nominal Diameter, in.	Minimum Breaking Strength in Tons of 2000 lb			Approximate Gross Metallic Area, $in.^2$	Approximate Weight/ft, lb
	Class A Coating Throughout	Class B Coating Throughout	Class C Coating Throughout		
3/8	6.5	6.2	5.9	0.065	0.24
7/16	8.8	8.4	8.0	0.091	0.32
1/2	11.5	11.0	10.5	0.119	0.42
9/16	14.5	13.8	13.2	0.147	0.53

Figure 6-2 – ASTM A603 Section Properties of Metallic-Coated Structural Steel Wire Rope

TABLE 8 Minimum Modulus of Elasticity of Prestretched Structural Wire Rope

Nominal Diameter Wire Rope		Minimum Modulus—Class A Coating[A]	
in.	mm	psi	GPa
⅜ to 4	9.52 to 101.60	20 000 000	140

Figure 6-3 – ASTM A603 Minimum Modulus of Elasticity of Prestretched Structural Wire Rope

In the SAP2000 model, we used linear springs to represent the guy wires. Although the drawings indicated four sets of guy wires at each tower, we noted three sets during our observations in February 2023; therefore, conservatively, we assigned three guy wire sets in our model. Each guy wire "spring" is defined as half the guy wire stiffness to account for opposing springs acting concurrently in the linear model. In other words, a guy wire in compression does not contribute to the restraint condition; however, opposing springs perform simultaneously in the model. The springs at each tower column corner are rotated 45° to represent the orientation of the actual guy wires (Figure 6-1 and Figure 6-4).

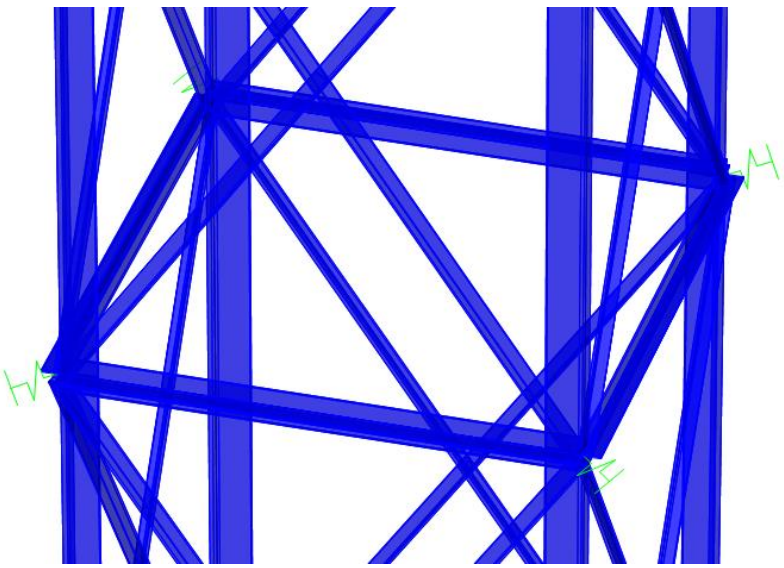

Figure 6-4 – Guy Wires Modeled as Springs in Structural Model

We referenced the structural drawings and field observations (Section 2.1.4) to account for the weight of the components on the tank tower, including the access level bridge, access level

platform, platforms at non-access levels, ladders, and piping/conduit. We do not have drawings that represent weights for the superimposed dead loads. Therefore, we reference current piping and ladder weights literature, assuming reasonably conservative demands. Member sizes and layouts of platforms and bridges are taken from the structural drawings. Where field measurements differ from the drawings, field measurements are used in the analysis.

AISC 360-16 and the Process Industry Practices (PIP) Structural Design Criteria provide nominal weights and design loads commonly used in the industry that we used when determining the component weights. We observed two perforated pipes that we assumed to be 6 in. diameter and four pipes that we assumed to be 3 in. diameter. We considered the possibility that the 3-in. steel piping is partially filled with conduit. The weight estimations for each component are summarized below. In the structural model, we assigned the weight of the components as point loads at the appropriate levels on the tank tower. Piping attachment, per field observations, appears to connect the pipe at each level directly to the beams via a welded tab. Therefore, this point load assumption appears appropriate. Connecting each platform are caged ladders that also run the full height of the tower (Figure 2-17).

The structure's total seismic mass includes the tank tower's self-weight and the weight of the components, including a 5% contingency to account for welds, connection elements, and other incidental superimposed loads. The estimated loads are as follows:

- Total piping load = 18 kips.
- Total weight of the caged ladders = 6 kips.
- Total weight of the platforms = 7 kips.
- At the access level, the bridge load on the tower (half of the total bridge weight) = 4.7 kips.

We performed a modal analysis of the tower, accounting for the mass of all self-weight and superimposed dead loads. Each primary horizontal mode contained approximately 77% mass participation, while the vertical primary mode contained approximately 80% mass participation. The primary X direction mode period is 0.51s, the primary Y direction mode period is 0.46s, and

the primary Z direction (vertical) mode period is 0.11s. The two primary horizontal modes (X and Y directions) have characteristic single curvature mode shapes.

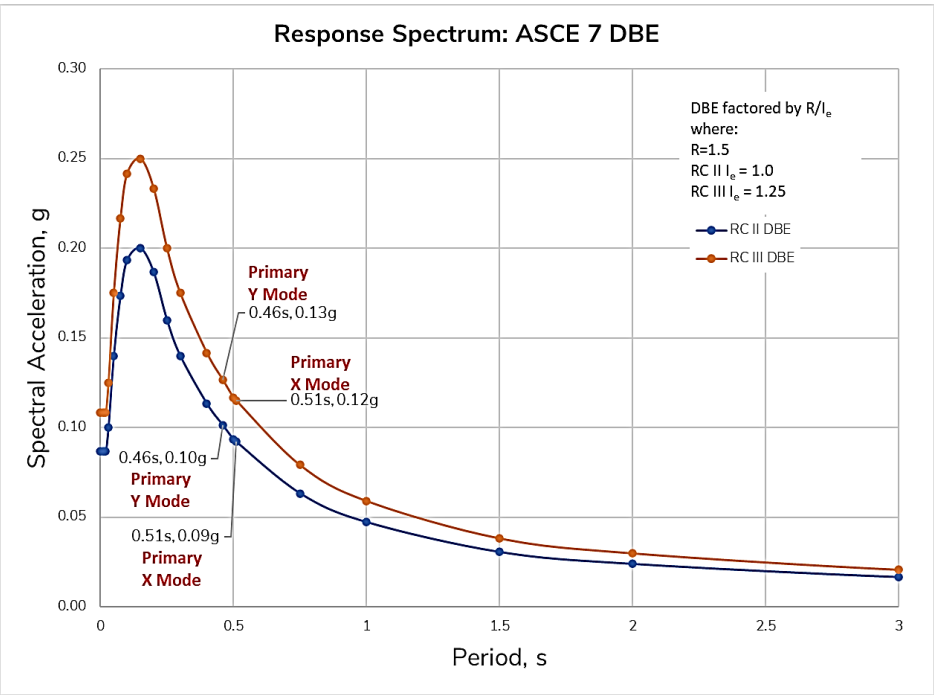

Figure 6-5 – Primary Horizontal Modes Relative to ASCE 7 DBE Response Spectrum

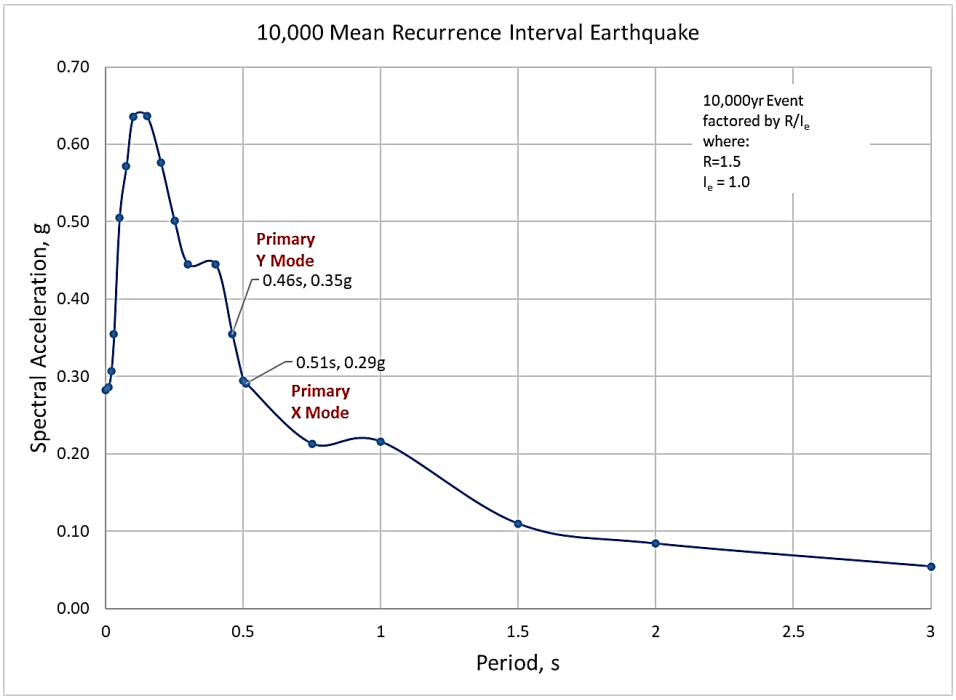

Figure 6-6 - Primary Horizontal Modes Relative to the 10,000-Year Response Spectrum

We used the equivalent lateral force (ELF) procedure to evaluate the seismic performance of the tank tower considering the Risk Category II and III DBE and the 10,000-year mean recurrence interval earthquake. We accounted for first-order and P-Δ second-order responses.

Our load combinations for each earthquake event consider orthogonal seismic demands. Load combinations are according to ASCE 7-22 Section 2.3.6 for LRFD:

$1.2D + E_h + E_v$, where

$E_h = \rho Q_E$

$\rho = redundancy\ factor, as\ defined\ in\ Section\ 12.3.4$

$Q_E = effects\ of\ horizontal\ seismic\ forces, such\ effects\ shall\ result\ from\ application\ of\ horizontal\ forces\ simultanesouly\ in\ two\ directions\ at\ right\ angles\ to\ each\ other, considering\ a\ 100\%/30\%\ relationship$

$E_v = 0.2 S_{DS} D$

We used a redundancy factor of 1.0 following Section 12.3.4 of ASCE 7-22. From the response spectra presented in Section 3, we used an S_{DS} = 0.3g and an $S_{10,000}$ = 0.94g.

6.2 Analysis Results

For the Risk Category II and Risk Category III DBE analyses, the tower performed well and remained in the elastic range, without failure, and thus with the expectation of fulfilling the Immediate Occupancy (IO) limit state. The controlling load combination for the Risk Category II analysis is $(1.2 + 0.2S_{DS})D + 0.3E_X - E_Y$, where E_X is the inertial demand in the X-direction, and E_Y is the inertial demand in the Y-direction. The largest demand-to-capacity (DCR) ratio for this analysis is 0.50 in the lowest set of braces. The primary demand in the brace in Figure 6-7 is axial compression, this component of the DCR alone being 0.49.

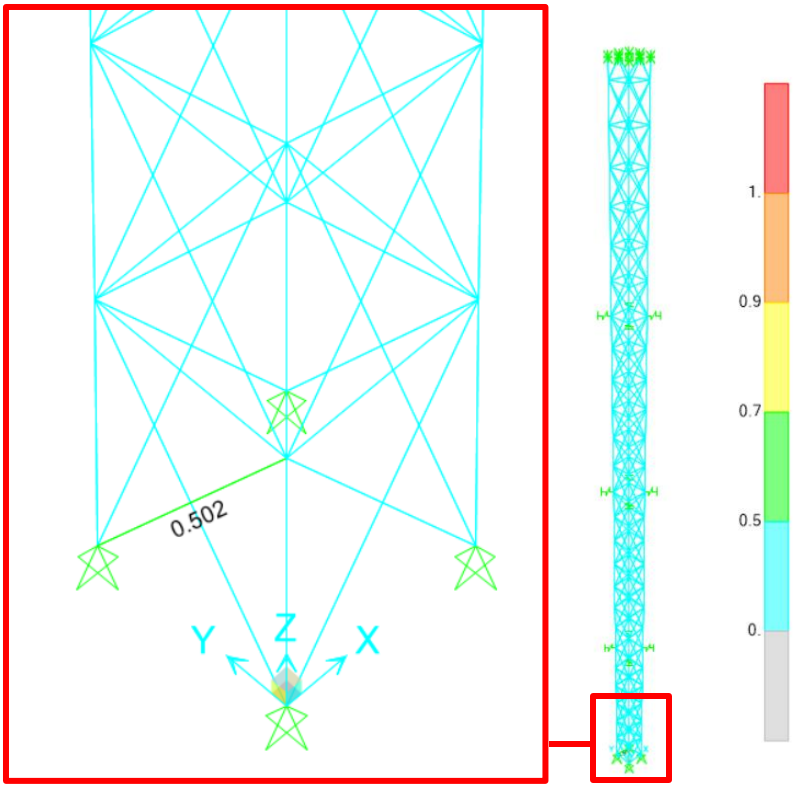

Figure 6-7 – ASCE 7 DBE Risk Category II DCRs

The controlling load combination for the Risk Category III analysis is again $(1.2 + 0.2S_{DS})D + 0.3E_X - E_Y$. The largest DCR for this analysis is 0.55 in the lowest set of braces. The primary demand in the brace in Figure 6-8 is axial compression, this component of the DCR alone being 0.53.

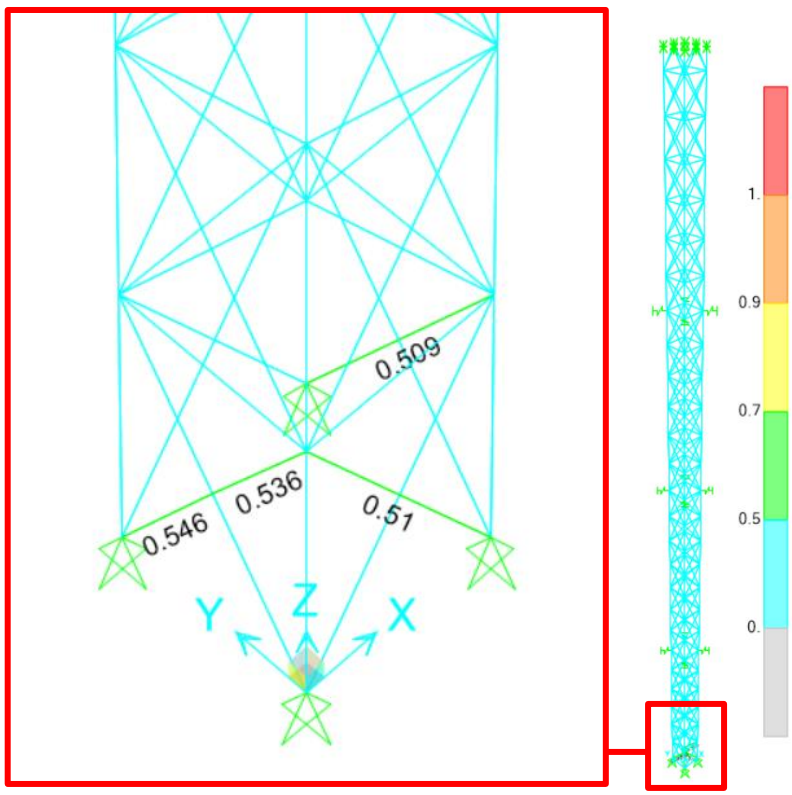

Figure 6-8 – ASCE 7 DBE Risk Category III DCRs

For the analysis with the 10,000-year MRI earthquake, with a resistance factor equal to 1.0 in accordance with the CP assumption that the structure continues to support gravity loads but retains no margin against collapse, the tower performed elastically, without failure and thus, with the expectation of fulfilling the CP limit state. The controlling load combination for the 10,000-year MRI earthquake analysis is $(1.2 + 0.2S_{10,000})D + 0.3E_X - E_Y$. The largest DCR for this analysis is 1.00 in the lowest set of braces. The primary demand in the brace in Figure 6-9 is axial compression, this component of the DCR alone being 0.99. A single brace with DCR = 1.00 in the lowest section of braces is considered acceptable for the CP limit state, given that we conservatively used an R-value of 1.5. The largest displacement for this controlling load combination is 1.39-in in the Y-direction (Figure 6-10).

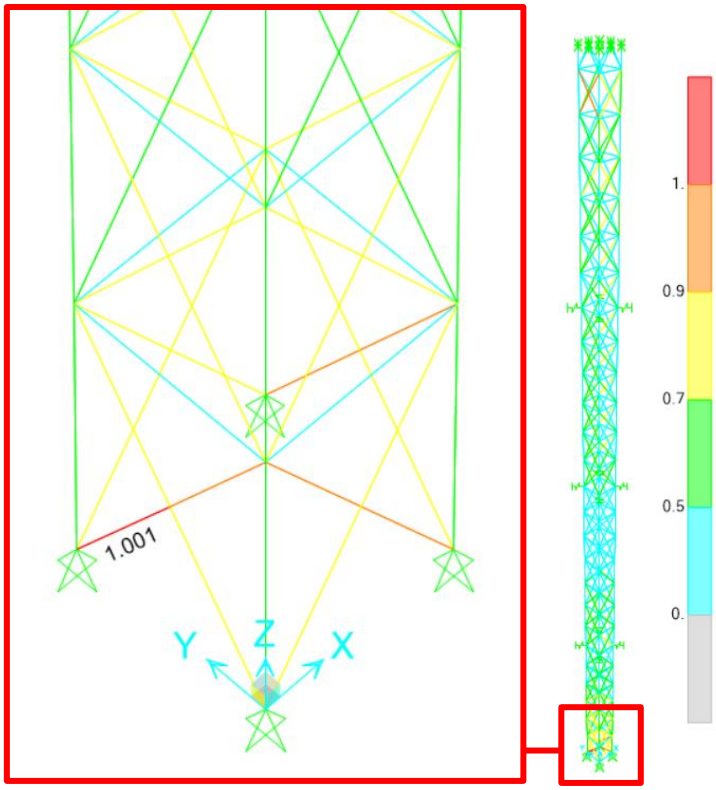

Figure 6-9 – 10,000-Year MRI Earthquake DCRs

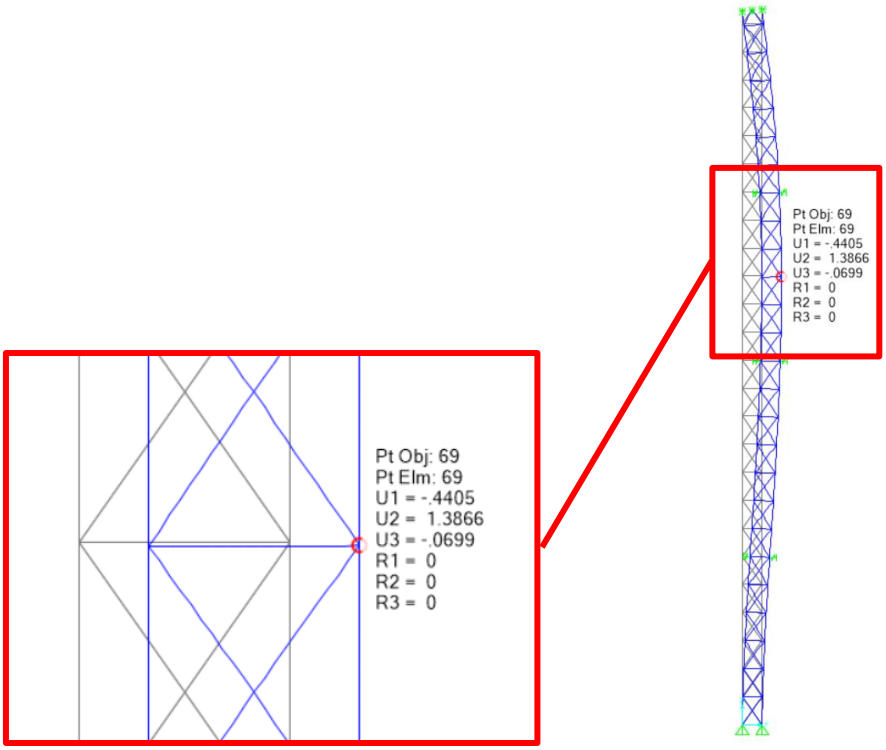

Figure 6-10 – 10,000-Year MRI Earthquake Maximum Displacement

The largest spring force at the guy wire locations for the larger 10,000-year event was 5.3 kips. The minimum breaking strength for these cables from ASTM 603 is 21 kips. Thus, the cables have sufficient capacity to withstand the 10,000-year event.

6.3 Discussion

Our analyses of the internal tank towers considered the ASCE 7-22 DBE for Risk Category II and Risk Category III assuming an immediate occupancy (IO) limit state and a 10,000-year return period event assuming a collapse prevention (CP) limit state.

The load combinations considering inertial demands for the ASCE 7-22 DBE resulted in maximum DCRs less than 0.6, indicating an additional margin in the tower system to withstand the DBE in Oahu.

For the load combinations considering inertial demands for the 10,000-year earthquake event, the performance of the tower structure meets the requirements of the CP limit state. The overall structure remains undamaged, although one brace at the lowest bay of the tower reached its capacity with a DCR of 1.0. An R-value of 1.5 was conservatively used at this limit state.

The tower members have sufficient capacity to achieve the respective limit states for both the ASCE 7-22 DBE and 10,000-year earthquakes.

Although the tower connection at the top of the tank is modeled as a vertical roller, the drawings indicate a pinned connection penetrating the top of the tank dome (Figure 2-16). The bottom tower connections are also embedded in the mass concrete plug below the lower tank dome (Figure 2-13). Therefore, the governing capacity of the top and bottom connections is the capacity of the column legs. Considering all analyses, the maximum DCR for the column leg members at the connections is 0.7. Thus, the tank-to-column connections at the top and bottom domes are judged to be adequate to withstand both the DBE and 10,000-year earthquakes. The splice connections along the column lengths have been assumed to have the same capacity as the columns, and given that the largest DCR in the columns is 0.7, the splice connections are also expected to be adequate.

The brace tension capacity is approximately 50 kips, while its compression capacity is approximately 6 kips. The midpoint and end gusset connections are designed to accommodate the largest tension forces; therefore, given the maximum demand in the braces for the 10,000-year event is approximately 6 kips in compression, the brace connections are deemed adequate for the seismic demands.

The largest DCR for the horizontal double-angle beams is 0.4. Assuming the connections have, at minimum, the capacity of the members, the connections are also expected to be adequate for the seismic demands.

Our analysis results show that three sets of guy wires have sufficient capacity to withstand earthquake demands from the 10,000-year event.

We considered the tower access bridge connecting the tank tower and the tank entrance at the upper access tunnel as gravity point loads on the tower. The structural drawings show a bolted connection between the access bridge and the internal tank tower (Figure 2-20). Photos from our site visits indicate cable stays between the bridge entrance access platform and the tank liner and welded/bolted connections between the bridge and the tank entrance (Figure 2-18).

Should the Navy choose to use the towers in the future to facilitate tank access, the seismic resistance and resilience of the tank access structures could be increased by adding seismically-rated restraint cables between the access bridge and the tank, as well as between the access bridge and the support tower. These seismically-rated restraint cables can assist in "catching" the access bridge should it disengage from its supports due to differential displacement between the tower and the tank. In addition, to prevent damage to the bolted connections that support the access bridge, the connection at one end of the bridge (either the tower end or the tank end) could be reconfigured to accommodate the anticipated differential displacement during a major earthquake.

Our analyses consider the tower, bridge, main level access platform, and other intermediate platforms to be in "good condition" with all members and connection hardware present, intact, and not in a degraded condition. To achieve the performance predicted by our analyses, the

tank towers and their connections should be inspected before the long-term closure of the facility and repaired/retrofitted as necessary to achieve the intended design capacity. An opportune time to perform this work would be at the time the Navy conducts their closure operations.

Additionally, we suggest periodic visual inspections for water at the bottom of the tanks. Should the towers be used for future tank access, pooling water should be avoided for long-term durability as water may jeopardize the capacity of the structural steel members since the steel makes direct contact with the bottom of the tank (Figure 2-15). If the fuel-oil-reclamation (FOR) line and main sump are adequately maintained, water accumulating in the tanks could be drained through this line.

7. LONG TERM DURABILITY

7.1 Concrete Components

7.1.1 Introduction

As described by Clifton (Clifton 1989), the service life of underground concrete "depends on both the physicochemical properties of the concrete materials and properties of the in-service environment," with the "major factors controlling the service life of underground concrete including the rate of ingress and movement of moisture in concrete, and the rate of reactions between the concrete and constituents of the groundwater."[1] In addition, there is relatively little experience with buried concrete structures older than 100 years, as few reinforced concrete highway tunnels are that old, and other types of structures of that age (pipelines, vaults, sewers, etc.) tend to be constructed of brick or stone masonry.

While concrete is generally durable, there are some conditions that can cause deterioration of buried concrete or damage to the concrete resulting from the corrosion of the embedded reinforcing steel. The mechanisms identified in the literature for tunnels (Allen et al. 2015, The National Academies of Sciences, Engineering, and Medicine 2015, Gannett Fleming, Inc. 2010) buried structures, and long-term storage of nuclear materials (Clifton and Knab 1989) include the following, as will be detailed in the following sections.

- Acid attack.
- Concrete leaching.
- Reinforcing steel corrosion due to carbonation.
- Reinforcing steel corrosion due to chlorides.
- External sulfate attack of concrete.
- Internal sulfate attack.
- Alkali silica reactivity.

[1] Note: "Concrete" is used generically throughout this section of the report to refer to concrete comprising portland cement, sand, water, and coarse aggregate, as no other cement types or other cementitious materials are identified in the record.

- Microbiological attack.
- Salt crystallization.
- Damage due to cyclic freezing and thawing.
- Direct attack by Low-Level Nuclear Waste (LLW).
- Serviceability issues related to leakage.
- Overloads and damage due to overburden slides (landslides).

7.1.2 Effect of Exposure

The degradation mechanisms listed above are typically related to (a) exposure to an external agent acting on the concrete or on the embedded reinforcing steel, environmental effects causing physical damage to the concrete, or (b) internal reactions causing damage within the concrete. All these mechanisms require some degree of exposure to water, either to dissolve and carry the aggressive agent, participate in the physical reaction, or provide an environment conducive to the internal reaction.

Because of the dependence of the deterioration mechanisms on the availability of water to the exterior or interior face of the tanks, the degree of water exposure will control the future performance of the tanks, with two different exposures – exterior and interior.

The exterior of the tanks will be exposed to water traveling down through the surrounding rock. While there is information available about the characteristics of the water passing through the rock (see below), the degree of exposure of the tank exteriors to the water is unknown and difficult to estimate or quantify because of the unknown effects and interaction of the 2 to 6 in. thick gunite applied to the excavation face, the red earth (clay slurry) separation layer between the gunite and the concrete, the concrete itself, and the post-concrete grouting. For example, the 2-in. to 6-in. thick shotcrete layer will provide a first barrier to exposure, supplemented by the pressure grouting that would have filled cracks and voids in the shotcrete and underlying rock. These unknowns effectively preclude the use of deterministic transport modeling, so the discussions below conservatively assume that the exterior of the concrete at the tanks is

directly exposed to the water flowing through the rock and ignores the effect of the gunite, red earth (clay slurry) and grouting.

At the interior of the tanks, there is a potential for any water that penetrates the concrete through cracks or joints or that forms due to condensation in the tank, to travel behind the steel liner through gaps, areas of poor bond, or areas where bleed water traveled during construction. This is supported by the limited observations identifying seepage of water between the steel liner plates and the inside face of the concrete tanks (Ackerson and Breetz 2018). The water test data also supports this, with the wells below the tanks showing a lower pH, lower dissolved oxygen, and lower oxidation-reduction potential (ORP) than the reference well, suggesting that steel corrosion occurred as the water traveled downward through the rock strata.

7.1.3 Acid Attack

Concrete has low resistance to acid attack and can be damaged by exposure to low pH water, such as when atmospheric carbon dioxide is dissolved in rainwater or by mineral or organic acids within the soil and rock that migrates to the concrete. The acidic water will attack the lime and, in extreme cases, the silicate hydration products present in the concrete.

A review of water chemistry data (NAVFAC 2023) shows a pH of 7.3 at Well RHMW04, away from the tank, suggesting that the exteriors of the tanks are not exposed to an acidic environment. The water testing at Wells RHMW01 to RHMW03 shows an average pH value of 6.8, slightly acidic and lower than that at reference Well RHMW04. As the well sampling locations are below the tanks, the difference between the wells could indicate that water interacts with the tanks (possibly due to the effect of the observed corrosion of the backside of the steel liner) as it moves through the rock, or that the water is being affected by the remnant fuel remaining in the rock strata below the tanks after the 2014 leakage event. The likelihood of water interaction with the tanks or remnant fuel is also indicated by the change in dissolved oxygen and ORP (an indicator of reactivity) in the water at the wells below the tanks compared to the reference well. The exact cause(s) of the changes in water chemistry cannot be determined from the limited test data, as the vertical separation between the sampling location

in the wells and the bottom of the tanks precludes identifying the elevation at which the changes in water chemistry occur.

7.1.4 Concrete Leaching

Although the tanks are above the water table, there will be water passing through the rock surrounding the tanks as it travels down to the water table. Therefore, there is some possibility of leaching of one or more of the concrete constituents into the passing water, although the exact potential for leaching cannot be determined because it is highly dependent on the concrete permeability and the chemistry of the water. The available water chemistry data (NAVFAC 2023) from the water at and below the tanks does not indicate an unusually aggressive leaching potential, with near-neutral pH and total dissolved solids concentration ranging from about 200 ppm to about 1,000 ppm for most sampling locations (within the range typical of freshwater, noting that freshwater typically contains less than 1,000 ppm dissolved solids).

Leaching deterioration occurs by the dissolution of components within the concrete and would first dissolve the alkali salts, followed by calcium hydroxide (Clifton 1989, Clifton and Knab 1989). The leaching could theoretically disrupt the main cement hydration products, although "the solubility of silica oxide [sic] is very low so that the decomposition rate, through dissolution of the calcium silicate hydrate [the main binder in portland cement concrete] is very slow" (Clifton and Knab 1989).

Leaching can also reduce the concrete pH by dissolving alkali and alkaline earth hydroxides from the concrete, but it is typically a very slow process, with leaching contributing to deterioration processes for "concrete…exposed to intermediately or continuously flowing underground water for 300 years" (Clifton 1989). A paper regarding LLW nuclear storage similarly notes that with a groundwater flux density of 10^{-10} m/s, it would take 500 years to cause leaching to extend to reinforcement at 100 mm of cover (Clifton and Knab 1989) and to decrease the concrete pH at the level of the reinforcement sufficiently to allow corrosion of the reinforcing steel to begin.

7.1.5 Reinforcing Steel Corrosion Due to Carbonation

Carbonation is the process through which the naturally-high pH of the concrete is decreased over time. It primarily occurs as the CO_2 in the atmosphere or dissolved in water as carbonic acid reacts with the Ca $(OH)_2$ in concrete to create $CaCO_3$. This reaction results in a decreased pH in the concrete, which can cause a loss of the corrosion protection offered by high pH environments to any embedded reinforcing steel. Once this natural corrosion protection is lost, the reinforcing steel can corrode if sufficient moisture and oxygen are available.

The depth of carbonation can be modeled as $D = Kt^{0.5}$, where K can be 3 to 4 mm/year for low-quality concretes (w/cm ~ 0.6) in the air (Neville 2012). Neglecting the effect of any protection from the groundwater offered by the shotcrete, red earth (clay slurry), and grout, neglecting the slowing effect of periodic wetting and drying on carbonation rate, and conservatively assuming that exposure to the groundwater is equivalent to exposure to air (noting that the past groundwater testing showed it to be slightly basic and not acidic), this would give a minimum time to carbonation at the 75 mm depth to the reinforcement on the order of 300 years.

7.1.6 Reinforcing Steel Corrosion Due to Chlorides

Similar to carbonation, exposure to chlorides can cause a loss of the corrosion protection offered by high pH concrete environments to any embedded reinforcing steel. The rate and depth of chloride penetration depend on the amount of chloride at the surface of the concrete and the concrete's permeability.

The SGH field observations from 30 – 31 March 2022 at the top of the tank domes (SGH 2022) and prior inspections did not identify any signs of corrosion (such as spalling, cracking, or the presence of corrosion products) of the embedded reinforcement within the concrete. Prior testing of the concrete also identified maximum chloride contents of 171 ppm (0.0171%) (Ackerson and Breetz 2018), although only limited information about the location and depth from which the samples were taken was provided. For context, a typical corrosion threshold is

taken as approximately 0.2% by mass of cement or about 0.033% by the total mass of concrete (ACI 2019) (assuming approximately 650 lbs of cement per cubic yard.)

The available water chemistry at the wells below the tanks and at the reference well indicates a chloride content ranging between 42 and 76 mg/L. Water with a chloride content of less than 1,000 ppm is acceptable for mixing water in conventionally reinforced concrete (PCA 2011, AASHTO 2020). Therefore, there is no apparent source of chlorides that will increase the chloride content within the concrete, so we do not expect that the chloride content within the concrete will increase above the corrosion threshold.

7.1.7 External Sulfate Attack on Concrete

Sulfates in water and soil can attack concrete, causing a loss of concrete strength and expansion and cracking of the cement hydration products within the concrete.

Typically distress due to sulfate attack manifests as map cracking of the concrete surface and softening of the concrete. Although the exterior surfaces of the tanks are not directly observable, the SGH field observations made between January and March 2023 and those of others do not identify any of this type of cracking or softening on the exposed areas of concrete at the plugs and upper hemispherical domes.

In addition, the available water chemistry data for sulfate (NAVFAC 2023) range between 10 and 16 mg/L in groundwater wells near the tanks. Combined with the field observations, this suggests that the sulfate is not a contributing factor to potential concrete deterioration because groundwater sulfate levels less than 150 ppm are considered low, and therefore, “injurious sulfate attack is not a concern” (ACI 2019).

7.1.8 Internal Sulfate Attack

Another form of sulfate attack is the internal formation of ettringite after setting, termed delayed ettringite formation (DEF). As in an external sulfate attack, the damage typically manifests as cracking of the concrete due to internal expansion. This typically occurs in concrete that sets and is cured at temperatures above approximately 160°F, such as in a

precast concrete manufacturing process. These temperatures can also be reached in large mass concrete placements such as those reported for the placements in Tanks 1-3 before active cooling measures were implemented (ASCE 1993). When it occurs, DEF typically occurs within twenty to thirty years of concrete placement.

As with external sulfate attacks, although the exterior surfaces of the tanks are not directly observable, the SGH observations did not identify any of this type of cracking on the exposed areas of concrete at the plugs and upper hemispherical domes that would indicate ongoing DEF.

7.1.9 Alkali-Silica Reactivity

Some silicious (silica-based) aggregates can cause a deleterious mechanism termed Alkali-Silica Reactivity (ASR). ASR occurs with certain forms of silica reacting with the available alkalis in the hardened concrete to create an amorphous "gel" that combines with water and expands after the concrete has set, cracking the associated aggregates and nearby concrete. ASR typically occurs shortly after the concrete is cast, although some slowly-reacting aggregates have been known to take twenty to thirty years to react enough to cause deterioration. ASR typically manifests as a map-like pattern of cracks on the concrete surface with associated gel deposits on the surface of the concrete at the cracks.

The SGH observations do not describe any crack patterns indicative of ASR at the plug concrete or the upper hemispheres, indicating no ongoing ASR, as we expect that any ASR would have occurred by this time.

Although we could not find any record of testing of the aggregates used that would have determined their susceptibility to ASR, the literature supports the lack of observed signs of ASR. A recent study (Robertson and Shen 2018) noted that ASR is not typical in Hawaii aggregates; the study included tests of multiple Hawaiian aggregate sources, including two aggregates from Oahu (Kapaa and Halawa quarries). The only aggregate they found vulnerable to ASR was from the Waikoloa quarry in Hawaii island. The Halawa coarse and fine aggregate from the nearby quarry that was reportedly used for some of the concrete at the site showed

expansion in short-term, aggressive, C1260 AMBT (Accelerated Mortar Bar Test) but not in the longer-term C1293 CPT (Concrete Prism Test) that is considered a more accurate predictor of in-service performance.

Another paper (Medeiros et al. 2019) states that in the Hawaii Archipelago, there is no history of aggregates being responsible for concrete deterioration due to alkali-silica reaction (ASR) and reports the results of testing of Hawaiian basalt aggregates. The study similarly identified expansion in three Hawaiian samples in the short-term, aggressive C1260 test but not in the longer C1293 test, which is considered more representative of in-service performance.

7.1.10 Microbiological attack

Corrosion of embedded reinforcing steel can result from a microbiological attack in which sulfate-producing bacteria can oxidize elemental sulfur and sulfides (iron sulfate, pyrite) to form sulfuric acid (Clifton and Knab 1989). No signs of this type of corrosion have been noted, although the exterior of the concrete cannot be observed for signs of damage in any locations where it would be routinely exposed to groundwater. However, the tanks contained fuels and had condensate water in the bottom of the tanks and behind the coatings on the steel tank walls. These localized environments likely could support microbiological activity and the associated generation of organic acids and mineral acids. This could have caused corrosion observed on the steel liner coupons in the 2018 study (Ackerson and Breetz 2018).

7.1.11 Salt Crystallization

If water carrying dissolved salts permeates the concrete, reaches the inside face of the concrete, and evaporates, it will leave behind the dissolved salts as crystalline deposits. These deposits can develop expansive pressures within the near surface of the concrete and cause scaling of the surface.

The presence of corrosion on the side of the steel liner in contact with the concrete indicates that some degree of water is passing through the concrete, but the low amount of dissolved solids in the water (as described previously) and the lack of observed salt crystallization damage and spalling in the access tunnels and exposed areas of concrete at the upper

hemispheres and lower plugs despite eighty-plus years of exposure indicate that the concrete will not likely undergo salt scaling.

7.1.12 Other Damage

Due to the future use and configuration of the tanks, other deterioration mechanisms considered for tunnels and low-level waste (LLW) from the nuclear industry are not applicable. These non-applicable items include damaged due to cyclic freezing and thawing (freezing temperatures are not reasonably expected), LLW attack (no LLW is or will be present), serviceability issues related to leakage (the tanks will not be in use), and overburden slides (the tanks are below a zone that may be affected by surface slides).

7.1.13 Suggestions For Potential Monitoring

We recognize the Navy's commitment to never again use the Red Hill tanks for fuel storage, and therefore, we do not recommend an extensive inspection and maintenance program for the tanks' concrete. Based on the identified potential damage mechanisms as discussed above, a long-term monitoring program could include:

- Periodically monitor the exposed concrete at the upper hemisphere and lower plugs for signs of pattern cracking typical of ASR (characterized by a finely-spaced map-pattern cracking with exuding gel and areas of persistent dark appearance even when dry, as shown in Figure 7-1).
- Monitor the steel liner for perforation loss (see Section 7.2 for more information). Monitor any exposed concrete for signs of acid attack, corrosion, and spalling, such as visibly displaced concrete (Figure 7-2), rust-colored staining (Figure 7-3), or exposed reinforcement (Figure 7-4).
- We believe an appropriate inspection interval would be every one to two years for the first few cycles and then every five to ten years thereafter if no issues are observed.

Figure 7-1 – Typical ASR Cracking (Not from Subject Site)

Figure 7-2 – Typical Incipient Spall (Not from Subject Site)

Figure 7-3 – Rust-Colored Staining (Not from Subject Site)

Figure 7-4 – Typical Exposed Reinforcement at Spall (Not from Subject Site)

7.2 Long-Term Corrosion Susceptibility of Red Hill Tank Steel Liners

The Red Hill tanks are currently lined with lap welded 1/4 in. (250 mils) thick steel plates. These liners have previously been internally protected with a corrosion-resistant coating system. Over the eighty-year life of the tanks, periodic non-destructive scans of the tank liner thickness have been conducted using ultrasonic and eddy-current techniques. Any thinned areas of the liners that were discovered have been repaired with patch plates.

We can assume that the steel liners of the emptied tanks will still have a uniform minimum thickness of 250 mils. The coating system inside these tanks includes a zinc-rich epoxy primer, an epoxy polyamide intermediate coating, and a polyurethane topcoat. These coatings have been inspected and repaired during the inspection cycle of the tanks, so we can assume that these coatings are in reasonable condition. This coating system is designed for immersion in aqueous/petrochemical solutions, and in the more benign atmosphere of an empty tank, they can be expected to have an extended life. We note that Tank 19 has been empty for

approximately twenty years, and a visual review of this tank shows the coating has not significantly deteriorated. We can therefore assume that the coating systems in emptied tanks will have a remaining life of at least twenty years.

Once the coating has deteriorated and no longer provides protection to the internal surface of the liner, the steel will start to corrode by an atmospheric corrosion mechanism. According to the Metals Handbook Volume 13C: Corrosion: Environments and Industries, in a tropical marine environment (Cape Canaveral, Florida, being similar to Hawaii), atmospheric corrosion will occur at a rate of approximately 5 mils per year. However, this rate is for the external environment; inside the tank, although the humidity could be elevated, the temperature will be lower, and there will be no chloride-bearing rain contaminating the surfaces. Therefore, the atmospheric corrosion rate will likely be similar to a more Northern rural environment, where typical corrosion rates are 0.5 to 1 mil per year. Given that the steel thickness is 250 mils, internal atmospheric corrosion of the steel liners will not be expected to corrode more than half their thickness for at least 100 years.

A greater unknown is corrosion on the outside of the tank liner. It is possible that gaps have formed between the steel liner and concrete tank wall, into which water can accumulate, resulting in crevice corrosion. There is no corrosion-resistant coating on the outside of these steel liners. We note that the groundwater adjacent to these tanks is low in chlorides, which can increase crevice corrosion rates. In the worst-case scenario, if the tank exterior was continually exposed to oxygenated flowing low-chloride water, a corrosion rate of up to 4 mils per year could be expected, giving a remaining life to through-thickness corrosion of sixty years. In reality, however, any water in crevices is likely to be stagnant rather than flowing, so it will have a limited supply of dissolved oxygen, reducing the corrosion rate to less than 1 mil per year. In addition, any such corrosion will likely be localized and will not affect the overall structural integrity of the concrete tank.

In summary, we do not expect any significant deterioration of the steel liner within the next fifty years.

8. SUMMARY, CONCLUSIONS, AND SUGGESTIONS

NAVFAC Hawaii commissioned SGH to assess the long-term structural and seismic risk for the Red Hill underground storage tanks under the assumption that the tanks will be left in place after the completion of defueling and the Navy's closure procedures. SGH performed the assessment as a subconsultant to Jacobs/B&V (Jacobs) under Jacobs Agreement No. 149001660, Rev. 1, with the scope of work as defined in the Amendment 26 SAES for IDIQ Contract N62478-20-D-5036 for the Red Hill Closure Structural Analysis at Joint Base Pearl Harbor-Hickam (JBPHH), Hawaii.

8.1 Summary of Key Tasks

The scope of work included the following primary tasks:

1. Determine seismic ground motion hazards at bedrock for a range of earthquakes at the site based on the USGS ground motion data.

2. Perform a site response analysis using a detailed model of the site-specific soil profile to determine soil and rock strains along the height of the soil column and Red Hill tanks, independent of the presence of the tanks.

3. Use the results of the site response analysis as inputs for an SSI analysis that considers a detailed model of the soil properties to calculate displacements and the pressures that would be experienced on the tank shell during an earthquake.

4. Use the loading from the SSI analysis on a detailed finite element model of a typical Red Hill storage tank to determine stresses and strains in the concrete tank shell and tank movement due to earthquake loading, both with and without the presence of the steel liner.

5. Perform a seismic evaluation of the access walkway and internal tank tower.

6. Evaluate the likely durability and extent of deterioration of both the steel liner and the concrete in the tank walls for a long exposure period, considering the groundwater chemistry.

Figure 8-1 schematically illustrates the overall analysis approach of Tasks 1 to 4 above. The following sections summarize the analysis results and findings for each of the key tasks.

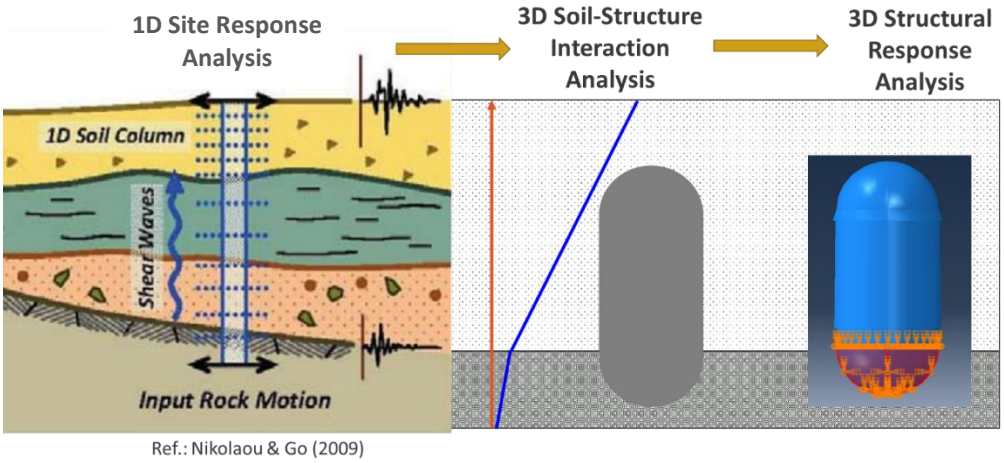

Figure 8-1 – Overall Seismic Response Analysis Approach

8.1.1 Seismic Hazards at the Site

For this project, we considered two levels of ground shaking. The first level is consistent with the building code requirements for new construction in Honolulu. The building code approach defines a Maximum Considered Earthquake (MCE) as one with a 2% probability of exceedance in a 50-year period, which equates to a 2,475-year return period. The intent of the building code is that there will be a low likelihood of structural collapse during an MCE event. Design code checks are then performed for a Design Basis Earthquake (DBE), which is defined as two-thirds of the accelerations of the MCE.

In this project, we have also considered ground motions from a 10,000-year return period event. This longer return period was selected to address the unspecified duration that the tanks will remain in their location beyond fifty years. Use of the 10,000-year return period event for seismic design is usually only performed for extremely important and critical infrastructure.

Figure 8-2 presents the seismic hazards at the Red Hill site in terms of peak ground acceleration (PGA) as a function of the annual probability of exceedance. The PGA is a measure of the maximum acceleration of the soil at the bedrock level during an earthquake. The PGA at the site is approximately 0.2 g for the MCE level event and approximately 0.4 g for the 10,000-year earthquake event.

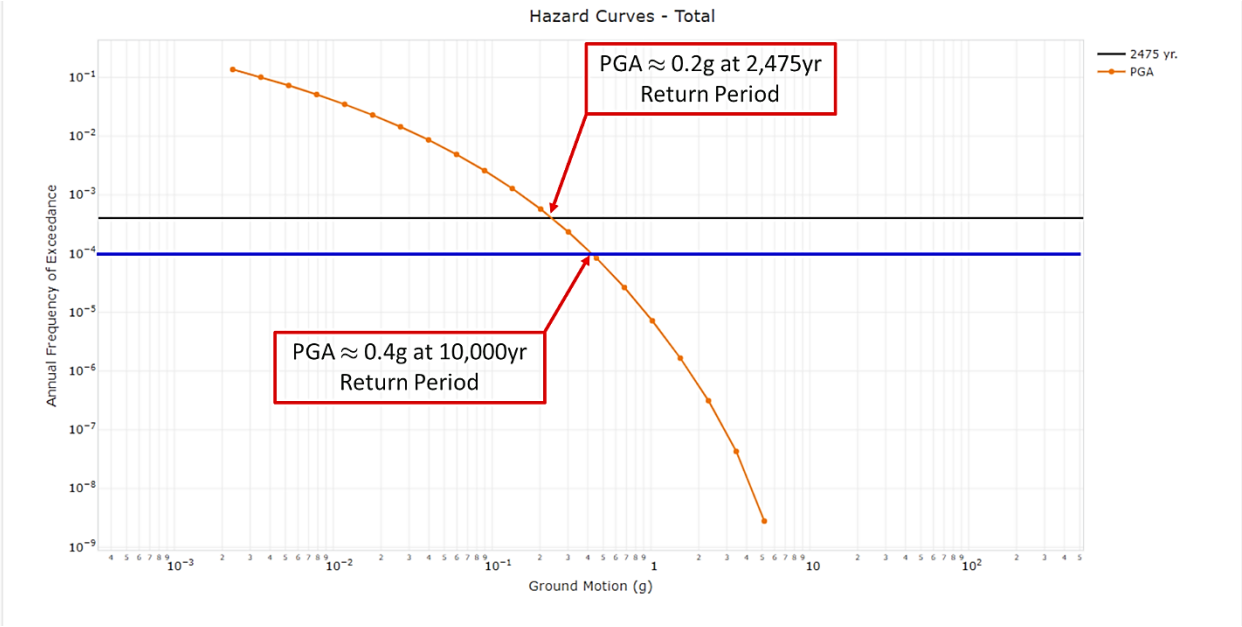

Figure 8-2 – Seismic Hazard Curve at the Red Hill Site

Figure 8-3 shows the response spectra associated with the MCE and the 10,000-year earthquake. A response spectrum is an indication of the maximum dynamic response of a structure with a given fundamental period and is related to the frequency content and magnitude of the earthquake.

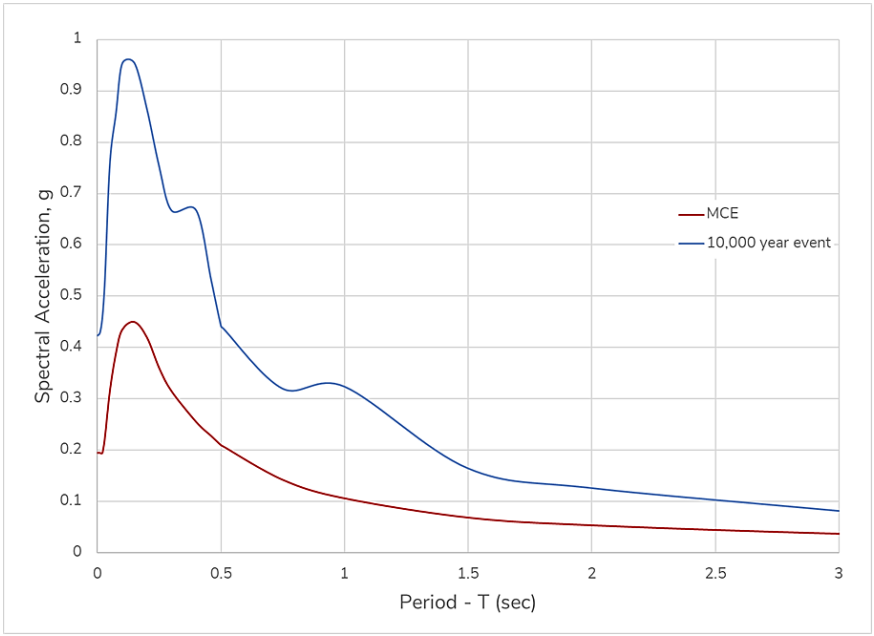

Figure 8-3 – Horizontal Response Spectra at the Site

8.1.2 Site Response

We evaluated the soil movements over the height of the tanks for representative soil profiles that include basalt rock and clinker layers. A 3D rendering of the log formations at each tank, showing the rock, clinker, grout, and lava tube layers, is shown in Figure 8-4. The concentration of rock is more pronounced in the tanks at the upper end of the tank gallery.

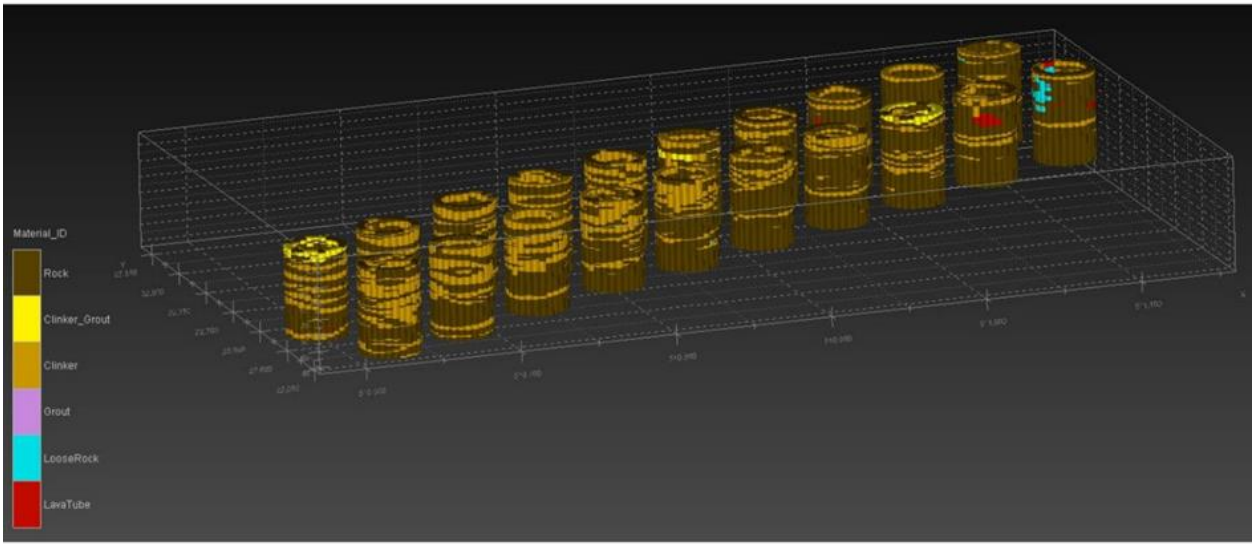

Ref.: AECOM 2019

Figure 8-4 – Excerpt from Conceptual Site Model Showing Clinker/Rock Strata

From our site response analysis, the maximum relative displacements over the height of the tanks range from 0.28 in. for the DBE to 1.05 in. for the 10,000-year earthquake.

Our sensitivity studies indicate that the calculated site response parameters are highly dependent on the mechanical soil properties, which have been conservatively estimated for this assessment.

8.1.3 Soil-Structure Interaction Analysis

Figure 8-5 shows the FE model we used for the analyses to capture SSI effects between the tank shell and the surrounding soil. For these analyses, we applied displacement output from the site response analysis to the soil to obtain tank displacements and soil pressures on the exterior of the tank.

The SSI analysis results indicate that some cracking may occur at the base of the tank during the 10,000-year earthquake.

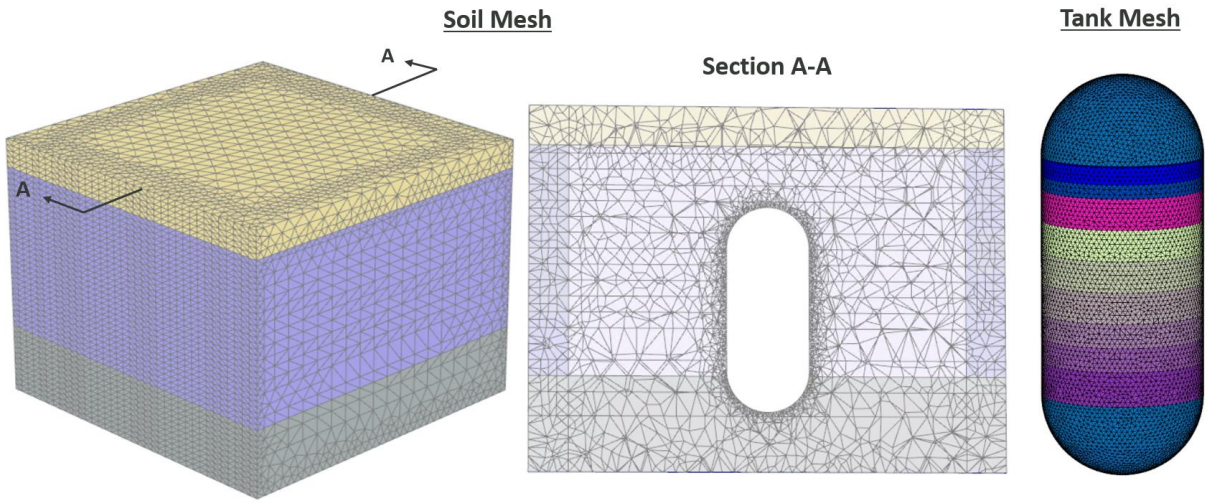

Figure 8-5 – 3D Soil-Structure Interaction Model

8.1.4 Tank Structural Response Analysis

We used the seismic loading from the SSI analysis as input to a more refined 3D model of the tank shell and performed a nonlinear FE stress analysis to evaluate the performance of the tank. We evaluated conditions both with the steel liner and without the liner, i.e., conservatively assuming a heavily corroded liner plate.

Figure 8-6 and Figure 8-7 show our nonlinear FE stress analysis model and modeling details. We modeled the concrete wall with varying thicknesses (4 ft at the base of the barrel section and 2.5 ft at the top of the barrel section). We also modeled the vertical and hoop reinforcement near the interior face of the barrel section and the reinforcement in the bottom dome. In addition, we modeled the 1/4 in. steel liner in the barrel section for the FE models that include the steel liner.

Figure 8-8 shows the deflected shape of the tank when the tank top is subjected to a lateral displacement of 1.1 in. for a 10,000-year earthquake for the condition without the steel liner. The lateral displacement of 1.1 in. corresponds to the worst-case scenario displacement from our SSI analysis. This analysis case represents the most conservative tank condition. For this

case, our analysis results indicate that the tank is stable and is able to sustain the lateral soil pressures due to the 10,000-year earthquake event with only localized cracking in the concrete.

For the DBE response, we did not observe any indication of cracking or other damage.

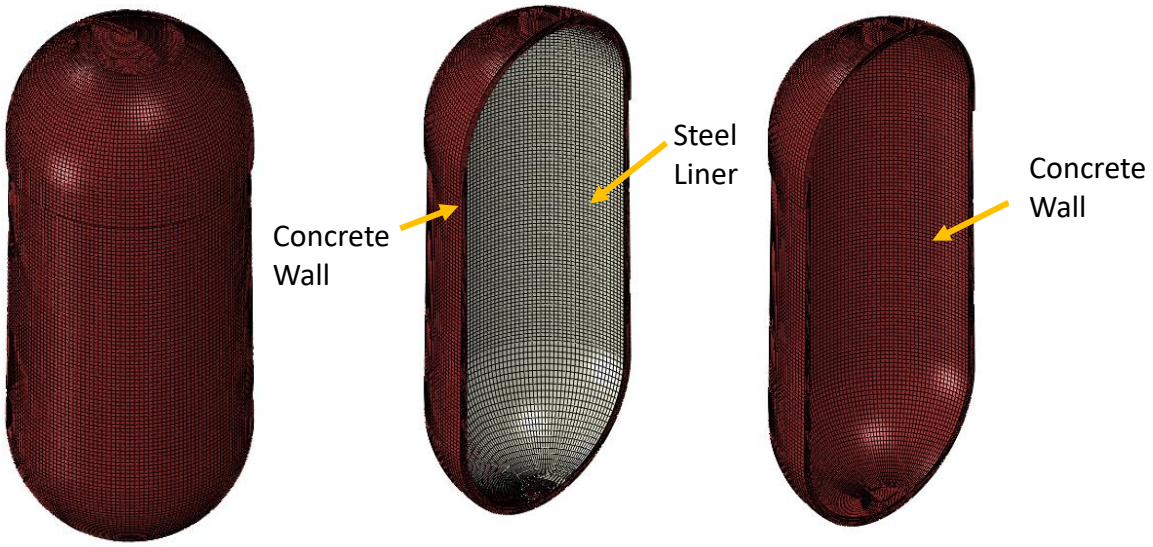

Figure 8-6 – Finite Element Model of Typical Underground Storage Tank

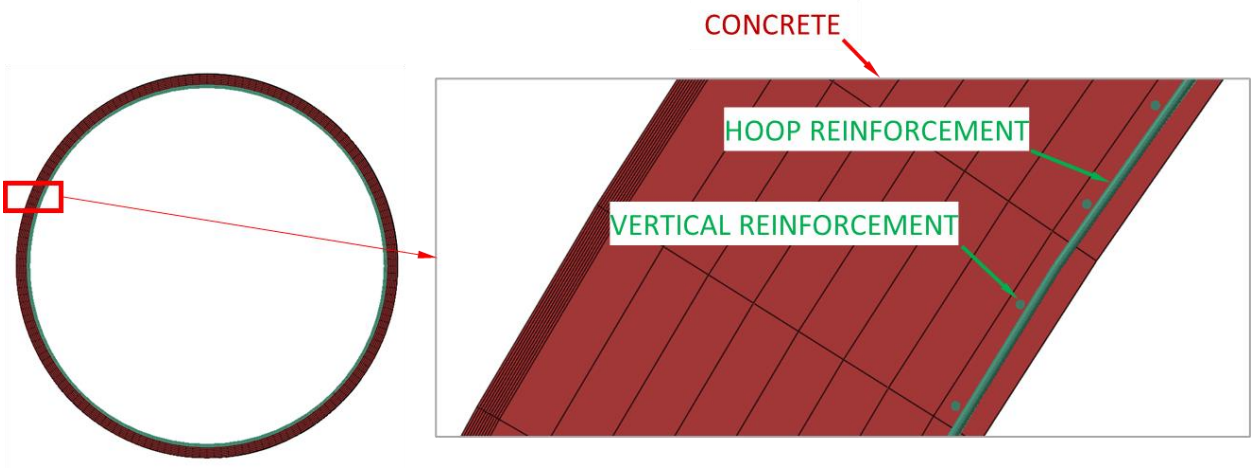

Figure 8-7 – Typical Reinforcement in Barrel Section of Tank

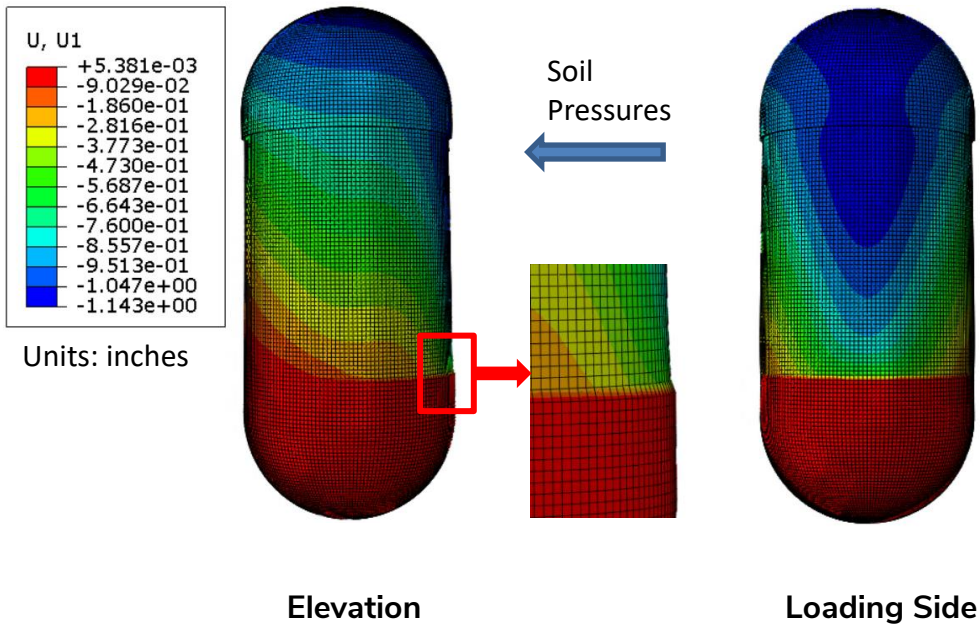

Figure 8-8 – Deflected Shape for 10,000-Year Earthquake Event (50% Rock-50% Clinker Strata, No Steel Liner)

8.1.5 Tank Access Bridge and Support Tower Structural Analysis

Internal tank access walkways and supporting towers were constructed to facilitate tank construction and periodic maintenance throughout the life of the tanks. We analyzed these structures for seismic loading, assuming they may be part of the Navy's tank access plans to access the tanks following a seismic event.

We generated an analysis model of the tower, as shown in Figure 8-9, and analyzed the tower for both the DBE and 10,000-year earthquake loads. We assumed that prior to closure, each tower would be inspected and repaired as necessary to ensure the original design capacity is still maintained. For all levels of the earthquake, our analysis results indicate that the tower remains undamaged.

Should the Navy choose to use the towers in the future to facilitate tank access, the seismic resistance and resilience of the tank access structures could be increased by adding seismically-rated restraint cables between the access bridge and the tank, as well as between the access bridge and the support tower. These seismically-rated restraint cables can assist in "catching" the access bridge should it disengage from its supports due to differential

displacement between the tower and the tank. In addition, in order to prevent damage to the bolted connections that support the access bridge, the connection at one end of the bridge (either the tower end or the tank end) could be reconfigured to accommodate the anticipated differential displacement during a major earthquake.

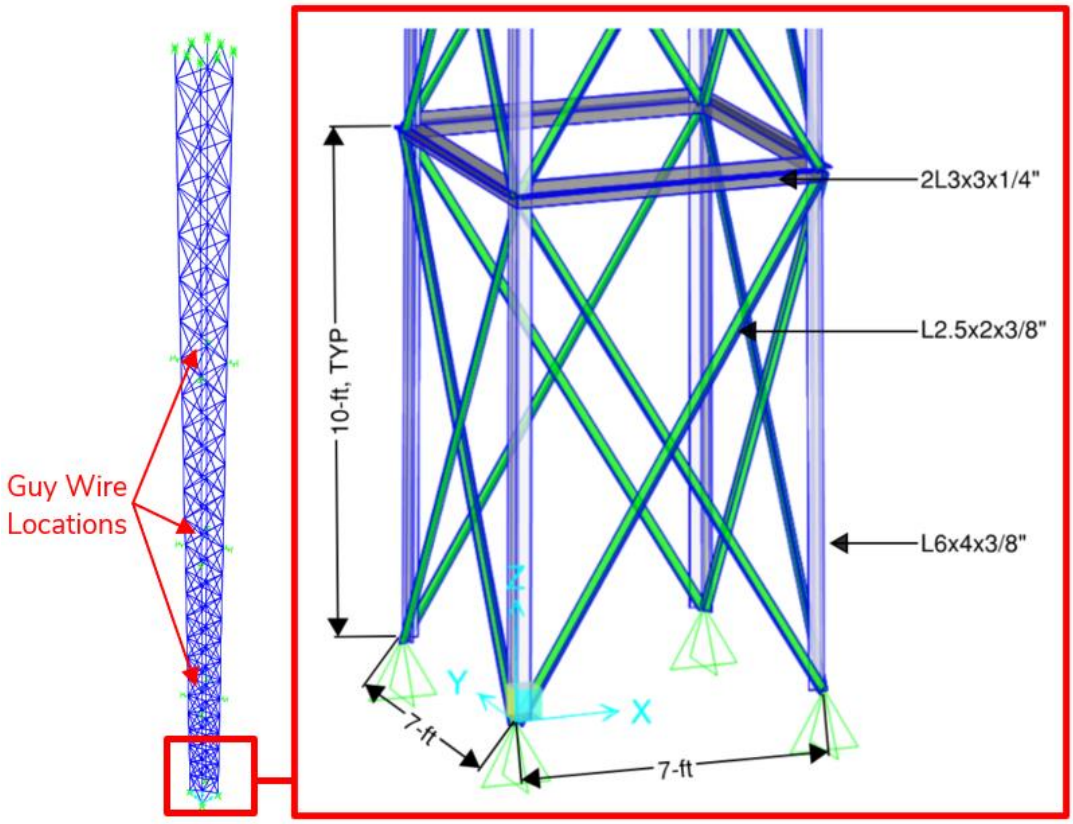

Figure 8-9 – Finite Element Model of Internal Tank Tower, Structural Elements, and Dimensions

8.1.6 Tank Durability

Concrete

We evaluated the durability of the concrete for extended exposure to site conditions, considering the available physical and chemical properties of the groundwater and concrete. In our evaluation, we considered numerous potential causes of degradation, including concrete acid attack, leaching, carbonation, chlorides, external sulfate attack, internal sulfate attack (delayed ettringite formation), alkali-silica reactivity (ASR), microbiological attack, salt crystallization, and others.

The deterioration mechanisms depend on the exposure to water, either to dissolve and carry the aggressive agent, participate in the physical reaction, or provide an environment conducive to the internal reaction. Our evaluation conservatively assumed that the exterior of the concrete at the tanks is directly exposed to water flowing through the rock and ignores the positive effects of the shotcrete layer, pressure grouting used to fill cracks and voids following concrete placement, and other protective measures applied to the tank wall during construction.

Our evaluation indicates that the governing mode of degradation for the tanks will likely be reinforcing steel corrosion due to carbonation, which is the process through which the naturally high acidity (pH) of concrete decreases over time, causing loss of corrosion protection offered to embedded steel by high pH environments. Using the information available, we estimate a timeframe on the order of 300 years would be needed for carbonation to reach the depth of the embedded reinforcing steel.

Steel Liner

We also evaluated the steel liner and estimate that because of the thickness of the steel liner and the use of protective coatings on the inside that have been periodically inspected and repaired over the 80-year lifetime of the tanks, no significant section loss is expected within the next 50 years and that internal atmospheric corrosion of the steel liners will not be expected to corrode more than half the thickness for at least 100 years. External corrosion due to exposure to oxygenated low-chloride water will likely be localized and not affect the overall structural integrity of the liner.

8.2 Considerations for Future Monitoring

We recognize the Navy's commitment to never again use the Red Hill tanks for fuel storage, and therefore, we do not recommend an extensive inspection and maintenance program. However, should the Navy wish to continue any future monitoring of the condition of the tanks, a long-term monitoring program could include the following considerations:

1. Periodically monitor any exposed concrete for signs of corrosion and spalling, such as visibly displaced concrete, rust-colored staining, or exposed reinforcement. Monitor the exposed concrete at the upper hemisphere and lower plugs for signs of pattern cracking

typical of ASR (characterized by a finely spaced map-pattern cracking with exuding gel and areas of persistent dark appearance even when dry). We believe an appropriate inspection interval would be every one to two years for the first few cycles and then every five to ten years thereafter if no issues are observed.

2. Should the Navy choose to use the towers in the future to facilitate tank access, the towers and their connections should be inspected before the long-term closure of the facility and repaired/retrofitted as necessary to restore their original capacity. To increase seismic resistance and resilience of the tank access structures, seismically-rated restraint cables could be added between the access bridge and the tank, as well as between the access bridge and the support tower. These seismically-rated restraint cables can assist in "catching" the access bridge should it disengage from its supports due to differential displacement between the tower and the tank. To increase seismic resistance and resilience of the tank access structures, the connection at one end of the bridge (either the tower end or the tank end) could be reconfigured to accommodate the anticipated differential displacement during a major earthquake.

8.3 Recommendations

We recommend that the Navy perform a visual review of the tanks should the site experience a future major earthquake (one with a peak ground acceleration at the site on the order of 0.2g) to identify sustained damage. A drone, the internal tank towers, or other means of safe access can facilitate this initial visual assessment.

9. REFERENCES

Ackerson and Breetz (2018). Destructive Analysis of 10 Steel Coupons Removed from Red Hill Fuel Storage Tank #14, Report No. 201801967, 17 December 2018.

Allen et al. (2015). Guide for the Preservation of Highway Tunnel Systems, NCHRP 14-27, July 2015.

American Association of State Highway Transportation Officials (2020). LRFD Bridge Specifications, 9th Edition, Washington DC.

American Concrete Institute (2019). Guide to Protection of Reinforcing Steel in Concrete against Corrosion, ACI Report 222R-9, 1 April 2019.

American Concrete Institute (2019). ACI 318 – Building Code Requirements for Structural Concrete and Commentary, American Concrete Institute.

American Institute of Steel Construction (2016). ANSI/AISC-360-16 Specification for Structural Steel Buildings. An American National Standard. Chicago, Illinois: American Institute of Steel Construction, 7 July 2016.

American Society of Testing Materials (2019). ASTM-A603 Standard Specification for Zinc-Coated Steel Structural Wire Rope.

American Society of Civil Engineers (1993). The Construction of the US Navy's Red Hill Underground Fuel Storage Facility, Hawaii, Enclosure 3.

American Society of Civil Engineers (2022). ASCE 7-22 Minimum Design Loads and Associated Criteria for Buildings and Other Structures.

American Society of Civil Engineers (2023). ASCE 7 Seismic Hazards Tool. Accessed at https://asce7hazardtool.online/

American Water Works Association (2014). Design of Prestressed Concrete Cylinder Pipe, AWWA C304-14.

AECOM (2019). Conceptual Site Model, Investigation and Remediation of Releases and Groundwater Protection and Evaluation, Red Hill Bulk Fuel Storage Facility. Comprehensive Long-Term Environmental Action Navy Contract Number N62742-12-D-1829, CTO18F0126, NAVFAC, Honolulu, 30 June 2019.

Brandes et al. (2011). Soil and Rock Properties in a Young Volcanic Deposit on the Island of Hawaii, Journal of Geotechnical and Geoenvironmental Engineering, June 2011.

Clifton, James (1989). Service life of Underground Concrete Structures, Structural materials: proceedings of the sessions related to structural materials at Structures Congress '89, San Francisco Hilton, San Francisco, CA, 1 – 5 May 1989.

Clifton, J. and Knab, L. (1989). NISTIPR 89-4086, Service Life of Concrete, US Department of Commerce, prepared for US NRC, June 1989.

Electric Power Research Institute (1993). Guidelines for determining design basic ground motions, v. 1: Method and Guidelines for Estimating Earthquakes Ground Motion in Eastern North America: EPRI Report TR-102293.

Gannett Fleming, Inc. (2010). Development of Guidelines for Rehabilitation of Existing Highway and Rail Transit Tunnels, Gannett Fleming, Inc., July 2010

Kramer. (1996). Geotechnical Earthquake Engineering, Pearson, 1st Edition. 1996.

Lee, J. A. (1998). Plastic-Damage Model of Cyclic Loading of Concrete Structures. Journal of Engineering Mechanics, 124(8), 892 – 900.

Lubliner, J.E. (1989). A Plastic-Damage Model for Concrete. International Journal of Solids and Structures, 25, 299 – 329.

Medeiros et. al. (2019). Evaluation of Basaltic Aggregates from Iceland and the Archipelagos of Hawaii and Azores Regarding Alkali-Silica Reaction: A Comparative Study, 17th EMABM, University of Toronto, Toronto, Canada, 20 – 23 May 2019.

National Academies of Sciences, Engineering, and Medicine. 2015. Guide for the Preservation of Highway Tunnel Systems. Washington, DC: The National Academies Press. https://doi.org/10.17226/21903.

NAVFAC (2023). Historical Groundwater Data, Received 23 March 2023.

Neville, A.M. (2012). Properties of Concrete, Trans-Atlantic Publications, Inc., 5th Edition.

Nikolau and Go (2009). Site-Specific Seismic Studies for Optimal Structural Design: Part II – Applications. Structure Magazine. Link: C-StructuralDesign-Nikolaou-Dec091.pdf (structuremag.org).

Picard and Beaulieu (1987). Design of Diagonal Cross Bracings Part 1: Theoretical Study. Engineering Journal, AISC.

Picard and Beaulieu (1988). Design of Diagonal Cross Bracings Part 2: Experimental Study. Engineering Journal, AISC.

Portland Cement Association (2011). Design and Control of Concrete Mixtures, 15th Edition.

Process Industry Practices (2017). Structural Design Criteria PIP STC01015.

Robertson, I, and Shen, L. (2018). Field Evaluation of Concrete using Hawaiian Aggregates for Alkali-Silica Reaction, Robertson, I, and Shen, L., MATEC Web of Conferences 199, 2018; https://doi.org/10.1051/matecconf/201819903005,

Simpson Gumpertz & Heger Inc. (2022). Assessment of the Red Hill Underground Fuel Storage Facility Pearl Harbor, Hawaii.

United States Geologic Survey (2023). Accessed at: https://earthquake.usgs.gov/nshmp/.

Wong et al. (2011). Shear-Wave Velocity Characterization of the USGS Hawaiian Strong-Motion Network on the Island of Hawaii and Development of a NEHRP Site-Class Map, Bulletin of the Seismological Society of America, Vol. 101, No. 5, pp. 2252 –,2269, October 2011.

\\sgh.com\offices\HOU\projects\2022\221162.00-RHDS\WP\008PBSummers-R-221162.00.dkh.docx